

**Geology and Geochemistry of the Amba Dongar
Carbonatite-Hosted Fluorite Deposit, India**

by

David A. S. Palmer

A thesis submitted to the Faculty of
Graduate Studies and Research in partial
fulfillment of the requirements for the
degree of Master of Science

Department of Earth and Planetary Sciences
McGill University, Montreal

© David Palmer, 1994

FRONTISPIECE



The Deccan Traps, viewed from Amba Dongar Village

ABSTRACT

The Zomba Dongar carbonatite complex, India is host to a large fluorite deposit (11% of 30% CaF₂). The complex consists of a small ring structure comprised of a central carbonatite breccia, a large, outer lining of calcitite and a number of smaller ankertitic carbonatite plugs. Surrounding the carbonatite ring are numerous dykes of nephelinitic and phonolitic syenites. The complex was intruded into the Cretaceous Bagh Sandstones and Late to Early Paleocene Deccan Volcanic.

The hydrothermal history of the complex is extensive, consisting of two main systems, the first resulted in large amounts of fensitization, causing extensive K and Na metasomatism of the surrounding sandstones and the second, dealt with a fluid was responsible for the silicification of large amounts of the calcitite and the deposition of economic quantities of fluorite.

The hydrothermal veins and vug fillings of blue, purple, white, yellow and colorless fluorite are the main ore zone, which is currently under production, and most of the fluorite is found near the carbonatite-sandstone contact.

Chemical and mass balance calculations show that the fluids responsible for silicification removed significant quantities of Ca from the rock while adding large amounts of Si, Al and F. Alteration associated with fluorite deposition involved the removal of Al from the rock and the addition of large quantities of F and Si.

Fluid inclusions in fluorite point to a low temperature-low salinity (<160°C-0.6 to 0.3 wt.% NaCl eq) ore fluid, which decreased in temperature and salinity with evolution. Crushing experiments performed on fluid inclusions in both fluorite and quartz reveal the presence of ~ 0.08 m of dissolved CO₂ in solution while analyses of leachates and decrepitate residues from fluid inclusions show significant concentrations of Ca, Al, Na, Cl and S in their fluids. Oxygen, hydrogen and carbon isotopic data from the fluids in fluid inclusions suggest that the dominant component of the ore fluid was meteoric, and that it had equilibrated with sedimentary carbonates. Log *f*O₂ and pH conditions of the fluid, at the time of ore formation, are interpreted to be >-42 and <3.5, respectively. The presence of Al and S in the fluid, the molar equivalence of Na and Cl, and the positive deviation of δ¹⁸O and δD from the meteoric water line point to a small contribution from orthomagmatic fluids.

A model is proposed in which the intrusion of a carbonatite magma at high crustal levels caused faulting and fracturing of the surrounding country rocks, and was accompanied by the release of orthomagmatic fluids, expressed as extensive K and Na metasomatism of the surrounding sandstones. With the decline of orthomagmatic activity, a meteoric water-dominated hydrothermal system was initiated by the heat of the intrusion. The interaction of Ca-bearing meteoric fluids with the last vestiges of F-bearing orthomagmatic NaCl brines caused deposition of vast quantities of fluorite at the site of mixing.

SOMMAIRE

Le complexe d'Amba Dongar, en Inde, de type carbonatite, contient un important gisement de fluorite (11.6 mt de 30% CaF₂). Le complexe présente une structure annulaire. Le plus petit anneau, formé de brèche carbonatitique, est entouré d'un plus large anneau de calcite. Aussi, plusieurs petits bouchons de carbonatite ankéritique sont présents. Plusieurs bouchons de syenites néphéitiques et phonolitiques se trouvent autour de l'anneau de carbonatite. Le complexe fut introduit dans les Grès de Bagh du Crétacé supérieur et dans les Volcaniques de Deccan du Paléocène inférieur et supérieur.

Le complexe montre un développement hydrothermal poussé pouvant être décrit par deux systèmes principaux. Le premier, a causé une fénitisation importante se traduisant par un métasomatisme considérable en K et Na des grès encaissants. Le second, a été responsable de la silicification de grandes quantités de calcite et de la déposition de quantités économiques de fluorite.

Le gisement est formé de veines et vacuoles remplies de fluorite bleue, violette, blanche, jaune ou incolore. La zone minéralisée principale, présentement sous production, ainsi que la majorité des occurrences de fluorite, se trouvent près du contact carbonatite-grès.

Des analyses chimiques et des calculs de bilan de masses démontrent que les liquides responsables de la silicification ont retiré de grandes quantités de Ca des roches, en y ajoutant, cependant, d'importantes quantités de Si, Al, et F. L'altération associée à la déposition de la fluorite a joué un rôle dans l'enlèvement de Al et l'addition de grandes quantités de F et Si.

Les inclusions fluides apparaissant dans la fluorite semblent indiquer un fluide minéralisant de faible salinité à basse température (<160°C-0.6 à 0.3% NaCl équivalent) dont la température et la salinité auraient baissé en évoluant. Des expériences de broyage d'inclusions fluides contenues dans la fluorite et dans le quartz, révèlent la présence de ≈ 0.08 m de CO₂ dissout en solution. Des analyses de résidus obtenus par lessivage et décrépitation d'inclusions fluides ont démontré de hautes concentrations de Ca, Al, Na, Cl et S dans les fluides. Des données isotopiques d'oxygène, d'hydrogène et de carbone des fluides contenus dans les inclusions indiquent la prépondérance d'un fluide minéralisant d'origine météorique ayant subi un équilibrage avec les carbonates sédimentaires. Lors de la formation du minerai, le log *f* O₂ et le pH du fluide auraient eu des valeurs de >-4.2 et <3.5 respectivement. La présence de Al et S dans le fluide, les équivalences molaires de Na et de Cl, et la déviation positive de δ¹⁸O and de δD de la ligne d'eau météorique indiquent une faible contribution de fluides orthomagmatiques.

Un modèle est proposé dans lequel l'intrusion d'un magma carbonatitique, à un niveau crustal élevé, aurait causé la formation de failles et de fractures dans les roches encaissantes, ainsi que le relâchement de fluides orthomagmatiques, démontré par l'ample métasomatisme en K et Na des grès avoisinants. Avec le déclin de l'activité orthomagmatique, un système hydrothermal, dominé par l'eau météorique, a été initié par la chaleur de l'intrusion. L'interaction des fluides météoriques, contenant du Ca, avec les derniers vestiges de saumures orthomagmatiques riches en NaCl et contenant du F, a entraîné la déposition de grandes quantités de fluorite au site du mélange.

ACKNOWLEDGMENTS

I would like to express my sincere gratitude to my supervisor, Dr. A.E. "Willy" Williams-Jones, for his assistance and for his helpful criticisms.

Dr. S. Viladkar is gratefully acknowledged for giving us the spark of an idea which developed into this thesis. Special thanks are also in order for his assistance in organizing the field work, acquainting us with the geology of the area and his helpful discussions on the complex. The Gujarat Mineral Development Corporation is also given many thanks for their hospitality, assistance and for providing us with complete access to the deposit and the surrounding area.

Field work was carried out with the assistance of Dr. Williams-Jones and Jeanette Roelofsen.

The author is indebted to Jeanette Roelofsen for her help with Scanning Electron Microscopy and for performing AEM analyses on samples from Amba Dongar. George Panagiotidis is gratefully acknowledged for his assistance with thin section preparation and the countless tips which saved the lives of many innocent glass slides. Atomic-absorption and ion-chromatography were performed by Glenna Keating and Sandra Lalli, with a special thanks for their patience.

The helpful advice of, and discussions with Jim. Clark, J. Roelofsen and Antoine Fournier contributed greatly to this thesis. Mia Boiridy, Georgia Spyros and their moms are given many thanks for their help in the production of this thesis. M. Boiridy is also thanked for her french translation of the abstract.

Most importantly, the author thanks his parents, Bill and Susan Palmer, who gave him the desire to pursue this goal, and immeasurable support throughout.

TABLE OF CONTENTS

FRONTISPIECE	i
ABSTRACT.....	ii
SOMMAIRE	iii
ACKNOWLEDGMENTS	iv
TABLE OF CONTENTS.....	v
PREFACE	xi
CHAPTER I INTRODUCTION	1
General Statement	1
Previous Work	6
Purpose and Methodology	7
CHAPTER II: GEOLOGY.....	8
Location	8
Regional Geology	8
Country Rock Geology	12
Deccan Basalt	12
Bagh Sandstone.....	13
Bagh Limestone	15
The Carbonatite Complex	15
Geology.....	15
Carbonatite Geology	16
Fenitization	19
CHAPTER III:.....	21
JOURNAL MANUSCRIPT	21
Abstract.....	23
Introduction	24
Regional Geology	27
Carbonatite Geology	29
Fenitization.....	30
Mineralization.....	31
Mode of Occurrence of Fluorite.....	31
Petrographic Characterstics	36
Barren Vein Systems	40
Alteration Associated with Quartz Veining	40

Fluorite Chemistry	42
Chemical Changes During Alteration.. .. .	47
Masses Gained and Lost	50
Mass Factors for Barren Quartz Vein Silicification	52
Mass Factor Associated with Quartz-Fluorite Alteration	54
Fluid Inclusions	56
Inclusions in Amba Dongar Fluorite	56
Inclusions in Quartz	59
Microthermometry	60
Crushing Experiments.. .. .	65
Estimates of Salinity Based on CO ₂ Concentration	66
Leachates	68
Results	69
Decrepitate Residues.. .. .	71
Results	72
Oxygen and Hydrogen Isotopes	75
Discussion..... .. .	76
Pressure and Temperature	76
Fluid Origin	78
Log f_{O_2} -pH Conditions	82
Fluid Evolution..... .. .	85
Transport and Deposition..... .. .	89
Comparison To Other Deposits	91
Conclusions.. .. .	92
CHAPTER IV: CONCLUSIONS.. .. .	94
General Conclusions.. .. .	94
Contributions to Knowledge	97
REFERENCES	98
APPENDIX..... .. .	107
Analytical Equipment and Methodology	107
Fluid Inclusion Microthermometry..... .. .	107
Leachate Analyses	107
Decrepitate Analyses	108

LIST OF FIGURES

- Figure 2.1 General geological map of West-Central India showing the Deccan Volcanic Province and the location of the study area. Map inset shows large-scale structural features of the region surrounding Amba Dongar. The course of the Narmada River is controlled by the Narmada Rift, a fault zone reactivated during the Late Cretaceous as the Indian plate crossed over a mantle plume (modified from Karakare and Srivistava, 1990). ... 9
- Figure 2.2 Geological map of the Amba Dongar carbonatite complex and surrounding area (modified from Deans *et al.*, 1972)... 11
- Figure 2.3 A) An outcrop of Bagh sandstone displaying cross bedding; B) Carbonatite breccia showing rough texture due to differential weathering of fragments (recessed) relative to the matrix..... 14
- Figure 2.4 A) An ankeritic carbonatite dyke intruding calcitite; B) Fenitized sandstone xenolith in calcitite. The xenolith shows complete replacement of quartz grains by K-feldspar 18
- Figure 3.1 The geology of the Amba Dongar carbonatite complex (modified from Deans *et al.*, 1972, Karkare and Srivistava, 1990).. 28
- Figure 3.2 A) A fluorite vein surrounded by a halo of silicified calcitite (dark); B) Silicified calcitite breccia cemented by fine-grained quartz... 32
- Figure 3.3 A) large yellow fluorite crystals coating vug wall; B) fine-grained purple fluorite crystals lining vug. 34
- Figure 3.4 A) A hand specimen of a vug showing early blue fluorite (B), against the wall, overgrown by later white fluorite (W), which in turn is overgrown by yellow fluorite (Y).; B) A hand specimen of a vug showing early blue fluorite (B), lining the wall, overgrown by colorless fluorite (C). The white fluorite layer is absent.. . . . 35
- Figure 3.5 A) Quartz encrusted yellow fluorite cubes. The ring in the picture is approximately 1.5 cm in diameter.; B) An SEM microphotograph of a fluorite vein showing growth, from left to right, of barite (Ba), purple fluorite (Fl) and quartz (Q) with disseminated barite. The quartz, fluorite and disseminated barite to the left of the barite layer is altered wall-rock (W).... 37

- Figure 3.6 A) A photomicrograph, taken using plane polarized light, showing crystals of an aluminosilicate mineral at the edge of the white fluorite layer. This phase is probably one of the kaolinite group minerals (i.e. kaolinite, dickite); B) An SEM photomicrograph of the aluminosilicate mineral in the white fluorite layer, showing the radiating, accordion-like habit of the mineral 38
- Figure 3.7 A) A photomicrograph, in plane polarized light, of unaltered calcite showing matrix composed of interlocking calcite grains. Photograph taken using plane polarized light, B) A photomicrograph of altered calcite immediately adjacent a fluorite vein. Quartz is now almost completely replaced by fluorite (Fl) and hematite (He). Further away from vein, quartz becomes the dominant alteration mineral. Crystal in the lower-center of the picture is euhedral pyrochlore. Photograph was taken using plane polarized light 41
- Figure 3.8 A) photomicrograph of calcite, which hosts barren quartz veins, that has been completely replaced by fine-grained quartz and minor fluorite. Photograph taken using cross polarized light, B) the same view in plane polarized light showing relationship between quartz (Q), hematite (He) and fluorite (Fl) 43
- Figure 3.9 Profiles showing abundances of selected major and trace elements in fluorite versus fluorite color. Units are in weight percent for Ca, Sc, SiO₂ and Fe₂O₃, and in ppm for the remaining elements 45
- Figure 3.10 Chondrite-normalized rare earth element abundances in fluorite. Chondrite values were taken from Boynton, 1983. Profiles show a slight positive slope with a distinct "well" between Nd and Sm 46
- Figure 3.11 A graph of Lu/La versus fluorite color showing the enrichment of LREE in early blue and purple fluorite relative to later yellow and colorless varieties 48
- Figure 3.12 Chondrite-normalized rare earth element abundances of altered and unaltered calcite. Chondrite values taken from Boynton, 1983. Samples AD008a and AD008b represent unaltered and altered calcite, respectively, associated with fluorite mineralization and samples AD053a and AD026a and AD053b and AD026b represent unaltered and altered calcite, respectively, associated with barren quartz veins 51

- Figure 3.13 Isocon diagram comparing a) sample AD053a with sample AD053b; and b) samples AD026a and AD026b. The dashed line represents the constant mass line (Mass Factor = 1) where an element is neither lost nor gained. The solid line is the isocon. If elements are above this line, they have been added to the rock, and if they are below the isocon they have been removed. For information about the samples refer to the text..... 53
- Figure 3.14 Isocon diagram comparing sample AD008a with AD008b, the alteration of calcite associated with fluorite mineralization. The behavior of this graph is the same for that of 3.13. For more information refer to the text. 55
- Figure 3.15 A) Primary fluid inclusions in fluorite, terminated by, and occurring along, growth zones; B) A plane of secondary fluid inclusions formed in fluorite. The decrease in size of the inclusions from the top to bottom indicates that they were trapped along a healing fracture..... 57
- Figure 3.16 A) A large, primary liquid-vapor fluid inclusion in fluorite; B) A primary, liquid-vapor fluid inclusion in fluorite displaying a negative-crystal habit C) A primary liquid-vapor fluid inclusion in quartz; D) A liquid-only fluid inclusion in quartz; E) Coexisting liquid-only and vapor-rich fluid inclusions in quartz..... 58
- Figure 3.17 Histograms of homogenization temperatures for liquid-vapor fluid inclusions in a) fluorite; b) and quartz.....61
- Figure 3.18 a) Histogram of initial ice melting temperatures for liquid-vapor fluid inclusions in fluorite and quartz; b) Histogram showing the final ice melting temperatures for fluid inclusions in fluorite and quartz..... 64
- Figure 3.19 A) An SEM photomicrograph of a fluid inclusion decrepitate residue on a silica plate; B) Energy dispersive scan from a typical Ca-, Na-, K-, Mg-, Fe-, C-, S- and Cl-bearing residue..... 73
- Figure 3.20 Oxygen and hydrogen isotopic data for Eocene and later, fluorite-hosted inclusion fluids and modern meteoric water. The meteoric water line (MWL) and primary magmatic water box (PMW) are shown in relation to the samples. The heavy dashed line in the field of PMW represents the typical $\delta^{18}\text{O}$ value for Amba Dongar carbonatites (Gwalani *et al.*, 1993). The lighter dashed lines between the meteoric water line and primary magmatic waters represent mixing lines for the Amba Dongar ore fluid..... 79

Figure 3.21 The fO_2 -pH stability fields of Fe-S-O minerals, calcite, barite, kaolinite, muscovite and the aqueous sulfur species at a) 125 °C (yellow and colorless fluorite) and b) 150 °C (blue and purple fluorite). Activities of ΣS , ΣC , Ba^{2+} , K^+ and Ca^{2+} in the ore fluid were determined to be 10^{-2} , 10^{-11} , 10^{-2} , 10^{-2} and $10^{-0.8}$, respectively, for yellow and colorless fluorite (125 °C), and 10^{-1} , 10^{-11} , 10^{-1} , 10^{-2} and $10^{-0.6}$, respectively, for blue and purple fluorite (150 °C). The shaded area in each of the diagrams represents the probable log fO_2 and pH conditions of the ore fluid at the time of fluorite deposition... .. 84

Figure 3.22 A plot of salinity (wt % NaCl eq.) versus homogenization temperature for fluid inclusions in fluorite and quartz 86

Figure 3.23 A plot of Tb/La versus fluorite color showing the chemical evolution from early purple and blue fluorite to the later yellow and colorless varieties..... 88

PREFACE

This thesis was written in the form of a journal manuscript, entitled Genesis of the Carbonatite-hosted Fluorite Deposit at Amba Dongar, India: Evidence from Fluid Inclusions, Stable Isotopes and REE Geochemistry, in accordance with the regulations put forth by the Faculty of Graduate Studies and Research, McGill University. In addition, an introduction, general geology and concluding chapter were written in order to provide a comprehensive description of the research

The following are excerpts from the Guidelines Concerning Thesis Preparation:

"Candidates have the option, subject to the approval of their Department, of including, as part of their thesis, copies of the text of a paper(s) submitted for publication, or the clearly-duplicated text of a published paper(s), provided that these copies are bound as an integral part of the thesis. If this option is chosen, connecting texts, providing logical bridges between the different papers, are mandatory"

"The thesis must still conform to all other requirements of the Guidelines Concerning Thesis Preparation and should be in a literary form that is more than a mere collection of manuscripts published or to be published. The thesis must include, as separate chapters or sections: (1) a Table of Contents, (2) a general abstract in English and French, (3) an introduction which clearly states the rationale and objectives of the study, (4) a comprehensive general review of the background literature to the subject of the thesis, when this review is appropriate, and (5) a final overall conclusion and/or summary."

CHAPTER I: INTRODUCTION

General Statement

Fluorite occurs in a variety of geological environments, including as a gangue mineral in certain types of ore deposits. It is commonly found as an accessory mineral in many granite-hosted tin deposits (Taylor and Pollard, 1985), Mississippi Valley Type lead-zinc ores (Kessen *et al.*, 1981) and REE deposits (Zhou *et al.*, 1980;). In some cases, it may form greater than 30% of the rock and constitute a primary ore mineral (Strong *et al.*, 1984; Roedder *et al.*, 1968; Ekambaram *et al.*, 1986; Ruiz *et al.*, 1980, 1985, Hein *et al.*, 1984, Barbieri *et al.*, 1983; Mariano, 1989). Strong *et al.* (1984) have classified fluorite deposits into two genetic types: those associated with sedimentary, dominantly carbonate, rocks, and similar in many respects to Mississippi Valley type deposits; and fluorite vein-type deposits related to alkaline-peralkaline rocks. A third group not considered by Strong *et al.* (1984) is represented by fluorite deposits hosted by carbonatites. Examples of the last class of fluorite deposit are rare and consequently relatively little is known about their genesis.

The association between carbonatites and fluorite is well documented (Le Bas, 1989; Kucilmer *et al.*, 1966; Flegg *et al.*, 1977, Woolley and Kempe, 1989; Wyllie, 1989). However, relatively few economic deposits of fluorite have been found (Mariano, 1989). Even though fluorite occurs as a primary mineral in carbonatites, and one deposit associated with the Choakhol'skiy carbonatite, Tuva, is thought to be magmatic in origin (Puzanov, 1975), most deposits of

economic significance are considered to be late-stage and hydrothermal (Mariano, 1989). Although most fluorite deposits are interpreted to have derived their fluorine from orthomagmatic fluids, often based on the geological setting of the deposit, few definitive studies on their origin have been undertaken. On the basis of $^{87}\text{Sr}/^{86}\text{Sr}$ isotopic data, Deans and Powell (1968) have suggested that deposition of fluorite in the carbonatites of Tororo, Uganda and Chilwa Island, Malawi was associated with late stage emanations from the carbonatitic magma. Based on their association with the carbonatite, reserves of fluorite at Okorusu, South Africa are also thought to have been deposited from carbonatite-derived fluids (Deans *et al.*, 1973). Late stage fluorite deposits hosted by carbonatites of the Bol'shaya Tagna pluton, Eastern Sayan were interpreted, through fluid inclusion data, to have been deposited from hydrothermal solutions that evolved from the magma chamber which produced carbonatite intrusions (Puzanov, 1977). Fluorite of the Mato Preto deposit in southern Brazil is also considered to be genetically related to its carbonatite host due to its enrichment in REE, and the slightly negative ϵ_{Nd} , indicating a possible mantle source for at least some of the components in the fluorite (Ronchi *et al.*, 1993). However, there is debate over the origin of the carbonatite-hosted fluorite deposits of Amba Dongar, India. Deans and Powell (1968) used strontium isotopic data to support a hypothesis that the fluorite was deposited by a mixture of meteoric and orthomagmatic fluids from the surrounding sandstones and the carbonatite (see also Kaul *et al.*, 1988). By contrast, Lahiry (1976) argued that the mineralizing solution was a mixture of meteoric and orthomagmatic fluids from the surrounding sandstones and basalts. In order to better understand the origin of the Amba Dongar deposit, the source of the fluid as well as the physico-chemical aspects of fluorite solution, transport and deposition must be considered.

Field relationships and experimental work are giving us a better idea of

the nature of carbonatitic magmas and their associated hydrothermal systems. It is evident that fluorine is an important constituent of carbonatitic liquids (Le Bas, 1977, 1989; Jones and Wyllie, 1983; Gittins *et al.*, 1990, Andersen and Austrheim, 1991). Whole rock analyses by Gittins (1989) have shown that carbonatites can contain up to 8 wt.% fluorine. The abundance of fluorine-bearing minerals in carbonatites, e.g., fluorite, fluoroapatite, phlogopite, bastnaesite, and pyrochlore, gives evidence of the importance of this element in carbonatite systems (Hogarth, 1989; Heinrich, 1966). In most carbonatite suites fluorine shows enrichment in the later stages of carbonatite activity (Woolley and Kempe, 1989), as shown by the increased abundance of fluorine-bearing accessory minerals (Hamilton *et al.*, 1989; Le Bas and Rubie, 1977, Jago and Gittins, 1991; Viladkar and Wimmenauer, 1992). It is for this reason that many authors have proposed that the hydrothermal fluids released by carbonatites during late stage activity are responsible for the formation of carbonatite-hosted fluorite deposits (Mariano, 1989; Deans and Powell, 1968; Deans *et al.*, 1972).

The nature of the hydrothermal fluids in equilibrium with carbonatite magmas has been studied by a number of researchers (Wyllie and Tuttle, 1960, Andersen, 1986; Gittins, 1989; Treiman and Essene, 1984). Early experimental work, in the system $\text{CaO-CO}_2\text{-H}_2\text{O}$, by Wyllie and Tuttle (1960) established that $\text{H}_2\text{O-CO}_2$ dominant fluids would be in equilibrium with carbonatitic liquids. This led many researchers to assume that fluids associated with carbonatites only vary in respect to their proportions of H_2O and CO_2 . However, Gittins *et al.* (1990), working with experimental carbonate systems containing fluorine, have postulated that aqueous fluids separating a carbonatite magma are not simply H_2O -dominant, but should contain a number of other components, including fluorine. The abundance of fluorine in aqueous fluids exsolved by carbonatitic magmas is evidenced by zones of fenitization containing fluorine-rich amphiboles

and micas (Le Bas, 1989). Further evidence lies in the fluorite deposits themselves which, as discussed above, may be genetically related to the carbonatite suites with which they are spatially associated. Chlorine may also be an important constituent in these fluids (Gittins, 1989). Currie and Ferguson (1971) have shown that fenitization surrounding the Callander Bay complex, Ontario was caused by an NaCl brine and Dawson (1989) and Gittins (1989) record high concentrations of Cl (up to 7800 ppm) in the carbonatite lavas of Oldoinyo Lengai. The ratio of Cl:F is typically <1 in the parental magma (Woolley and Kempe, 1989), however, it would be considerably larger in the exsolved fluid as chlorine partitions strongly into the aqueous phase while fluorine prefers the melt (Gittins, 1989).

The solubility of fluorite and its behavior in hydrothermal systems has been investigated by a number of workers (Booth and Bidwell, 1950; MacDonald and North, 1974; Richardson and Holland, 1979a,b). The early studies indicated that hydrothermal solutions containing calcium could not carry the amounts of fluoride ions necessary to form the large fluorite deposits that are observed, due to the very low solubility of fluorite. A two solution model, or separate sources of Ca and F, was then proposed to explain these deposits (Hall and Friedman, 1963). Subsequently, Richardson and Holland (1979a) suggested that it might be possible to carry larger amounts of fluorine as ion pairs with one of the major cations in solution (i.e., Na^+ , Ca^{++} , K^+ , Mg^{++}). This study showed that, in NaCl solutions, fluorite solubility increases with increasing temperature, at all concentrations of NaCl, to about 100°C . At temperatures between 100°C and 150°C , solutions more dilute than $1.0m$ NaCl reached a maximum of fluorite solubility, and possibly a minimum at greater temperatures. Solubility also increased with increasing NaCl concentration, due to the effect of the change in the ionic strength on the ion activity coefficients (Richardson and Holland,

1979a). The pH of the fluid likewise has a strong effect on fluorite solubility. NaCl-HCl-bearing fluids show a large increase in fluorite solubility at HCl concentrations greater than $10^{-3}m$ (Richardson and Holland, 1979a). Fluorite deposition can be accomplished by a number of methods including decreases in solution temperature or pressure (Richardson and Holland, 1979b). In hydrothermal solutions with greater than $1.0m$ NaCl, cooling of the fluid below $260^{\circ}C$ (the limit of the experimental data) is an effective mechanism for lowering the solubility of fluorite. However, in dilute solutions ($<1.0m$ NaCl) fluorite transport and deposition can only occur at temperatures below $150^{\circ}C$ (Richardson and Holland, 1979a). Studies of the effect of pressure on fluorite solubility by MacDonald and North (1974) have shown that a decrease in pressure will lower the solubility of fluorite but that the accompanying temperature drop will far outweigh this effect. Wall rock interaction can also be an effective method for precipitating fluorite. Such interaction may increase the pH and/or calcium ion activity (e.g. through dissolution of calcite) both of which will favor deposition of fluorite (Richardson and Holland, 1979a).

The carbonatite complex of Amba Dongar, India provides an excellent setting in which to study hydrothermal events related to carbonatite activity. The economic potential of the complex was first revealed in 1962 with the discovery of large amounts of fluorite originally thought to be associated with mobilized limestones and Deccan volcanics. It wasn't until 1963 that the host rocks were shown to be carbonatites and that the genesis of the fluorite deposits was intimately related to their emplacement (Sukheswala and Udas, 1963).

Amba Dongar is a ring-structured carbonatite which is located approximately 400 km northeast of Bombay, India. The complex consists of numerous, distinct, carbonatitic bodies hosted by Early to Late Cretaceous quartzitic Bagh sandstones and Late Paleocene to Early Eocene Deccan flood

basalts (Chiplonkar *et al* , 1977; Wellman and McElhinny, 1970; Viladkar, 1981). Fluids released during intrusion of the carbonatite are thought to have caused localized K-metasomatism (finitization) of the surrounding sandstones.

Hydrothermal fluids of unknown origin were responsible for depositing large quantities of fluorite within the carbonatite. The Geological Survey of India estimated the initial reserves of fluorite at 11,600,000 tonnes of 30% CaF₂. The deposit is currently being mined by the Gujarat State Mining Company by open pit methods.

Previous Work

The geology of the Amba Dongar complex has been studied by a number of workers (Sukheswala and Udas, 1963; Deans and Powell, 1968; Deans *et al.*, 1972; Viladkar, 1981; Srivastava, 1989; Gwalani *et al*, 1993) and a small number of microthermometric measurements have been carried out on the fluid inclusions in fluorite (Roedder, 1973; Lahiry, 1976; Kaul *et al*, 1988). No data is available for fluid inclusions in quartz associated with silicification or mineralization. Homogenization temperatures reported in these studies range from 106-162°C and are lower for the late yellow and colorless fluorite than the early blue fluorite. Roedder's (1973) study contained the only reliable final ice-melting temperatures, with those for early blue fluorite being -0.9 to -1.0°C and that of late fluorite being -0.5°C. Although the nature of the carbonatite has been well documented, there is still considerable debate on the origin of the fluorite. Viladkar & Wimmenauer (1992), Kaul *et al.* (1988) and Deans *et al* (1972) consider that the fluids responsible for fluorite deposition were genetically related to the carbonatite. By contrast, Lahiry (1976), on the basis of the similar Sr

isotopic compositions of the fluorite and Bagh sandstone, has argued that the fluorite was deposited by a mixture of meteoric water from the sandstone, which supplied the calcium, and a F-bearing aqueous orthomagmatic fluid derived from the magma that produced the Deccan basalts.

Purpose and Methodology

This study has investigated the genesis of the fluorite at Amba Dongar, with a number of methods, in order to establish the nature of the fluids responsible for fluorite deposition, their origin and the physico-chemical controls of their deposition. Microthermometric studies of fluid inclusions were used to constrain the temperature of deposition and to obtain a partial composition of the fluid. Leachate and decrepitate analyses were performed to obtain additional compositional information. Crushing tests were used to identify any dissolved gas species. Analyses of the fluorite chemistry were used to gain insight into fluid composition, and mass balance calculations were carried out to establish the role of wall rock alteration in fluorite deposition. Stable isotope data have provided information on origin of the fluids.

A large amount of research has been carried out on fluorite deposits of sedimentary or alkaline-peralkaline association (see previous references). However, relatively little is known about the genesis of carbonatite-hosted fluorite deposits. This research was used to develop a model for fluorite deposition at the Amba Dongar complex which could find application in helping to interpret the genesis of other carbonatite-hosted fluorite deposits. It may also shed light on the role of the late stage hydrothermal processes which are thought concentrate other elements, most notably REE, into economic quantities.

CHAPTER II: GEOLOGY

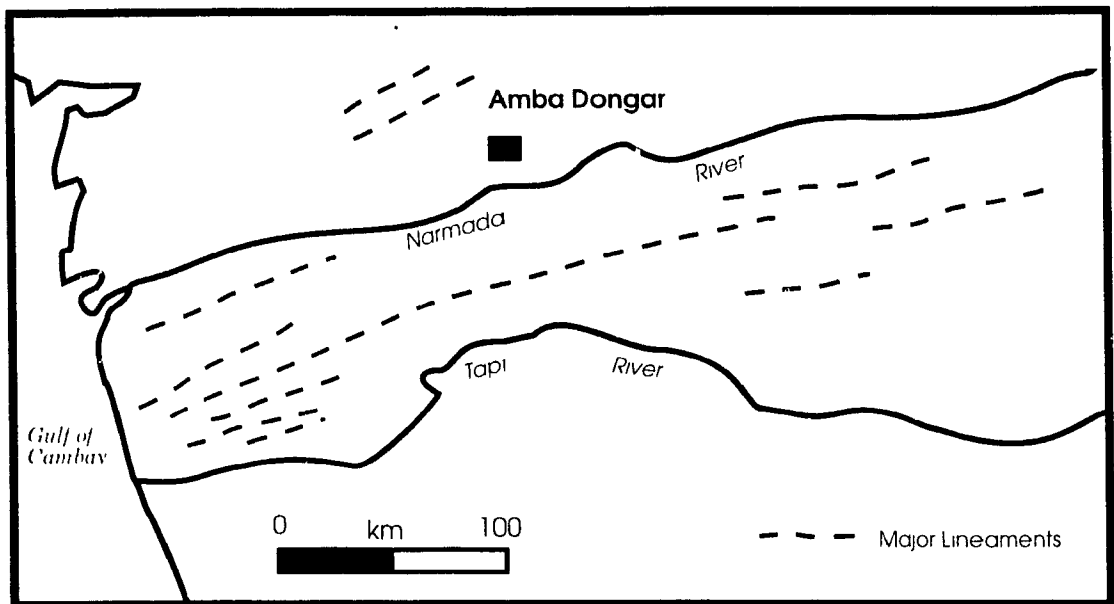
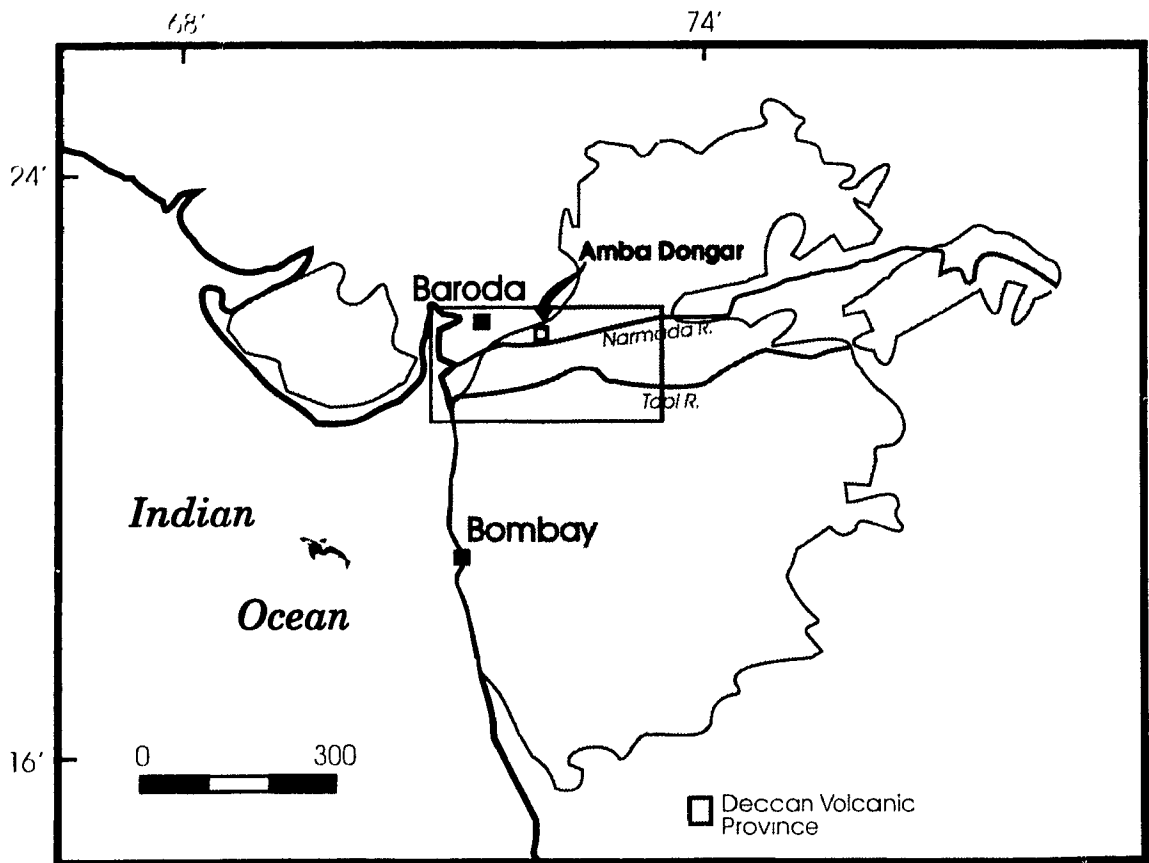
Location

The Amba Dongar complex is situated approximately 400 km northeast of Bombay, India in the Baroda district of Gujarat State. It outcrops over an area of approximately 3.5 km and lies at a minimum elevation of 380 meters above sea level with a maximum relief of 61 meters.

Regional Geology

The carbonatite complex of Amba Dongar was emplaced into the northern part of the Deccan Volcanic Province which covers an area of approximately 500,000 km² of West-Central India, and forms one of the largest geological formations of the country (Krishnan, 1982) (Fig. 2.1). The Deccan province consists of a large thickness of plateau flood basalts. Extrusion of the basalts is thought to have occurred during rifting, along reactivated lineaments, as a result of the upwelling of tholeiitic magma when India passed over a mantle thermal center at around 65 Ma (Dietz and Holden, 1970; Gupta and Gaur, 1984; Srivastava, 1989; Karkare and Srivastava, 1990;). A general chronology for the area is: 1) eruption and extrusion of voluminous flood basalts; 2) intrusion of alkaline and carbonatitic bodies; and 3) emplacement of late picritic and basaltic dykes (Gwalani *et al.*, 1993; Srivastava, 1989; Sukheswala *et al.*, 1976).

Figure 2.1 General geological map of West-Central India showing the Deccan Volcanic Province and the location of the study area. Map inset shows large-scale structural features of the region surrounding Amba Dongar. The course of the Narmada River is controlled by the Narmada Rift, a fault zone reactivated during the Late Cretaceous as the Indian plate crossed over a mantle plume (modified from Karakare and Srivistava, 1990).



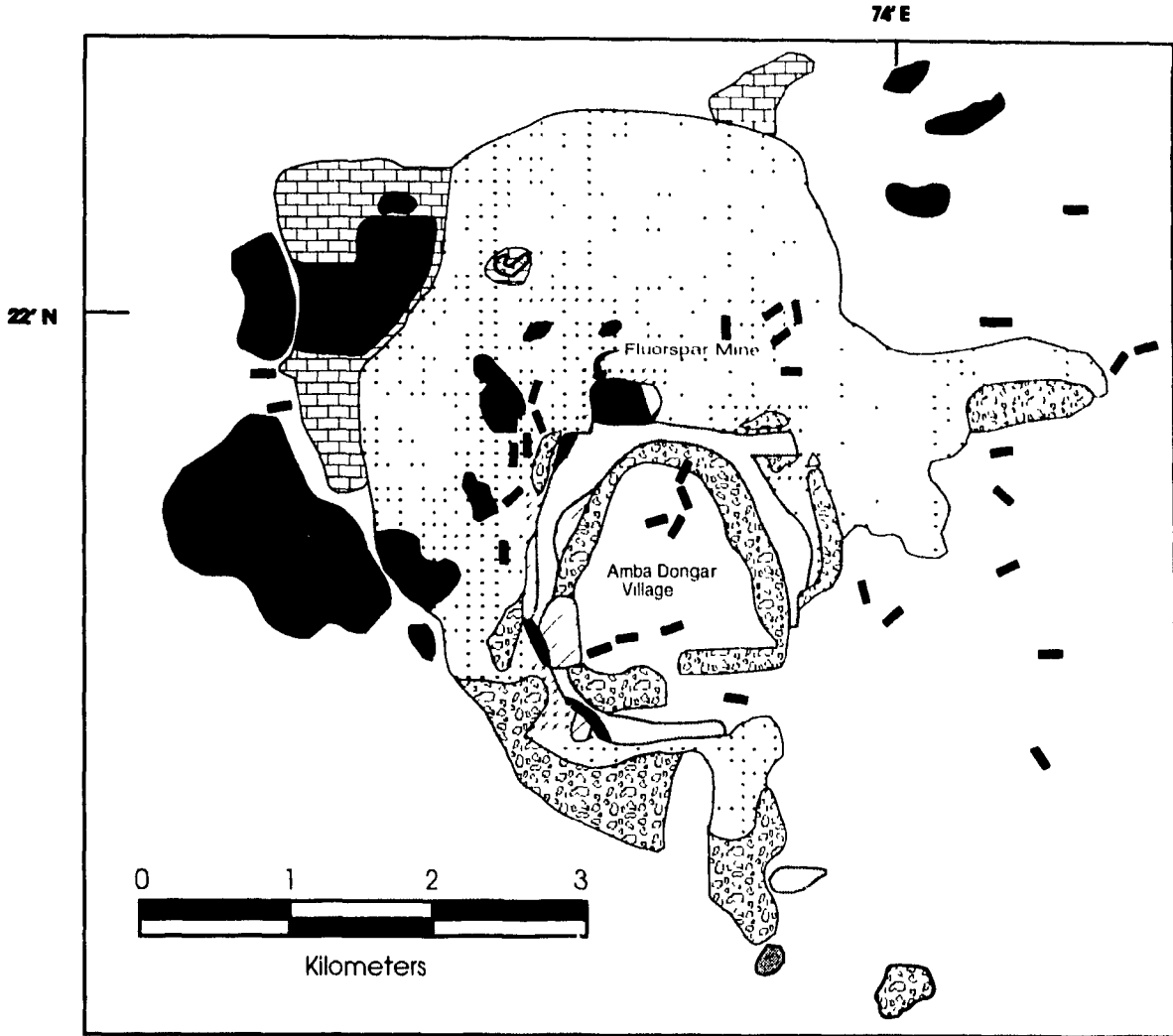
Gwalani *et al.* (1993) have divided the Deccan Province into three subprovinces, based on observations of alkaline magmatism. Amba Dongar has been included in the Chota Udaipur sub-province, which is characterized by abundant alkaline intrusions, and is unique in that it is the only one to contain feldspar-free rocks such as carbonatites. The Chota Udaipur sub-province has been further subdivided into five sectors, each containing a main geographic formation (Gwalani *et al.*, 1993). The Amba Dongar complex has been assigned its own sector owing to the fact that it is the only ring structure in the subprovince.

The complex lies within a major zone of structural weakness represented by the ENE trending Narmada rift, which is located nine kilometers to the south (Fig. 2.1 inset). To the north of the complex, is a sympathetic set of faults related to the Narmada rift (Viladkar, 1981). The rift system is thought to be the arm of a failed triple junction that originated along the older Vindhayan fault (Karkare and Srivastava, 1989; Deans *et al.* 1972, Courtillot *et al.*, 1988). Structural expressions of this zone of weakness consist of numerous parallel (to the rift), mafic dyke swarms and NE trending strike-slip faults (Srivastava, 1989).

Intrusion of the carbonatite caused updoming of the country rock which is reflected in dips of 35 to 60 degrees outwards from the body. These structural features are evident up to 5 km away from the ring. Numerous faults are distributed radially around from the complex and have given rise to steep valleys and scarps.

The carbonatite ring structure was intruded into Deccan basalts, which comprise its southern and southwestern boundaries, and a small inlier of Late Cretaceous Bagh sandstones and limestones (Viladkar, 1981), which flank the intrusion on all other sides (Fig. 2.2). Deccan basalts are also present inside the ring structure, and are interpreted by Deans and Powell (1968) to represent

Figure 2.2 Geological map of the Amba Dongar carbonatite complex and surrounding area (modified from Deans *et al.*, 1972).



**Post-Carbonatite Intrusives
(Eocene and Later)**

 Basalt and
Dolerite Dykes

**Amba Dongar Alkaline
Complex
(Eocene and Later)**

 Fluorite
Mineralization

 Fenitized
Sandstone

 Ankeritic
Carbonatite



Calcite



Carbonatite
Breccia



Nephelinite

**Deccan Volcanic
Province
(Late Cretaceous
to Eocene)**



Basalts

**Bagh Formation
(Late Cretaceous)**



Sandstone



Limestone

a roof over the intrusive site which collapsed during emplacement of the carbonatite. Viladkar (1981), however, has suggested that the basaltic core may represent a later igneous event following carbonatite emplacement. The underlying basement rocks consist of Precambrian granitic gneisses which are poorly exposed and do not outcrop in the area (Srivastava and Karkare, 1991; Deans *et al.*, 1972). Surrounding the carbonatite, and less commonly within the carbonatite, are plugs of nephelinite and phonolitic nephelinite which are interpreted to be genetically related to the carbonatite (Viladkar, 1984).

Country Rock Geology

Deccan Basalt

By far the most common rock type in the surrounding area is the flood basalt of the Deccan Traps. The latter consist predominantly of tholeiitic flows and yield whole rock K-Ar dates of 65 Ma to 50 Ma which place them in the Late Paleocene to Early Eocene period (Wellman and McElhinny, 1970). The area surrounding the Narmada Rift belongs to one of a number of alkali olivine basalt subprovinces which occur within the Deccan province (Chatterjee, 1964; Srivastava, 1989; Gwalani, 1981).

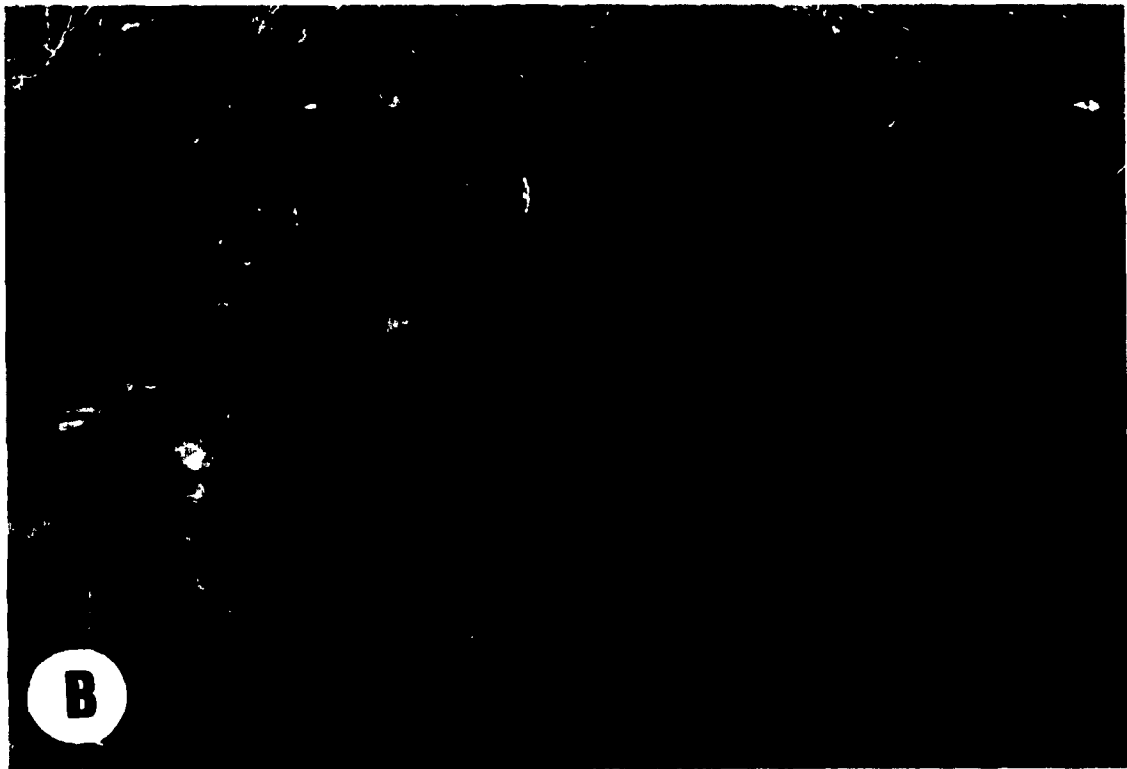
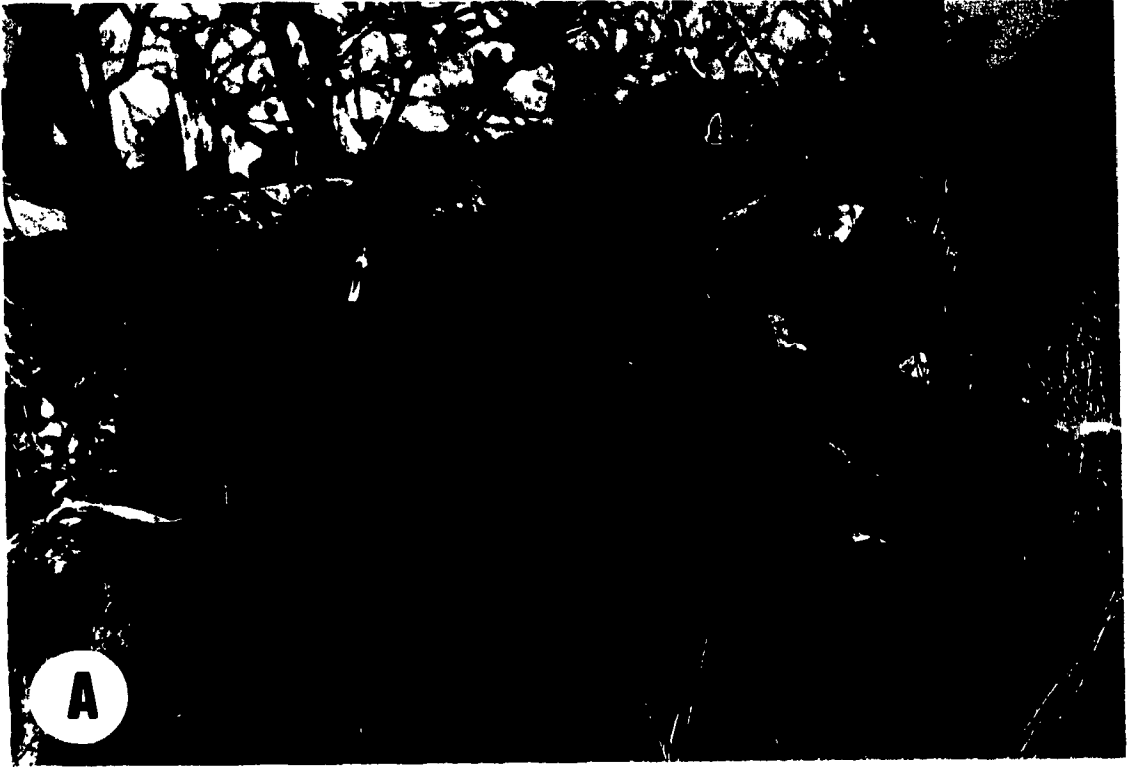
The dominant lithologies of the Trappean beds are basaltic lavas and agglomerites. Dykes of glassy basalt and dolerite are also common, and trend parallel to the Narmada lineament (Srivastava, 1989). Basalt is typically porphyritic and locally glomerophytic. Phenocrysts, as well as the groundmass, consist of augite and labradorite which, modally, make up 70 to 80 % of the rock. Accessory minerals include olivine, calcite, zeolites and apatite. Evidence of

vesiculation is common in the basalts, typically in the form of amygdules. Dolerite forms dark gray dykes which range in width from 0.5 to 15 m and can be followed for distances of up to 1.5 km (Srivastava, 1989). Modally, plagioclase is more important in the dolerite than in the basalt, and the percentage of plagioclase plus augite is at least, 80%. The texture is commonly ophitic to sub-ophitic and locally porphyritic with labradorite occurring as the micro-phenocrysts (Srivastava, 1989). Minor minerals include olivine and iron oxides.

Bagh Sandstone

The only other rock type which borders the complex is the Late Cretaceous Bagh sandstone. The sandstones belong to a wave-dominated shelf sequence (Bose and Das, 1986). Bose and Das (1986) have divided the Bagh sequence into five main facies: 1) a conglomeratic lag deposit; 2) coarse-grained sandstone; 3) sandstone; 4) mudstone; and 5) limestone. Chiplonkar *et al.* (1977) have interpreted the sequence as being between Upper Albian to Turonian in age (100 Ma - 88.5 Ma), based on paleontological observations. The Bagh sandstone consists of an almost pure quartz sandstone (>96% quartz) which, in outcrop, appears white to light gray. The grain size varies from medium to coarse, and there are local concentrations of small quartz pebbles. The sandstones have a generally well sorted groundmass of spherical quartz grains which commonly show evidence of recrystallization, possibly due to pressure solution. Sedimentary features observed in outcrop include cross-bedding, normal grading and asymmetric ripple marks, indicating a moderate velocity, shallow fluvial environment (Fig. 2.3A). In some areas adjacent to the ring complex the Bagh sandstone has been intensely fenitized, which is evident as K-feldspar pseudomorphs after quartz. In these areas the sandstone takes

Figure 2.3 A) An outcrop of Bagh sandstone displaying cross bedding; B)
Carbonatite breccia showing rough texture due to differential
weathering of fragments (recessed) relative to the matrix.



on a reddish hue.

Bagh Limestone

To the west of the complex, and separated from it by the sandstones, is a unit of limestone that was deposited after the quartz-rich sediments (Viladkar, pers. comm.). The limestone is a thinly to moderately thickly bedded, fine-grained, tan-colored unit which displays gentle folding in outcrops nearest the complex.

The Carbonatite Complex

Geology

The carbonatite complex of Amba Dongar is a ring structured intrusion with a diameter of approximately two kilometers, and consists mainly of a prominent ridge of calcitite, which forms the principal topographical feature of the ring, and an inner lining of calcitite breccia (Fig. 2.2). Breccias also occur around the circumference of the ring as variably sized, isolated plugs, parallel to the ring's border. Along both margins of the calcitite ring are numerous small plugs of ankeritic carbonatite. Small dykes (<1 m) of ankeritic carbonatite and calcitite cut the above lithological units. In the calcitite, intense fracturing, indicated by numerous jasper and quartz-fluorite veins, may have provided the pathway for fluids which deposited large amounts of fluorite in open space-filled veins and vugs. In a number of areas the calcitite shows intense silicification surrounding barren quartz veins. Formation of the complex also included the intrusion of a

number of moderately sized (200m -1500m in diameter) syenitic plugs in the surrounding country rock.

Deans *et al.* (1972) and Viladkar (1981) have developed a chronological sequence for intrusion of the ring. Formation of the structure is interpreted to have begun with the emplacement of the calcitite breccia followed by intrusion of the calcitite and finally the plugs of ankeritic carbonatite. Silicification and fluorite deposition are thought to have post-dated all igneous activity.

Carbonatite Geology

The calcitite breccia consists mainly of fragments of calcitite and minor metamorphic rocks, sandstone, basalt and nephelinite all set in a matrix of calcitic or ankeritic material (Fig. 2.3B). Differential weathering of the fragments and the harder matrix give the breccia a very rough, irregular appearance

Calcitite, which forms the main component of the ring system at Amba Dongar, shows a large variation in grain size, texture and color. Early calcitite tends to be coarser-grained, occurring as xenoliths in the later, fine-grained calcitite. The most frequently observed texture consists of interlocking, equigranular calcite crystals. A porphyritic texture is well developed, locally, with larger calcite phenocrysts set in a matrix of finer grained calcite. The proportions of other minerals in calcitite vary greatly; comprising from 1% to over 30% of the rock by volume. In decreasing order of importance, martite, apatite, fluorite, barite, galena, pyrochlore, zircon, phlogopite and aegirine are the most commonly found of these other minerals. Color variations of the calcitite are numerous, ranging from white to red, brown or a mottled white and black. This range in color is due mainly to the nature of the dominant accessory minerals.

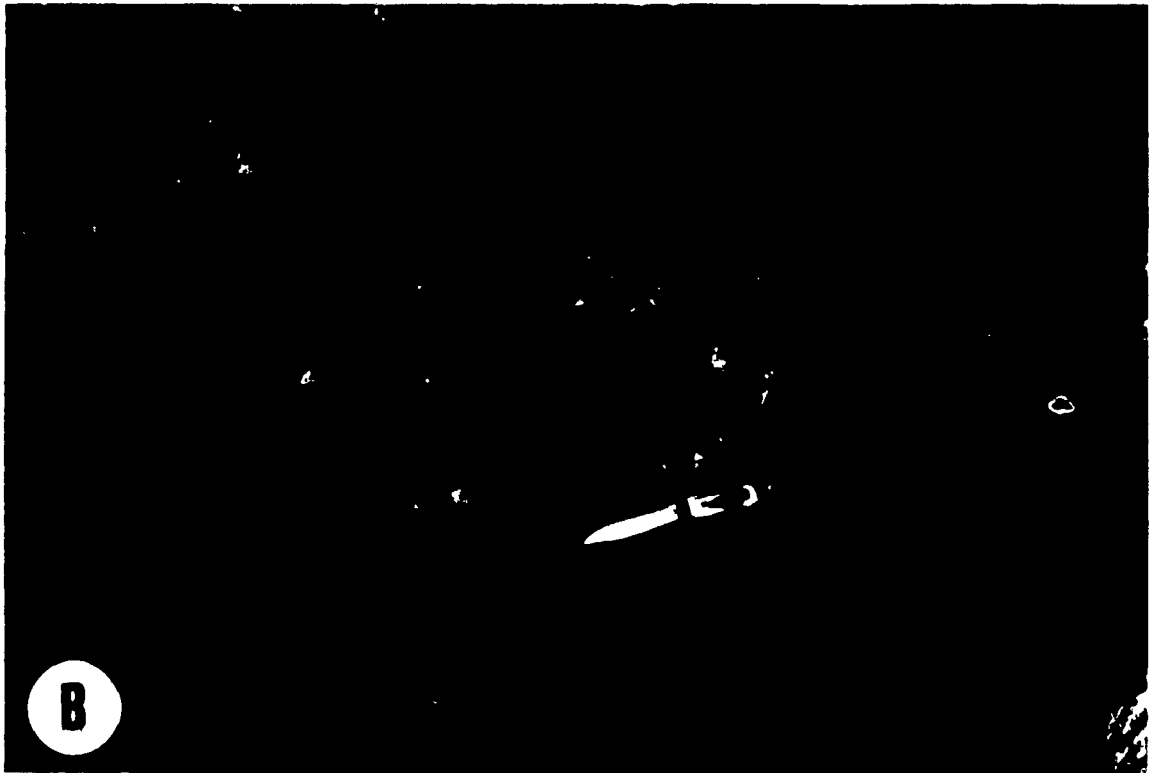
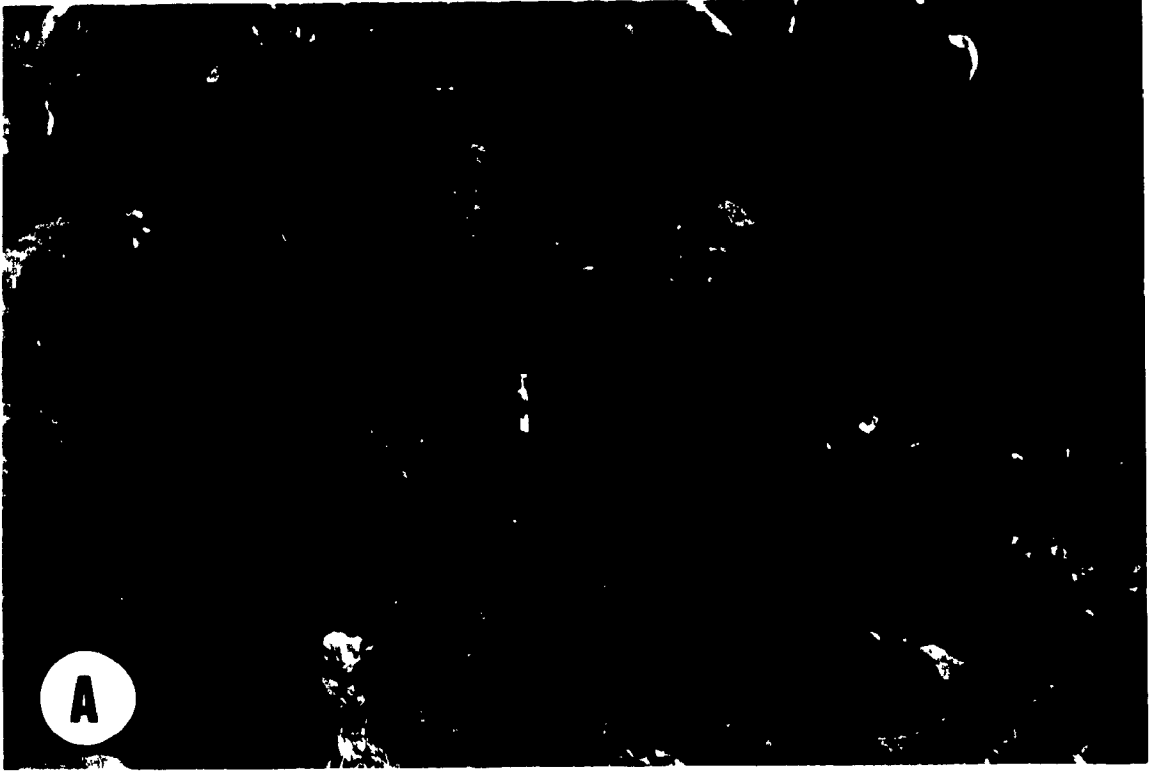
Flow banding is commonly observed in the calcitite, and is recognized

either by grain size variations or by the alignment of accessory minerals. The orientation of the flow banding is variable, but typically it is at an oblique angle to the ring with a near vertical or steep northerly dip. Small ankeritic carbonatite dykes, as well as fenitized xenoliths of Bagh sandstone are found in the calcitite (Fig 2.4A)

Ankeritic carbonatite is generally a dark red, highly oxidized, fine-grained rock. Accessory minerals are abundant in this unit, the most important of which is martite, in some samples martite can comprise over 50% of the volume of the rock. Other minor constituents include fluorite, barite, apatite, bastnaesite, pyrochlore, monazite, thorite, pyrite, galena and chalcopyrite (Viladkar and Wimmenauer, 1992). Calcitite dikes as well as small jasper veins are found within the ankeritic carbonatite. Following carbonatite intrusion, a hydrothermal event caused silicification of large volumes of calcitite surrounding zones of pervasive quartz veining. Hydrothermal activity also caused the formation of numerous fluorite deposits scattered throughout the calcitite. The fluorite mineralization occurs as vein and replacement deposits. Deposition of fluorite occurred in two stages; an early stage characterized by a blue to purple variety and a later stage characterized by yellow to colorless fluorite. Fluorite occurs as large, euhedral cubic crystals in the larger veins and vugs, and as anhedral groups of interlocking crystals in the smaller veins. Minor amounts of quartz can also be found in the veins and vugs along with small quantities of barite, hematite, galena, pyrite and chalcopyrite.

Surrounding the ring complex are a number of plug-like intrusions which are expressed as topographic highs. The plugs vary in diameter from 200m to 1.5 km, and are hosted by Bagh sandstones and limestones, and Deccan volcanics. These intrusive rocks are of two types; nepheline syenites and phonolitic syenites (Viladkar, 1984). They are generally brown to dark green in

Figure 2.4 A) An ankeritic carbonatite dyke intruding calcitite; B) Fenitized sandstone xenolith in calcitite. The xenolith shows complete replacement of quartz grains by K-feldspar.



color and consist of a fine-grained, glassy matrix with phenocrysts of nepheline, alkali feldspar, pyroxene and melanite garnet. Magnetite occurs as a minor phase in some samples. The rocks tend to be highly weathered, and are commonly pink to red in color.

Fenitization

A distinctive feature of the Amba Dongar complex is the occurrence of a well developed zone of fenitization in the sandstone surrounding the carbonatite. Xenoliths of nephelinite in the carbonatite also show the effects of fenitization, typically as intense phlogopitization of pyroxene. Fenitization of sandstones, associated with the carbonatites, was of two types, with some gradation between the two. The first, potassic fenitization, is evident at higher levels of the complex; whereas the second, sodic fenitization, is only recorded in deeper sections (Viladkar, 1986). Owing to the nature of the sandstone, almost pure quartz, fenitizing effects can be readily quantified. Potassic fenites are the most common of the altered rocks, occurring within the carbonatite and around its periphery. The amount of metasomatism is variable, with sandstone xenoliths within the carbonatite typically showing complete replacement of quartz by potassium feldspar (Fig. 2.4B) and fenite outside the ring containing as little as 5% potassium feldspar. Proximal sandstones may show up to 70% replacement of quartz and at distances of between 100 m to 150 m away from the ring, sandstones will contain only 5-10% feldspar. Further out they are essentially unaltered.

In outcrop, potassium-fenitized sandstone varies in color from white to light pink with various degrees of mottling depending on the extent of fenitization. Megascopically, quartz retains many of the characteristics of quartz in unaltered

samples, although there appears to have been some recrystallization. Within potassic fenites, feldspar consists of both lath-like orthoclase crystals and small irregular grains which appear to be pseudomorphs after quartz. The color of the feldspar ranges from white to pink.

Sodic metasomatized rocks are relatively uncommon in the complex except where they have been uncovered during mining operations. These rocks have been divided into two types: sodic fenites, consisting of albitized, aegirine-augite bearing rocks; and ultrasodic fenites, or albitites, which are composed only of albite (Viladkar, 1986). The precursor rocks in both cases are reported to be the Bagh sandstone (Viladkar, 1986). Albitites consist of a monomineralic groundmass of small anhedral to subhedral albite. Accessory minerals include rare aegirine-augite and relict quartz grains (Viladkar, 1986). Sodic fenites are the rarest of the metasomatized rocks, occurring in only one outcrop in the northwestern section of the complex (Viladkar, 1986). The rock is made up of over 50% albite with intergrown pale green aegirine-augite and small amounts of relict quartz grains (Viladkar, 1986).

**CHAPTER III:
JOURNAL MANUSCRIPT**

**Genesis of the Carbonatite-Hosted Fluorite Deposit
at Amba Dongar, India: Evidence from Fluid Inclusions,
Stable Isotopes and REE Geochemistry**

by

David A.S. Palmer and Anthony E. Williams-Jones

Department of Earth and Planetary Sciences

McGill University

Montreal, Quebec

Canada H3A 2A7

Abstract

Since their discovery, carbonatite-hosted fluorite deposits have received very little attention with respect to their genesis. The Amba Dongar carbonatite complex, India, hosts one such deposit, consisting of 11.6 mt of 30% CaF_2 . The complex comprises a carbonatite ring dyke, which hosts the fluorite, and a number of syenitic intrusions which were emplaced into Late Cretaceous Bagh sandstones and Late to Early Eocene Deccan volcanics.

Hydrothermal activity associated with the intrusion was responsible for fenitization of the surrounding sandstones, and later silicification of calcite and the deposition of economic quantities of fluorite. Fluorite mineralization occurs as veins and vug fillings, localized along fractures, near its contact with the sandstone.

Chemical analyses and mass balance calculations show that the fluids responsible for silicification removed large quantities of Ca from the rock while adding similarly large quantities of Si, and lesser amounts of Al and F. Alteration associated with fluorite deposition involved the removal of Al from the rock and the addition of large quantities of F and Si.

Fluid inclusions in fluorite point to a low temperature-low salinity (<160°C-0.6 to 0.3 wt.% NaCl eq.) ore fluid, which decreased in temperature and salinity with evolution. Crushing experiments performed on fluid inclusions in both fluorite and quartz reveal the presence of ≈ 0.08 m of dissolved CO_2 in solution while analyses of leachates and decrepitate residues from fluid inclusions show significant concentrations of Ca, Al, Na, Cl and S. Oxygen, hydrogen and carbon isotopic data from the fluids in fluid inclusions suggest that the dominant component of the ore fluid was meteoric, and that it had equilibrated with sedimentary carbonates. Log $f\text{O}_2$ and pH conditions of the fluid, at the time of ore formation, are interpreted to have been >-42 and <3.5 , respectively. The presence of Al and S in the fluid, the molar equivalence of Na and Cl, and the positive deviation of $\delta^{18}\text{O}$ and δD from the meteoric water line point to a small contribution from orthomagmatic fluids.

A model is proposed in which the intrusion of a carbonatite magma at high crustal levels caused faulting and fracturing of the surrounding country rocks, and was accompanied by the release of orthomagmatic fluids, expressed as extensive K and Na metasomatism of the surrounding sandstones. With the decline of orthomagmatic activity, a meteoric water-dominated hydrothermal system was initiated by the heat of the intrusion. The interaction of Ca-bearing meteoric fluids with the last vestiges of F-bearing orthomagmatic NaCl brines caused deposition of vast quantities of fluorite at the site of mixing.

Introduction

Fluorite is commonly found in carbonatites. It exists as a liquidus phase in late stage carbonatite melts and also within hydrothermal assemblages hosted by the carbonatite bodies (Kuellmer *et al.*, 1966; Flegg *et al.*, 1977; Le Bas, 1989; Woolley and Kemp, 1989; Wyllie, 1989; Viladkar and Wimmenauer, 1992). However, economic fluorite deposits associated with carbonatites make up a very small proportion of the overall number of exploitable fluorite deposits. There are approximately 330 recognized carbonatites throughout the world (Woolley, 1989) and, of these, only seven contain economic deposits of fluorite (Table 3.1). All but two of the deposits are considered to be hydrothermal in origin (Mariano, 1989). The latter, associated with the Bol'shaya Tagna carbonatite, Eastern Sayan and with the carbonatites of the Tuva Basin, are considered to have formed by direct crystallization of fluorite from a carbonatite melt (Puzanov, 1975, 1977). On the basis of radiogenic isotopes, REE chemistry, limited fluid inclusion data and geological setting, hydrothermal fluorite deposits are considered to be derived primarily from orthomagmatic fluids exsolved from the carbonatite (Deans and Powell 1968; Deans *et al.*, 1973; Puzanov, 1975; Bredikhina and Bobrov, 1993; Ronchi *et al.*, 1993). However, the conditions under which these deposits form has been poorly documented, and there has been no comprehensive study of their genesis.

The Amba Dongar carbonatite ring complex, India contains dilatant veins and replacement bodies of fluorite with reserves of 11,600,00 tons of 30% CaF_2 , and is thus an ideal example around which to develop a model for the genesis of hydrothermal carbonatite-hosted fluorite deposits. The complex has been studied by a number of researchers (Sukheswala and Udas, 1963; Deans and

Table 3.1 Carbonatite-hosted fluorite deposits.

Locality	Mineralization	Reference
Amba Dongar, India	Hydrothermal dilatant veins and replacement bodies in carbonatite, 11.6 mt of 30 wt.% fluorite	Deans et al (1972)
Okorusu, Namibia	Hydrothermal veins in carbonatite and replacement bodies in limestone in contact with the complex, 7-10 mt 35 wt.% fluorite	Deans et al. (1972)
Mato Preto, Brazil	Hydrothermal veins and replacement bodies at the contact between calcitite and phonolite dykes, 2.6 mt of 60 wt % fluorite	Ronchi et al (1993)
Tchivira, Angola	Hydrothermal bodies at the contact between carbonatite and ijolite	Mariano (1989)
Karasugskiy, Tuva	Primary magmatic fluorite	Puzanov (1977)
Choakhol'skiy, Tuva	Primary magmatic fluorite	Puzanov (1977)
Bol'shaya Tagna, Eastern Sayan	Early magmatic precipitation of fluorite followed by late, hydrothermal vein-deposition	Puzanov (1977)

Powell, 1968; Deans *et al.*, 1972; Roedder, 1973; Lahiry, 1976; Viladkar, 1981; Kaul *et al.*, 1988; Srivastava, 1989; Gwalani *et al.*, 1993, Simonetti and Bell, 1993). The study by Roedder (1973) provided microthermometric data for fluid inclusions, in several samples of fluorite. These data show that the fluorite formed at low temperatures (115-160°C) from low salinity fluids. Limited fluid inclusion homogenization temperatures are also reported in Lahiry (1976) and Kaul *et al.* (1988). However, the nature of the late stage hydrothermal processes responsible for silicification and fluorite deposition is still debated. Based on $^{87}\text{Sr}/^{86}\text{Sr}$ data presented by Deans and Powell (1968), which gave values that were not consistent with an origin of fluorite from the carbonatite, Deans *et al.* (1972) proposed that fluorite deposition was a result of mixing of meteoric water from the sandstones and residual hydrothermal fluids from the carbonatite. Lahiry (1976), using the same data, postulated that the fluorite was deposited when Ca-bearing meteoric fluids from the sandstone mixed with fluorine-bearing orthomagmatic fluids exsolved from the Deccan basalt magma.

As stated above, relatively little is known about carbonatite-hosted fluorite deposits. To the authors' knowledge no comprehensive research has been undertaken, until now, on the genesis of these deposits. In this paper we make use of fluid inclusion data, stable isotope geochemistry, and whole-rock and mineral geochemistry to characterize the fluids responsible for fluorite deposition at Amba Dongar and to determine the source of this mineralization. The information gained from these studies is used to develop a model for the genesis of carbonatite-hosted fluorite deposits.

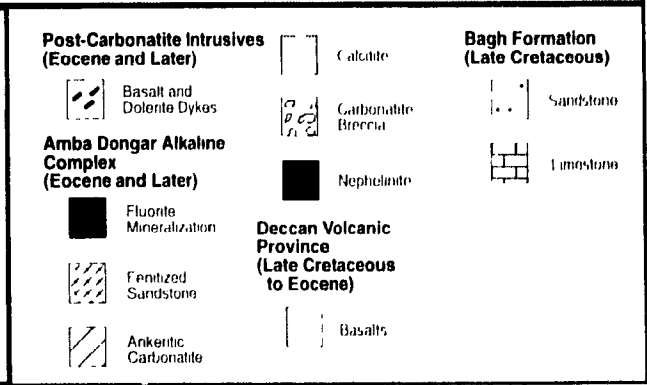
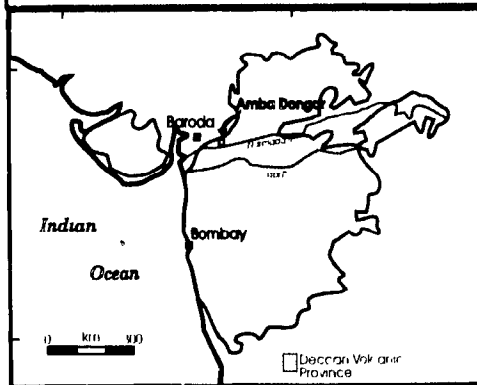
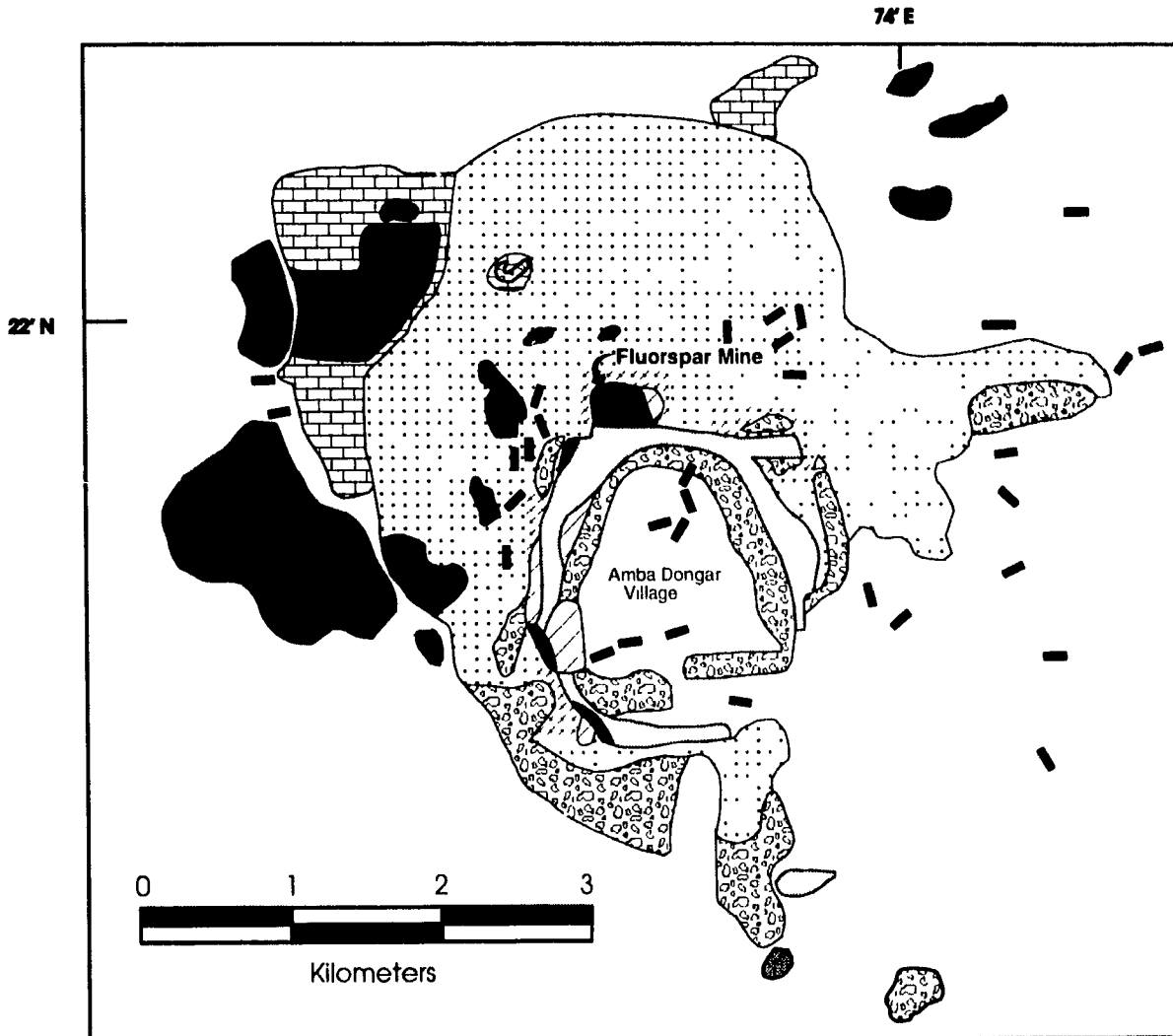
Regional Geology

The Amba Dongar complex is located approximately 400 km northeast of Bombay, India in the Baroda District of Gujarat State, and consists of subvolcanic intrusions composed of carbonatites and associated syenites (Fig. 3.1). It was emplaced into tholeiitic and alkaline plateau flood basalts of the Deccan Volcanic Province. The complex is situated adjacent to the ENE trending Naramada Rift, which formed along an ancient plane of crustal weakness, reactivated as India passed over a mantle plume during the Early Paleocene (65 Ma). Carbonatite activity occurred following extrusion of the flood basalts, and prior to intrusion of numerous doleritic and picritic dykes (Gwalani *et al.*, 1993; Srivastava, 1989; Sukheswala *et al.*, 1976; Viladkar, 1981)

The Amba Dongar area belongs to the Chota Udaipur sub-province (Gwalani *et al.*, 1993), which is characterized by numerous alkaline intrusions and the presence of the only feldspar-free rocks in the region. Structure in the area was controlled by the Naramada Rift and a sympathetic fault system to the north, and is expressed as numerous mafic dike swarms, oriented parallel to the rift, and NE trending strike-slip faults (Viladkar, 1981; Srivastava, 1989).

Country rocks surrounding the complex consist of flood basalts to the south of the complex and quartzitic sandstones (orthoquartzites) and limestones of the Late Cretaceous Bagh Formation to the west, north and east (Fig. 3.1). The sandstone is fine- to coarse-grained and consists of greater than 96% quartz. Limestone is typically fine-grained with variable amounts of sand grains, and ranges from pure limestone to marl. The core of the Amba Dongar intrusion is composed of basalt which Deans and Powell (1968) consider to be a syn-emplacment collapse structure of the overlying Deccan basalts. Viladkar

Figure 3.1 The geology of the Amba Dongar carbonatite complex (modified from Deans *et al.*, 1972; Karkare and Srivistava, 1990).



(1981), however, ascribed the core to post-emplacement basaltic activity. The area is underlain by Precambrian granitic gneisses of the Dharwar Formation (Srivastava, 1989). Within the surrounding sandstones and limestones are numerous plugs of nephelinite and phonolitic nephelinite, interpreted to be genetically related to the carbonatite (Viladkar, 1981).

Carbonatite Geology

The Amba Dongar complex consists of a carbonatite ring dyke, with a diameter of approximately two kilometers, and a number of syenite intrusions which are randomly distributed around the ring (Fig. 3.1). The bulk of the ring structure is composed of calcitite which is also responsible for the topographic expression of the structure. Calcitite consists of a fine- to coarse-grained matrix of interlocking calcite crystals with a locally developed porphyritic texture. The accessory minerals consist of, in decreasing order of importance, martite, apatite, pyrochlore, fluorite, phlogopite, barite and galena, and comprise between 1 and 30% of the rock's volume (Viladkar, 1981; Srivastava, 1989, Viladkar and Wimmenauer, 1992). Flow banding, delineated by concentrations of accessory minerals or grain size variations, is common and is generally subvertical and subparallel to the ring.

Lining the interior edge of the calcitite is a ring of carbonatite breccia. This unit consists dominantly of angular to rounded fragments of calcitite, plus fragments of metamorphic rocks, sandstone and basalt set in a matrix composed of fine-grained calcite crystals. Differential weathering has roughened the surface as a result of the recession of calcitite fragments relative to the matrix.

Ankeritic carbonatite occurs as small, rounded, irregularly shaped plugs

on both borders of, and in one case cutting, the calcitite. It is generally dark red in color and typically fine-grained. Accessory minerals are varied and abundant in this unit, locally making up over 50% of the rock. These phases consist predominantly of martite with minor apatite, bastnaesite, pyrochlore, monazite, thorite, pyrite, galena and chalcopyrite (Viladkar, 1986).

A general chronology for intrusion of the ring has been developed by Deans *et al.* (1972) and Viladkar (1981). According to these authors, emplacement began with a fluidization event which caused ring fractures in the country rock, along which the breccia formed. This was followed by intrusion of the calcitite and then the ankeritic carbonatite. Following carbonatite emplacement, hydrothermal fluids were responsible for formation of quartz vein systems and silicification of large parts of the calcitite ring. Large fluorite deposits of hydrothermal origin were also deposited in the calcitite

Numerous plugs of nephelinitic and phonolitic syenite, varying in diameter from 200 meters to 1.5 km, were intruded contemporaneously with the carbonatite into the surrounding Bagh sandstone and limestone, and in the Deccan basalt. They are brown to dark green rocks with a fine-grained glassy matrix and numerous phenocrysts of nepheline, alkali feldspar, pyroxene and melanite garnet.

Fenitization

Immediately adjacent to the ring is an discontinuous zone of potassic fenite, up to 150m wide, in which quartz of the Bagh sandstone has been variably replaced by potassium feldspar (Fig. 3.1). This fenitization is also evident in xenoliths of sandstone in the calcitite which now consist almost

entirely of K-feldspar, and nephelinite xenoliths in which pyroxene has been replaced by phlogopite. Rare sodic fenites have been exposed by mining operations in the northern section of the ring. These fenites comprise albite-aegirine-augite-bearing rocks or rocks composed only of albite (albite).

Mineralization

Mode of Occurrence of Fluorite

Although fluorite can be found as an accessory mineral within all carbonatite lithologies, economic quantities only occur within the calcitite. These deposits are situated along the contact of the host rock and the Bagh orthoquartzites, and are commonly found near ankertic carbonatite plugs. The main ore zone contains reserves of 11,600,000 tonnes of ore grading 30% CaF_2 , mostly as vug fillings, and is located within the calcitite near its contact with the fenites in the north (Fig. 3.1). Veins of fluorite, as well as larger fluorite zones, fill concentric fractures and dip from steep northerly to vertical. Host rocks surrounding fluorite occurrences are pervasively silicified, but silicification is generally limited to 10 cm from the vein-wallrock contact (Fig. 3.2A). Unmineralized quartz vein systems also occur within the calcitite, and are accompanied by pervasive silicification of the host (Fig. 3.2B).

Fluorite veins are typically thin (1 cm to 20 cm wide) structures which can occur discretely or in networks of randomly oriented, irregular veins. However, some veins may reach widths of up to 50 cm. Fluorite also fills vugs in large

Figure 3.2 A) A fluorite vein surrounded by a halo of silicified calcitite (dark);
B) Silicified calcitite breccia cemented by fine-grained quartz.



lenticular zones within the calcitite, ranging in length from centimeters to 2 meters (Fig 3.3A, B). They are generally oblong in shape. Contacts between wallrock and fluorite are typically irregular. Fragments of wall-rock occur in fluorite as small rounded grains or long thin slivers which have not been transported for any distance. Silicification in the surrounding calcitite consists of fine-grained quartz which, in turn, has been partially replaced by fluorite. Proximal to the veins, quartz-fluorite alteration is uneven in distribution, imparting a patchy appearance. At distances greater than approximately three centimeters from vein-wallrock contacts, alteration consists almost entirely of silicification.

The planar morphology of fluorite veins and their sharp wallrock contacts suggests that silicification and dilation preceded deposition. Vug fillings of fluorite, however, show concave, irregular wall rock boundaries as well as more irregular silicification, suggesting simple replacement of the carbonatite.

Within both vein- and replacement-type bodies, fluorite occurs as massive anhedral to euhedral crystals making up to 95% of the vein or vug material. Euhedral crystals of fluorite are common in both types of mineralization, and can grow up to 30 cm in diameter, although most crystals are between 1 and 5 cm in diameter (Fig 3.3A, B).

One of the most distinctive features of the Amba Dongar fluorite is its color zonation. Fluorite occurs in blue, purple, white, yellow and colorless varieties. From field relationships the crystallization order was determined to have been blue and purple fluorite, which are commonly interlayered, followed by the white and finally the yellow and colorless varieties (Fig. 3.4A, B). The latter two fluorite types are the most commonly encountered followed closely by the blue variety. Purple fluorite is relatively uncommon and white fluorite appears to

Figure 3.3 A) large yellow fluorite crystals coating vug wall; B) fine-grained purple fluorite crystals lining vug.

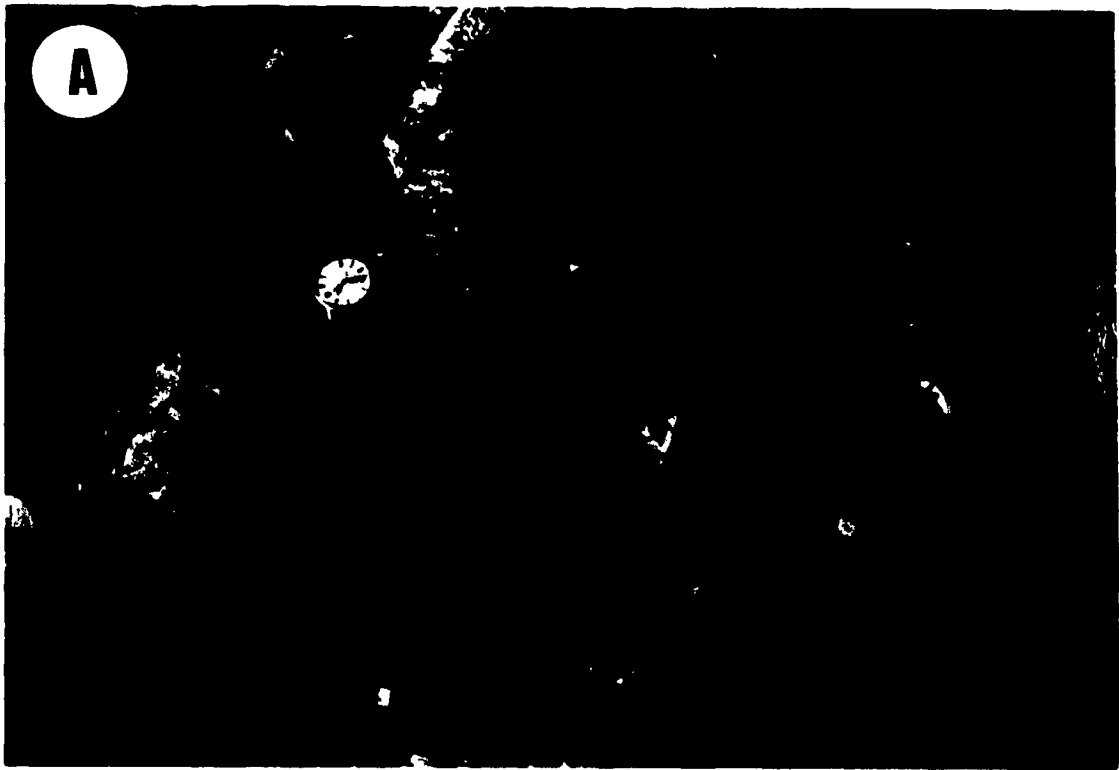
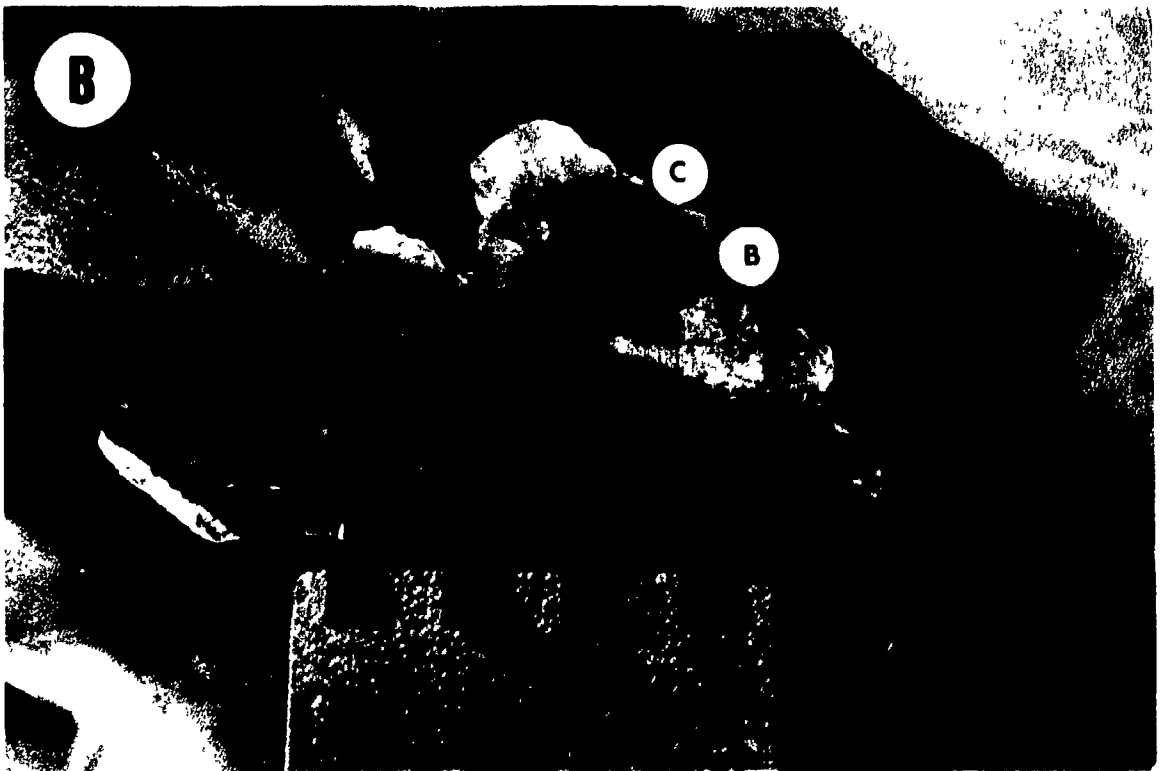
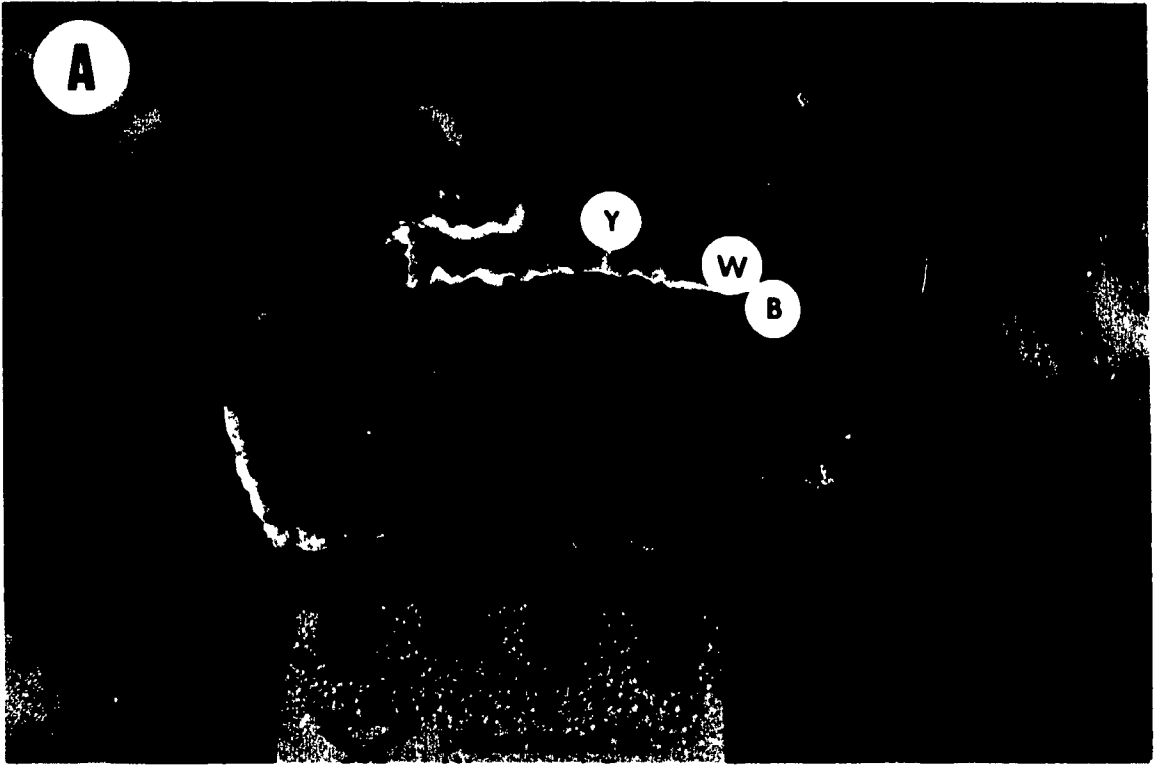


Figure 3.4 A) A hand specimen of a vug showing early blue fluorite (B), against the wall, overgrown by later white fluorite (W), which in turn is overgrown by yellow fluorite (Y).; B) A hand specimen of a vug showing early blue fluorite (B), lining the wall, overgrown by colorless fluorite (C). The white fluorite layer is absent



be a rare, localized occurrence. All fluorite, with the exception of the white variety, is extremely clear with few solid inclusions; white fluorite is opaque. In addition to the initial silicification of the host rock, fluorite mineralization at Amba Dongar shows an intimate association with quartz. Within fluorite veins, quartz occurs as inclusions within fluorite or as separate layers making up between 5 to 40% of the vein material. Quartz also occurs as fine-grained encrustations that post-dated fluorite deposition (Fig. 3.5A)

Minor quantities of barite, hematite and galena were observed as inclusions in both quartz and fluorite in a very small number of samples. The distribution of these phases is not homogeneous, with barite found most commonly in purple fluorite (Fig. 3.5B) and hematite in yellow fluorite. A kaolinite group mineral was identified, based on SEM analyses and Analytical Electron Microanalysis (AEM), in white fluorite (Fig 3.6A, B). Pyrite and chalcopyrite have also been reported to occur in the deposit (Deans and Powell, 1968; Deans *et al.*, 1972; Viladkar and Wimmenauer, 1992; Srivastava and Karkare, 1989). Sulfide minerals typically occur as open space growths on the surface of fluorite. More rarely, they are found as inclusions in both fluorite and quartz.

Petrographic Characteristics

The parageneses of the fluorite bodies are readily evident in thin section. Silicification of the host rocks occurred first as replacement of calcitite by quartz. Following replacement of calcitite, quartz was deposited along vein and vug walls. Quartz grains lining vein/vug walls are typically small (100-200 μ m in diameter), subhedral to euhedral crystals that grow perpendicular to wallrock contacts. Within the first quartz layer, local aggregations of acicular hematite crystals can be found which penetrate the succeeding fluorite layer.

Figure 3.5 A) Quartz encrusted yellow fluorite cubes. The ring in the picture is approximately 1.5 cm in diameter.; B) An SEM microphotograph of a fluorite vein showing growth, from left to right, of barite (Ba), purple fluorite (Fl) and quartz (Q) with disseminated barite. The quartz, fluorite and disseminated barite to the left of the barite layer is altered wall-rock (W)

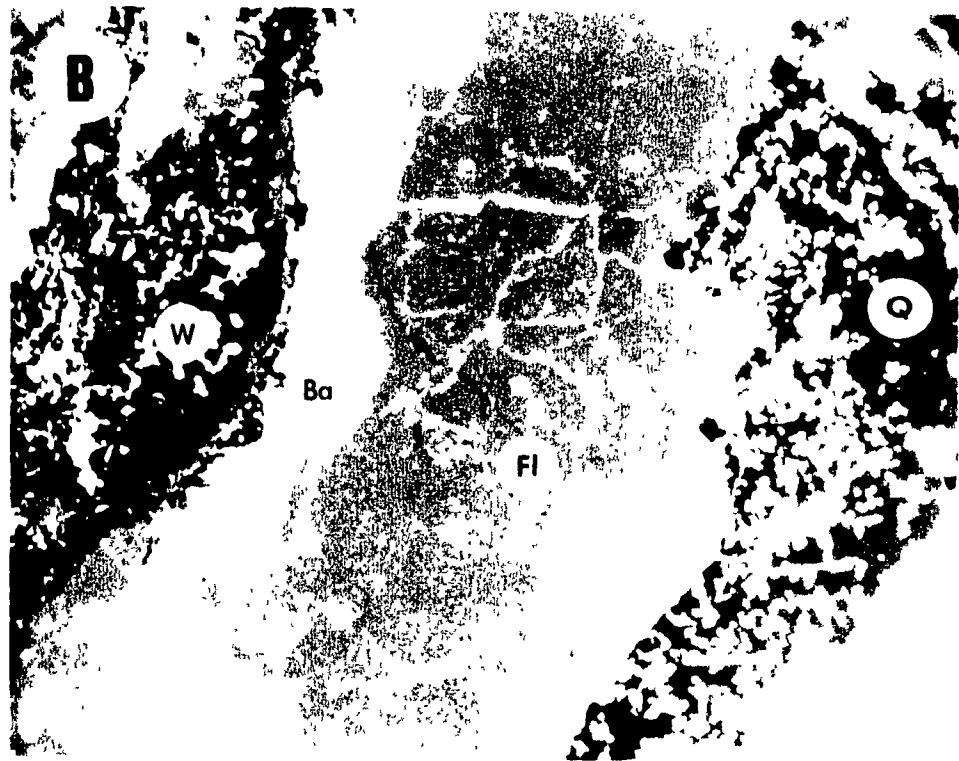
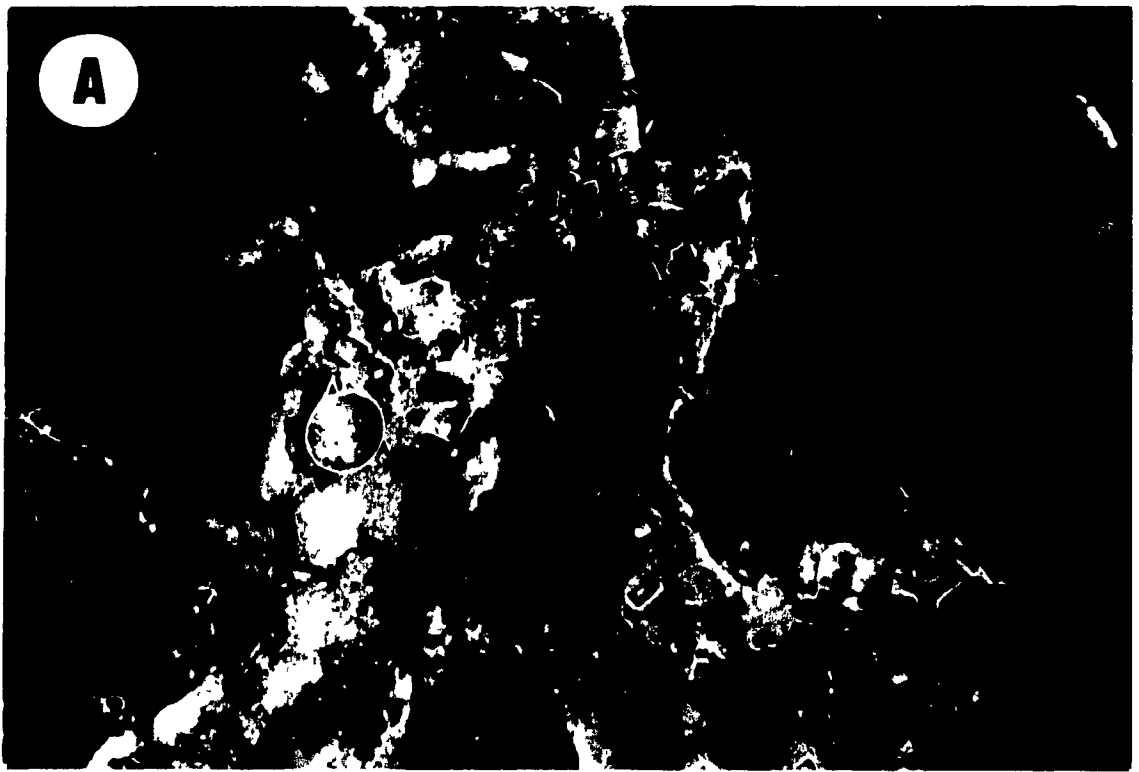
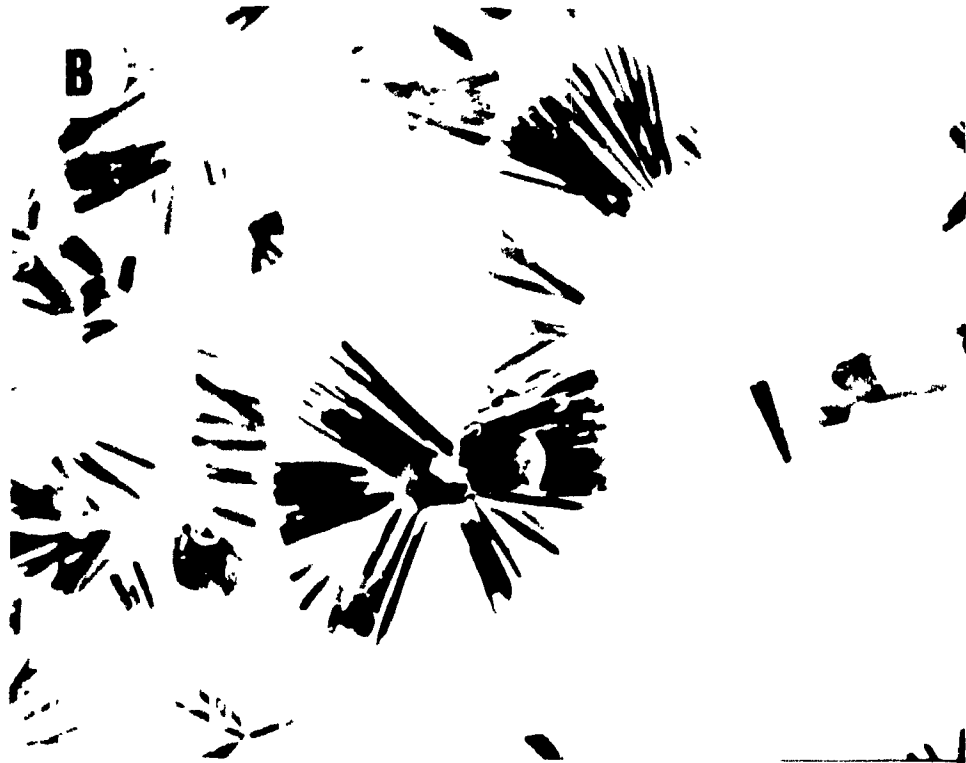


Figure 3.6 A) A photomicrograph, taken using plane polarized light, showing crystals of an alumino-silicate mineral at the edge of the white fluorite layer. This phase is probably one of the kaolinite group minerals (i.e. kaolinite, dickite); B) An SEM photomicrograph of the alumino-silicate mineral in the white fluorite layer, showing the radiating, accordion-like habit of the mineral.

A



B



Crystals are between 100 and 500 μm in length and 20-60 μm in width. They are commonly missing, leaving only an outline of their shape in the fluorite. The presence of this cast in fluorite suggests that their removal was a later event occurring after fluorite deposition. Fluorite is the next phase to occur. It is generally of massive, homogeneous morphology, consisting of a matrix of anhedral to subhedral interlocking crystals. The fluorite layers are typically monomineralic, although they may contain inclusions of quartz. The accessory quartz occurs either as intergrowths, doubly terminated crystals, or small euhedral, singly terminated prisms, which were probably removed from vein walls by the fluorine-bearing fluids. This first fluorite layer can be of any color, depending on which generation of fluid has invaded (Fig. 3.3 A, B, 3.4A). If multiple generations of fluorite are present, which is generally not the case, an intermediate white, solid inclusion-filled fluorite may be present separating the earlier blue or purple fluorite from the yellow and colorless varieties (Fig. 3.4A). The white fluorite layer is generally less than 1 cm in thickness and outlines the euhedral nature of the earlier crystals. This variety of fluorite contains a large proportion of small (<10 μm), accordion-shaped crystals with an aluminosilicate composition (Fig. 3.6B). Small subhedral to euhedral quartz grains are also present in the white fluorite, but in relatively small numbers. Following the white fluorite are layers of colorless and yellow fluorite, similar in morphology to the first formed fluorite layer. The final stage of vein/vug filling, which only occurred locally, consisted of encrustations of fine-grained quartz on fluorite surfaces (Fig. 3.5A).

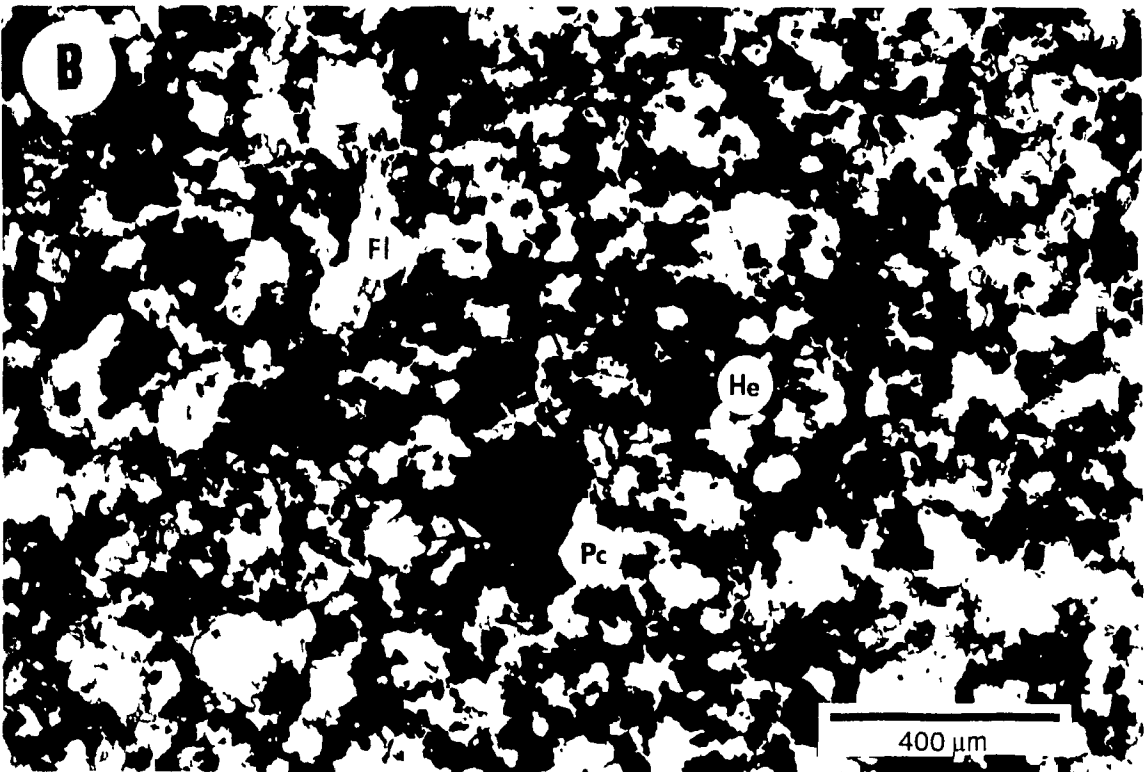
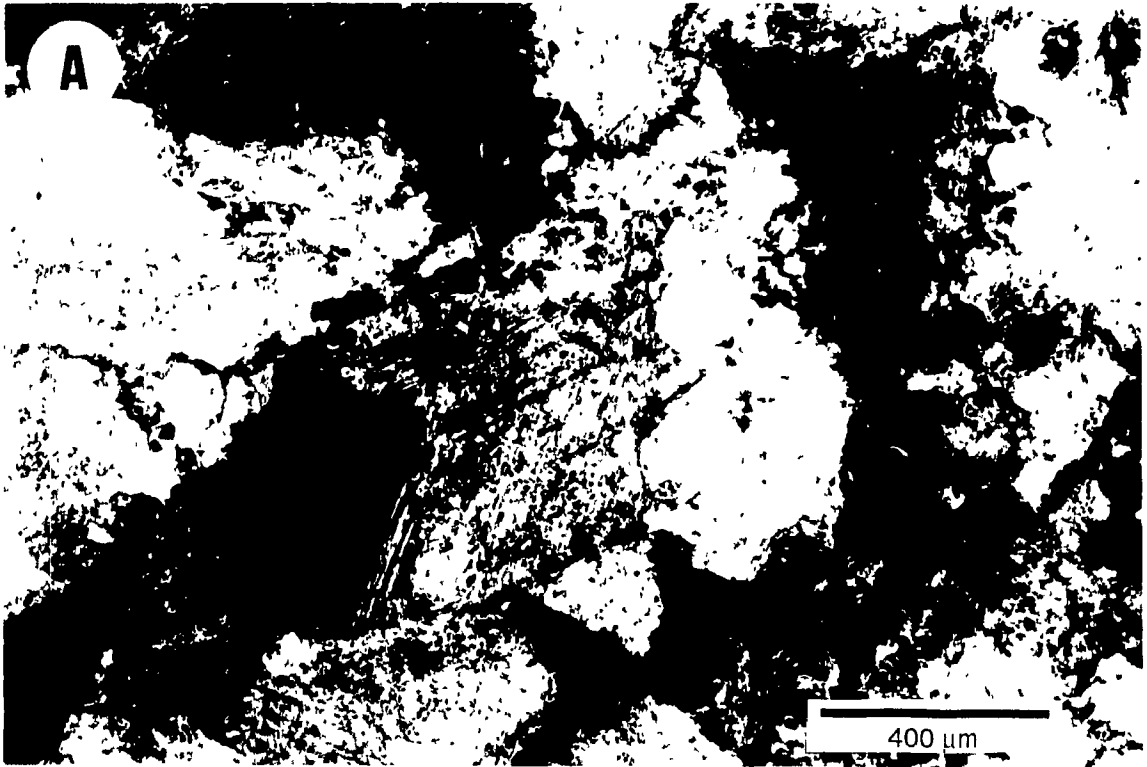
Barren Vein Systems

The calcitites of Amba Dongar contain a number of zones of intense silicification associated with quartz veining. Quartz veins are surrounded by extensive silicification, covering areas of 10's to 100's of meters. The veins occur as separate, irregular veins or in large networks, commonly accompanied by brecciation of the host rock (Fig. 3.2B). On an outcrop scale, alteration forms large irregular zones which are parallel to the vein systems. The veins themselves are completely surrounded by silicification and, due to the intensity of alteration, haloes surrounding particular veins cannot be distinguished. The veins consist of massive anhedral quartz or euhedral, open space-filled quartz crystals. Vein-width is typically less than 5 centimeters. The orientation of quartz veins is variable, but is most commonly concentric with the ring structure, with dips being either vertical or steep northerly. Less commonly, zones of silicification are oriented radially to the ring structure, parallel to fault valleys. Fluorite occurs as an accessory mineral in most veins, either within the vein material or on the surface of quartz crystals, as open space terminations. Iron oxides are also present along grain boundaries.

Alteration Associated with Quartz Veining

In hand sample, silicified calcitite retains many of the textures and characteristics of the unaltered rock. Differences between the two include a more glassy appearance of the silicified rock and the presence of small (1-3 mm diameter) isolated pore spaces. In thin section, the difference between the altered and unaltered rock is more apparent. The matrix of interlocking carbonate grains, as well as accessory minerals, in the calcitite (Fig 3.7A) have

Figure 3.7 A) A photomicrograph, in plane polarized light, of unaltered calcite showing matrix composed of interlocking calcite grains. Photograph taken using plane polarized light; B) A photomicrograph of altered calcite immediately adjacent a fluorite vein. Quartz is now almost completely replaced by fluorite (Fl) and hematite (He). Further away from vein, quartz becomes the dominant alteration mineral. Crystal in the lower-center of the picture is euhedral pyrochlore. Photograph was taken using plane polarized light.



been completely replaced by finer-grained anhedral quartz (Fig. 3.8A). Small fluorite grains (< 0.5 mm), of indeterminate color, occur with quartz, modally making up to 5 % of the rock,. Hematitic staining, as well as small rhombic to rectangular iron oxides, are found along grain boundaries.

Fluorite Chemistry

Mineral separates of fluorite from samples representing all color zones were hand picked and analyzed for major elements by ICP, trace elements by ICP and neutron activation, and rare earth elements (REE) by neutron activation (Table 3.2). Figure 3.9 shows profiles of selected major and trace elements plotted against the color of fluorite. Barium, SiO_2 and Fe_2O_3 have their highest contents in purple fluorite, and progressively lower contents in the blue, yellow and colorless fluorite. The behavior of SiO_2 is consistent with the occurrence of thin quartz layers in purple fluorite, numerous quartz inclusions in blue fluorite, and rare quartz inclusions in late yellow and colorless fluorite. Ba contents are likewise consistent with the occurrence of abundant inclusions of barite in the purple fluorite, rare inclusions in blue fluorite and the absence of barite in late yellow and colorless fluorite. In contrast to Ba, SiO_2 and Fe_2O_3 , Ca is most depleted in purple fluorite and increases in content from blue to yellow varieties, i.e. as the proportion of solid inclusions decreases. Both Sr and Sc also show a significant enrichment in the later yellow and colorless varieties of fluorite. Zr, Y, K_2O and P_2O_5 show no zonation from the earlier blue and purple fluorite to the later yellow and colorless varieties.

The total REE content of all of the samples is low, and chondrite-normalized plots of REE show a slight positive slope with a "well" at Nd and Sm

Figure 3.8 A) photomicrograph of calcitite, which hosts barren quartz veins, that has been completely replaced by fine-grained quartz and minor fluorite. Photograph taken using cross polarized light; B) the same view in plane polarized light showing relationship between quartz (Q), hematite (He) and fluorite (Fl).

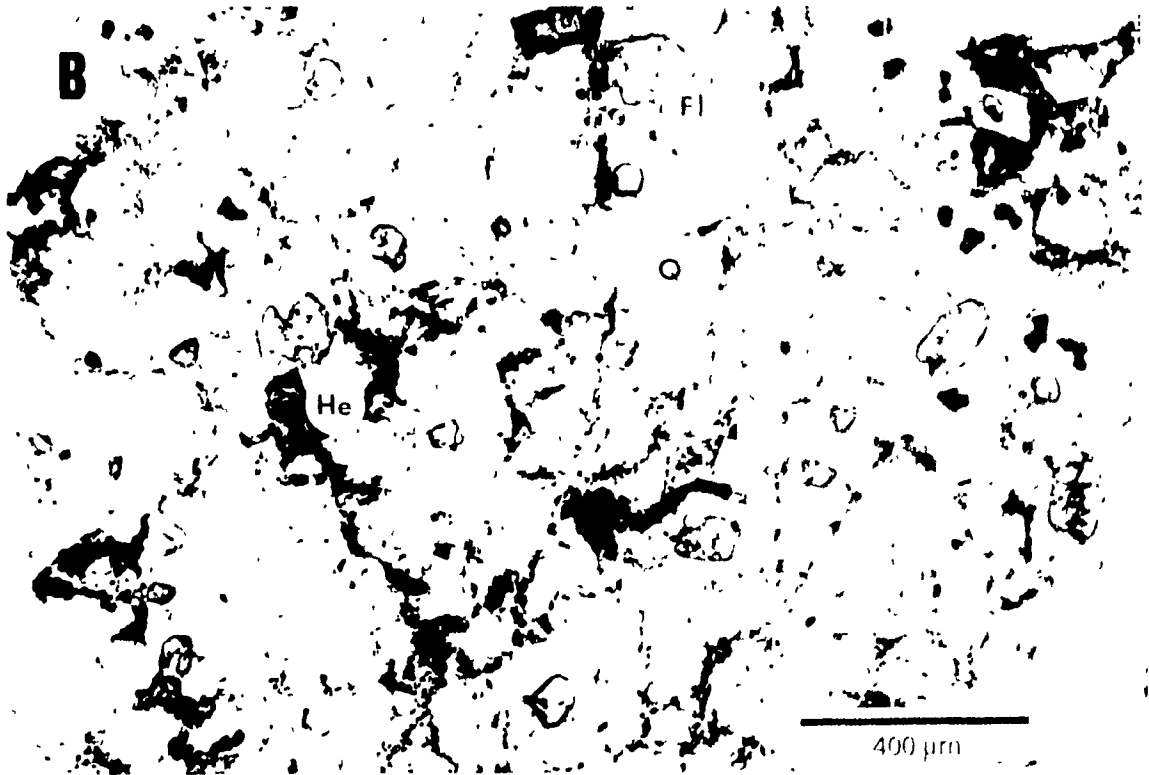
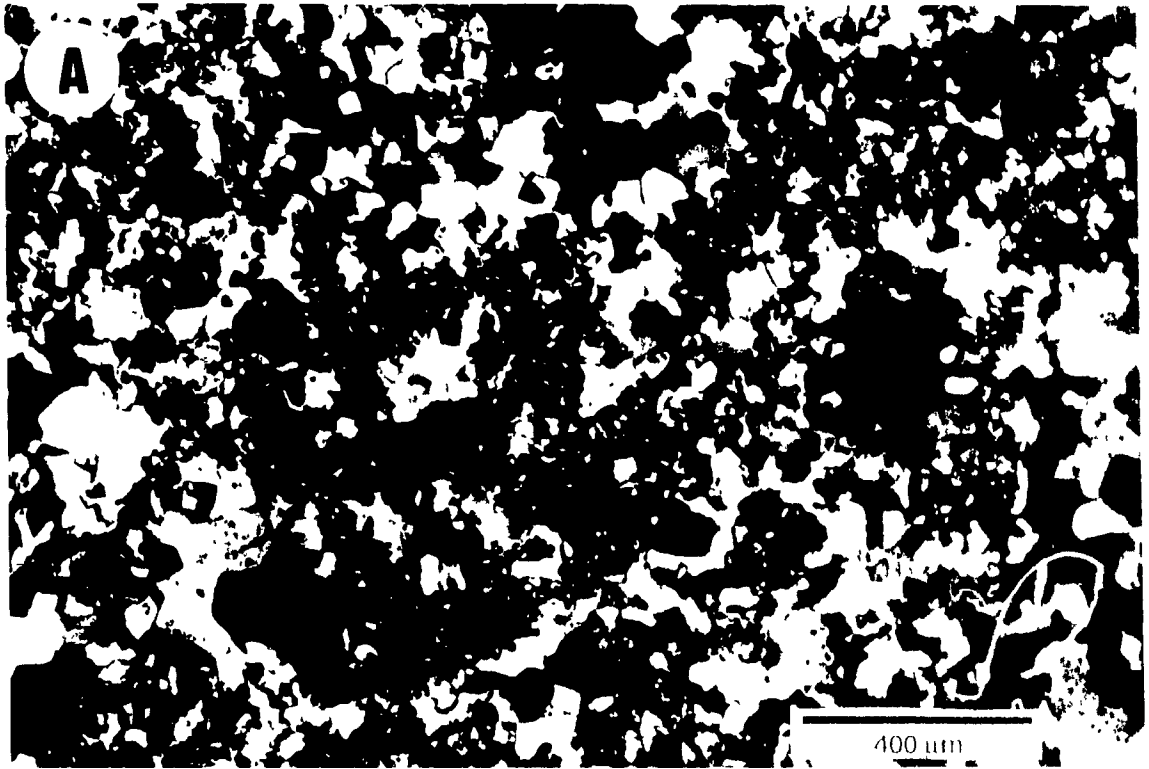


Table 3 2 Chemical analyses of fluorite mineral separates

Sample	AD066Z	AD050B	AD066XB	AD066W	AD008A	AD066XY	AD050C
	Blue	Blue	Blue	Purple	Yellow	Yellow	Colorless
	wt. %						
SiO ₂	0.77	1.4	1.88	4.68	0.26	0.82	0.26
Al ₂ O ₃	ND	ND	ND	ND	ND	ND	ND
Fe ₂ O ₃	0.07	0.05	0.06	0.1	ND	ND	0.05
MgO	0.03	ND	ND	0.03	ND	0.03	ND
CaO	93.5	92.85	92.2	87.7	94.05	93.15	93.89
Na ₂ O	ND	ND	ND	ND	ND	ND	ND
K ₂ O	0.18	0.12	0.07	ND	0.08	0.12	ND
P ₂ O ₅	0.03	0.02	ND	0.02	0.02	0.03	ND
MnO	ND	ND	ND	ND	ND	ND	ND
	ppm						
Ba	151	998	88	3339	12	11	11
Sr	423	256	357	215	2004	1616	937
Zr	22	138	10	104	10	32	13
Y	148	90	151	78	74	59	185
Sc	0.6	0.1	0.3	0.2	1.1	0.9	1.5
La	7	5	9	12	6	3	5
Ce	25	17	27	33	27	13	22
Nd	9	9	11	11	8	5	9
Sm	3.3	2.2	2.7	2.5	3.3	1.3	3.7
Eu	2.2	1.4	1.8	1.3	1.8	0.8	2.7
Tb	2.2	1.1	1.9	0.9	1.7	0.9	2.8
Yb	7.9	3.5	8.2	3	12.7	8.8	11.9
Lu	1.04	0.46	0.95	0.4	1.99	1.3	1.66

ND Not Detected

All oxides analysed by ICP methods (analyses performed by Acme Labs, Vancouver)

Trace elements and REE analysed by Neutron Activation (Activation Labs, Ontario)

Figure 3.9 Profiles showing abundances of selected major and trace elements in fluorite versus fluorite color. Units are in weight percent for Ca, Sc, SiO₂ and Fe₂O₃, and in ppm for the remaining elements.

Figure 3.10 Chondrite-normalized rare earth element abundances in fluorite. Chondrite values were taken from Boynton, 1983. Profiles show a slight positive slope with a distinct "well" between Nd and Sm.

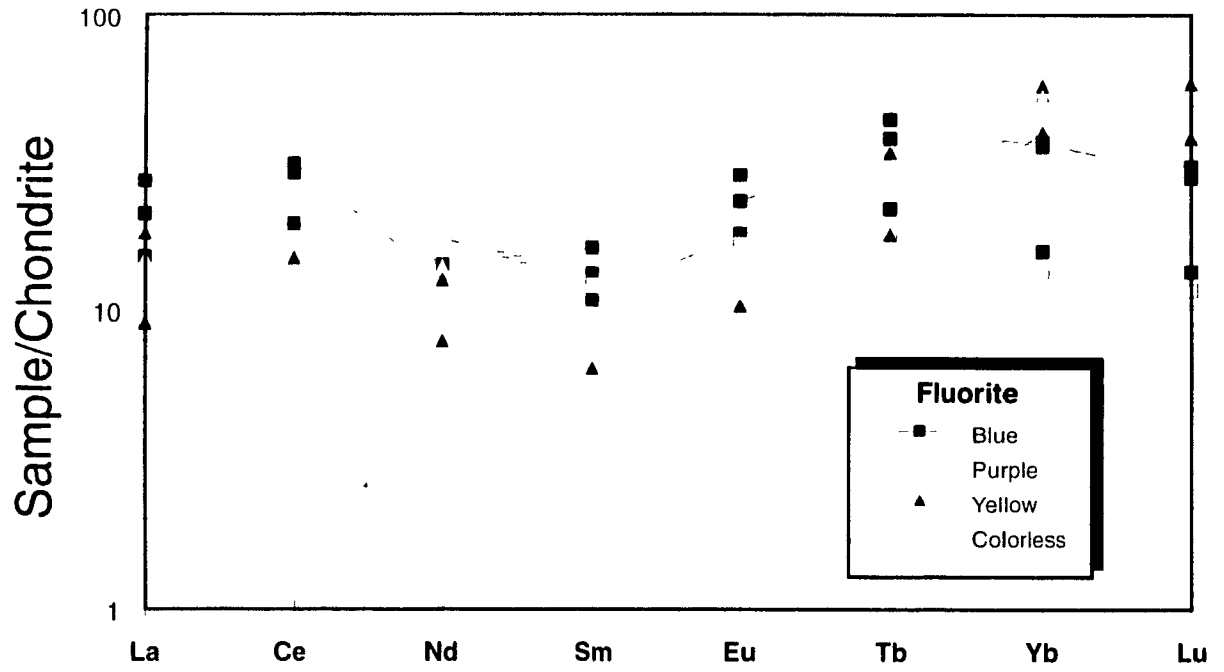


(Fig. 3.10). Late fluorite can be distinguished from early fluorite by the greater depth and breadth of these wells and by the maximum at Tb for early fluorite and Yb for late fluorite. Moreover, when compared on the basis of Lu/La, it is evident that blue and purple fluorite are enriched in LREE with respect to the late fluorite and depleted in HREE (Fig. 3.11). The negative Eu anomaly commonly reported for fluorite (Ganzeyev and Sotskov, 1976; Ekambaram *et al.*, 1986; Collins and Strong, 1992; Ronchi *et al.*, 1993) is absent.

Chemical Changes During Alteration

Three samples of unaltered calcitite and its silicified counterpart were analyzed for major and trace elements by XRF and for REE by neutron activation (Table 3.3). Sample AD 008b consists of silicified calcitite surrounding a fluorite vein and samples AD052b and AD026b are silicified calcitite associated with barren quartz veins. Samples AD008a, AD053a and AD026a are the respective precursors.

Owing to the nature of the alteration, SiO_2 increases dramatically in all altered samples. Total Fe as Fe_2O_3 , as well as Th, behave similarly to SiO_2 , increasing in all of the altered samples, although to a lesser extent than SiO_2 . The increase in iron is expressed by the increase in iron oxides in the altered samples. In contrast, MgO decreases considerably in the altered equivalents, possibly due to the dissolution of small amounts of dolomite, which have been reported in calcitite (Viladkar and Wimmenauer, 1992). Differences between the silica-fluorite and barren quartz vein associated alteration can be seen in a number of elements. Aluminum content increases considerably in silicified samples AD053b and AD026b, but decreases in the silica-fluorite altered rock.

Figure 3.11 A graph of Lu/La versus fluorite color showing the enrichment of LREE in early blue and purple fluorite relative to later yellow and colorless varieties.

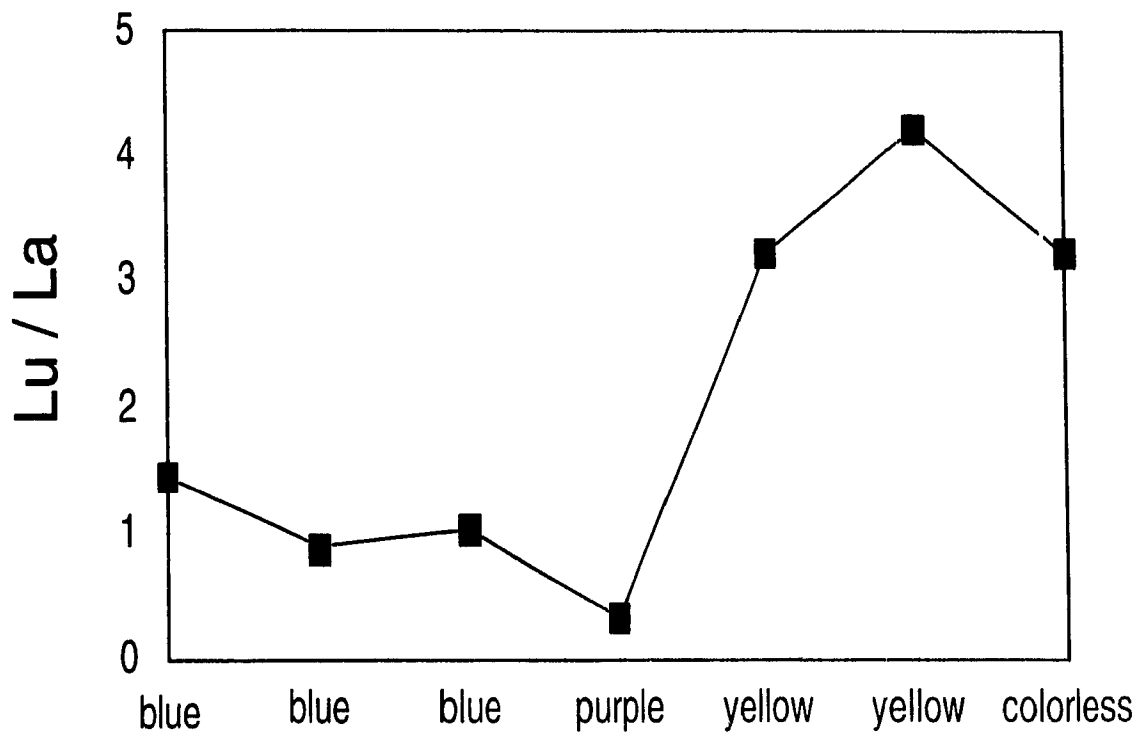


Table 3.3 Chemical analyses and Mass Transfers (MT) and corresponding % changes of elements in calcite (original) and its altered equivalent (altered)

Sample	AD 008a AD 008b				AD 053a AD 053b				AD 026a AD 026b			
	original	altered	MT	% change	original	altered	MT	% change	original	altered	MT	% change
g/100 g precursor												
SiO ₂	9.01	25.6	10.19	113	3.76	89.31	52.51	1396	6.13	74.86	41.03	669
Al ₂ O ₃	0.45	0.13	-0.35	-78	0.06	0.4	0.19	320	0.11	0.66	0.31	278
Fe ₂ O ₃ *	2.37	5.2	1.53	64	1.9	2.77	-0.15	-8	3.39	3.33	-1.29	-38
MgO	0.18	0.02	-0.17	-92	0.08	0.02	-0.07	-84	1.87	0.06	-1.83	-98
CaO	50.49	61.87	-4.09	-8	53.77	5.06	-50.58	-94	45.21	8.29	-39.99	-88
SrO	0.22	0.11	-0.14	-61	0.32	0.04	-0.29	-92	0.21	0.09	-0.16	-74
BaO	0.26	0.11	0.08	-67	0.64	0.42	-0.37	-59	0.92	2.08	0.39	43
F	0.2	9.99	7.29	3646	0.54	3.7	1.79	332	0.17	4.6	2.73	1605
Na ₂ O	0.1	0.12	-0.01	-11	ND	ND			ND	ND		
K ₂ O	0.22	0.08	-0.16	-73	ND	ND			ND	ND		
P ₂ O ₅	0.64	0.61	-0.18	-29	2.19	0.57	-1.83	-84	0.63	1.06	0.04	6
MnO	0.27	0.48	0.09	33	0.24	0.14	-0.15	-63	0.54	0.37	-0.31	-57
Cr ₂ O ₃	ND	ND			0	0.01	0	5	0	0.01	0	-15
TiO ₂	0.04	0.17	0.09	219	0.07	0.08	-0.02	-28	0.12	0.03	-0.1	-84
g/1000 kg precursor												
Y	60	167	65	109	117	83	-65	-55	111	113	-40	-36
Zr	113	153	2	2	94	31	-74	-79	62	136	24	38
Nb	32	1907	1398	4370	97	165	7	7	418	34	-397	-95
Sc	0.8	5.6	3.4	425	1.4	0.9	-0.8	-60	7.6	11	-0.67	-9
Th	30	190	113	375	86	91	-29	-33	61	93	-2	-4
U	ND	ND			130	31	-110	-85	27	ND		
W	ND	ND			ND	ND			415	40	-2	-7
Zn	ND	ND			114	294	71	62	ND	ND		
La	790	880	-130	-16	510	900	57	11	1400	2000	-140	-10
Ce	1400	1800	-50	-4	880	1400	2	0.23	2000	3100	-47	-2
Nd	430	550	-18	-4	260	350	-40	-15	590	1100	103	17
Sm	44	61	2	4	27	39	-2	-9	60	110	9	16
Eu	14.9	21.7	1.38	9	10	13.7	-1.37	-14	19.2	37	4.11	21
Tb	5.2	7.9	0.73	14	3.7	2.5	-2.13	-57	10	6.5	-5.91	-59
Yb	4.4	14.9	6.78	154	16.9	6.7	-12.68	-75	8.04	7.54	-3.29	-41
Lu	0.69	2.3	1.04	150	2.76	1.06	-2.09	-76	1.33	1	-0.7	-53

*Total Fe as Fe₂O₃

Oxides analysed by ICP methods (except for SrO and BaO) (analyses performed by Acme Labs, Vancouver)

Trace elements, REE, Sr and Ba analyzed by Neutron Activation (analyses performed by Activation Labs, Ontario)

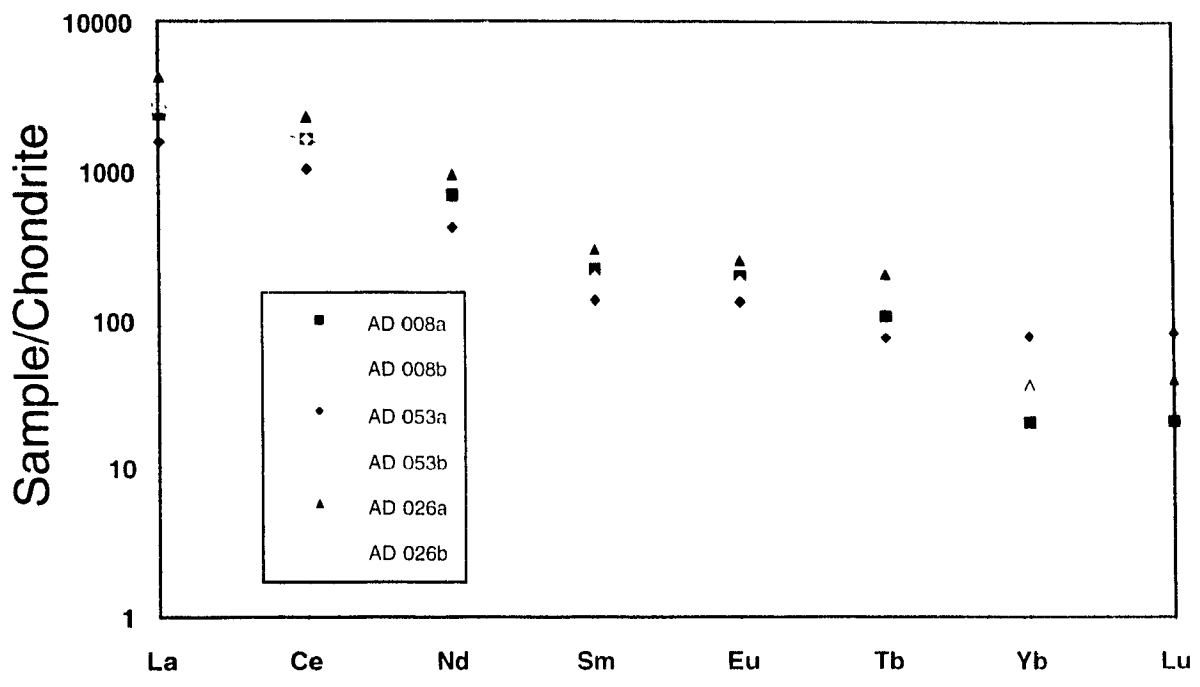
Barium also shows the same behavior as Al_2O_3 , but with smaller differences. In sample AD008b, CaO, MnO and Y all increase in small amounts, but decrease in silicified samples, AD053 and AD026. The loss of calcium in samples AD053b and AD026b is easily explained by replacement of calcite by quartz, and the increase of calcium in AD008b, by replacement of quartz by fluorite. Chromium, although not available for samples AD008a,b, shows a slight increase in the silicified samples AD053b and AD026b. No trends are apparent for P_2O_5 and TiO_2 .

Profiles of REE are shown in figure 3.12 for samples AD008, AD026 and AD053. Results show an overall moderately negative slope from La to Lu, with horizontal hiatuses between Sm and Eu and Yb and Lu. A small, but regular interval is maintained between sample-pairs for La through Tb, with altered samples being apparently more enriched than their unaltered equivalents. Values for Tb to Lu show a difference in the trend maintained between La and Eu, for all samples. Samples AD053 and AD026 show a reversal in enrichment for Tb to Lu, with higher values of HREE in the unaltered samples. The interval between unaltered and altered sample pairs also changes, with that of AD026 becoming smaller and more erratic, and that of AD053 increasing considerably. In sample AD008 the HREE maintain their enrichment in the altered sample but the interval between the pair increases.

Masses Gained and Lost

Mass balance calculations were performed using analyses of altered and unaltered calcite pairs in order to relate mass and volume changes to the actual exchange of elements between the rock and fluid. The above samples were selected so that the unaltered calcite was as proximal to the altered calcite as

Figure 3.12 Chondrite-normalized rare earth element abundances of altered and unaltered calcitite. Chondrite values taken from Boynton, 1983. Samples AD008a and AD008b represent unaltered and altered calcitite, respectively, associated with fluorite mineralization and samples AD053a and AD026a and AD053b and AD026b represent unaltered and altered calcitite, respectively, associated with barren quartz veins.



possible, in order that problems of precursor heterogeneity, with respect to the altered rock, would be minimized. Calculations were based on the isocon method of Grant (1986), a graphical representation of Gresens' (1967) volume factor method, rather than the multi-sample, single mobile element method of MacLean and Kranidiotis (1987) because of the small number of samples. The method of MacLean and Kranidiotis (1987) requires a number of altered samples with a common precursor, whereas that of Grant (1986) allows for the comparison of only two samples, an altered rock and its precursor. The results of these calculations are presented in Table 3.3.

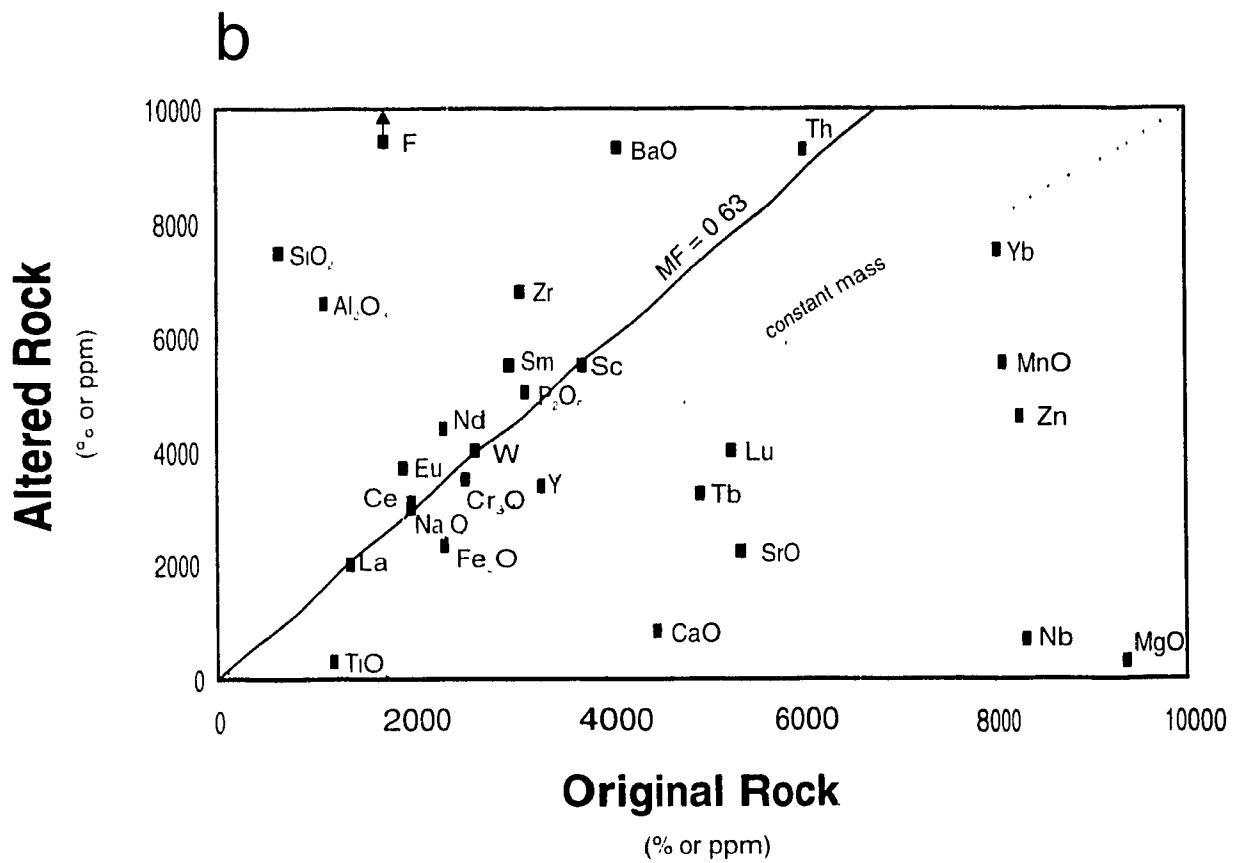
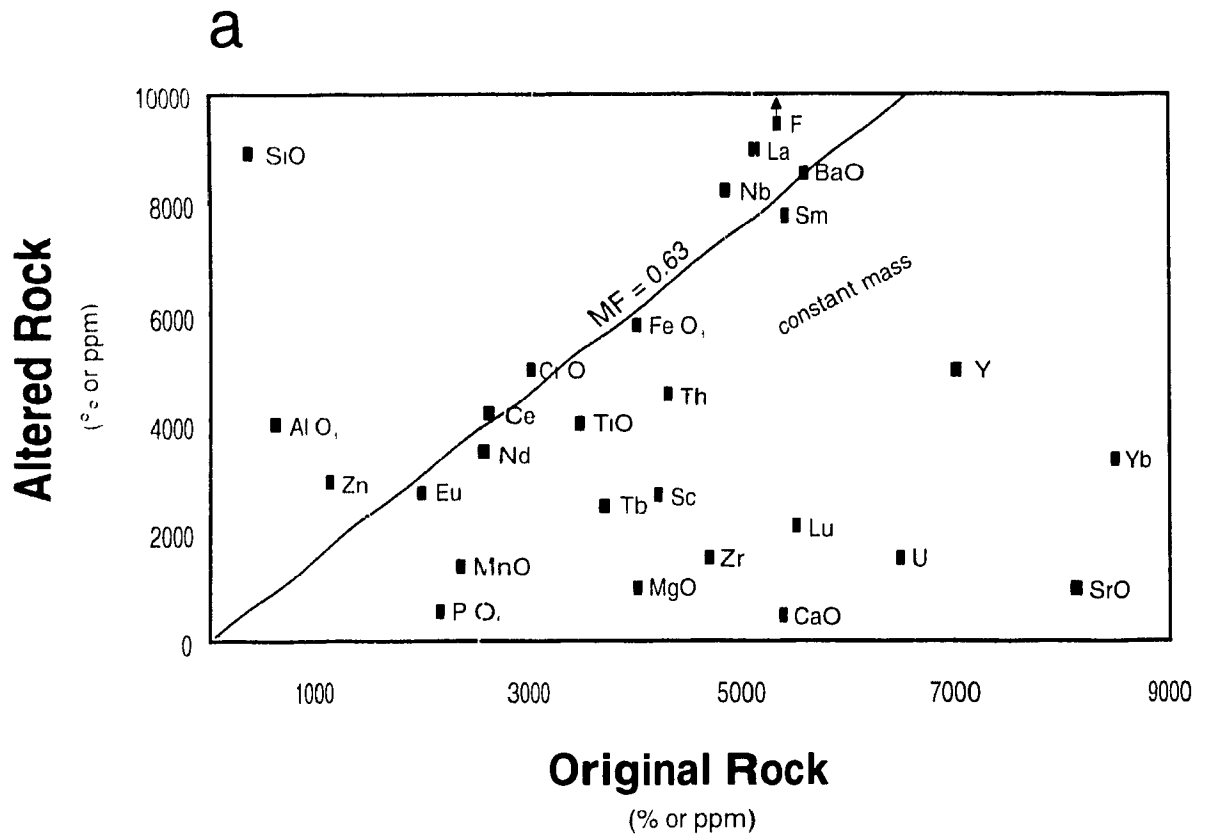
Mass Factors for Barren Quartz Vein Silicification

Figure 3 13a and b shows isocon diagrams for samples of unsilicified and silicified calcitite pairs AD053a and b and AD026a and b, respectively. The diagram for AD053a and b has a moderately well defined isocon, which passes through the origin, and through or near to La, Ce, Nd, Sm, Eu, Cr, Ba and Nb. The slope of this isocon is 1.57 which corresponds to a mass factor of 0.63 and therefore a mass loss of 37%. Using the equation

$$f_v = (M^A/M^0)/(g^A/g^0) \quad (1)$$

relating the mass factor to Gresens (1967), volume factor, where f_v is the volume factor, (M^A/M^0) is the ratio of the mass of the altered rock to the mass of the original and (g^A/g^0) is the ratio of the densities, a value of 0.64 was determined for the volume factor corresponding to a volume loss of 36%. Silicon, aluminum and fluorine were the only elements to be added in quantity to the rock, with

Figure 3.13 Isocon diagram comparing a) sample AD053a with sample AD053b; and b) samples AD026a and AD026b. The dashed line represents the constant mass line (Mass Factor = 1) where an element is neither lost nor gained. The solid line is the isocon. If elements are above this line, they have been added to the rock, and if they are below the isocon they have been removed. For information about the samples refer to the text.

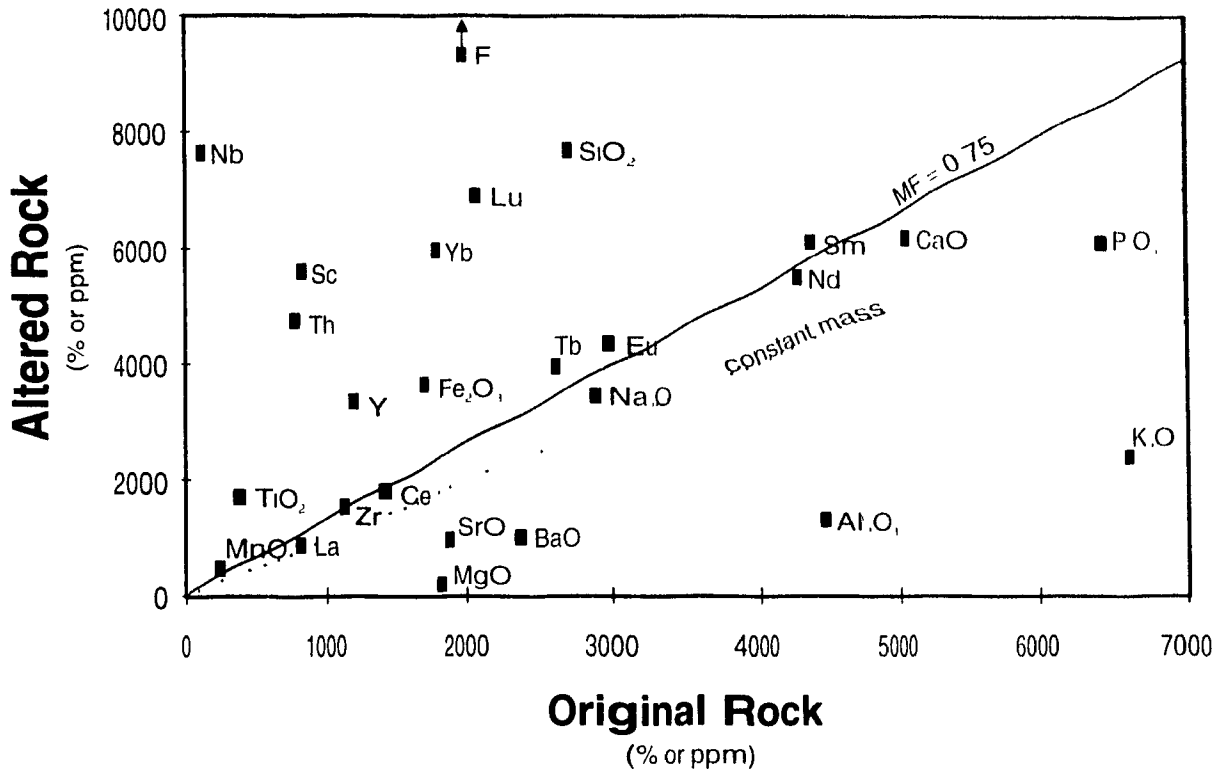


mass changes of 1396, 320, and 332%, respectively, while CaO, SrO, BaO and MgO were removed in large amounts (mass losses of 94, 92, 59 and 84%, respectively). Comparison of samples AD026a and b yields similar results to AD053, the isocon being determined by La, Ce, Nd, Sm, Eu, Cr, Na, Sc, P and Th. The isocon has a slope = 1.57 which corresponds to a mass factor of 0.63, identical to that of sample AD053. The volume factor and volume loss are also the same (0.64 and 36%) due to the similarity in the two rock types. In both samples, components added include SiO₂, Al₂O₃, F and Ba with 669, 278, 1605 and 43% increases, respectively. CaO, SrO, MgO, Fe and MnO were lost in amounts of 88, 74, 98, 38 and 57%, respectively.

Mass Factor Associated with Quartz-Fluorite Alteration

Figure 3.14 shows a plot of unaltered versus altered rock for Sample AD008, the fluorite-associated alteration. Comparison of the two samples yields an isocon, delineated by La, Ce, Nd, Sm, Eu, Tb, Mn, Zr and Na, with a slope of 1.32, corresponding to a mass factor of 0.75 (mass loss of 25%) and a volume factor of 0.69, indicating a volume loss of 31%. Mass changes involved in the alteration of the precursor included large gains of SiO₂, F and Fe, with respective increases of 113, 3646 and 64%. Elements which show mass losses are Al, K, Sr, Mg, Ba, and P in amounts of 78, 73, 61, 92 and 67%. Calcium shows neither a significant loss nor gain, plotting close to the isocon. This behavior is explained by the addition to the rock of significant amounts of fluorite. Calcium, however, is not considered to have been an immobile element due to the Sr isotope data of Deans and Powell (1968) which suggests that calcium in the calcite was not the major source of the calcium in the fluorite.

Figure 3.14 Isocon diagram comparing sample AD008a with AD008b, the alteration of calcitite associated with fluorite mineralization. The behavior of this graph is the same for that of 3.13. For more information refer to the text.



Fluid Inclusions

A fluid Inclusion study was undertaken in order to gain compositional and geothermometric data on fluid(s) responsible for silicification and fluorite deposition. Fluid inclusions occur in both fluorite and quartz from all samples taken from the Amba Dongar complex, although they are much more numerous in fluorite. The distribution of fluid inclusions within the fluorite is, however, uneven with the purple and blue varieties containing the largest quantity of inclusions, and yellow and colorless fluorite having only a small proportion.

Inclusions in Amba Dongar Fluorite

Primary inclusions were identified in all stages of fluorite. They are isolated and randomly oriented, or are concentrated in planes parallel to growth zones (Fig. 3.15A). Their diameters range from a few microns to over 300 microns, and their shapes vary from irregular to rounded or negative crystal (Fig. 3.16A, B). Necking-down of inclusions is common and generally recognizable. Those inclusions suspected of being necked-down were disregarded.

Secondary inclusions are also present in fluorite, occurring as planar trains crosscutting mineral boundaries. Their shapes are predominantly rounded and less commonly irregular. These inclusions are typically smaller than primary inclusions, ranging in diameter from 5 to 50 microns. In some cases the size of these inclusions decreases towards the termination of a healed fracture (Fig. 3.15B).

Primary inclusions in fluorite are of two types: liquid-vapor (Fig. 3.16A),

Figure 3.15 A) Primary fluid inclusions in fluorite, terminated by, and occurring along, growth zones; B) A plane of secondary fluid inclusions formed in fluorite. The decrease in size of the inclusions from the top to bottom indicates that they were trapped along a healing fracture.

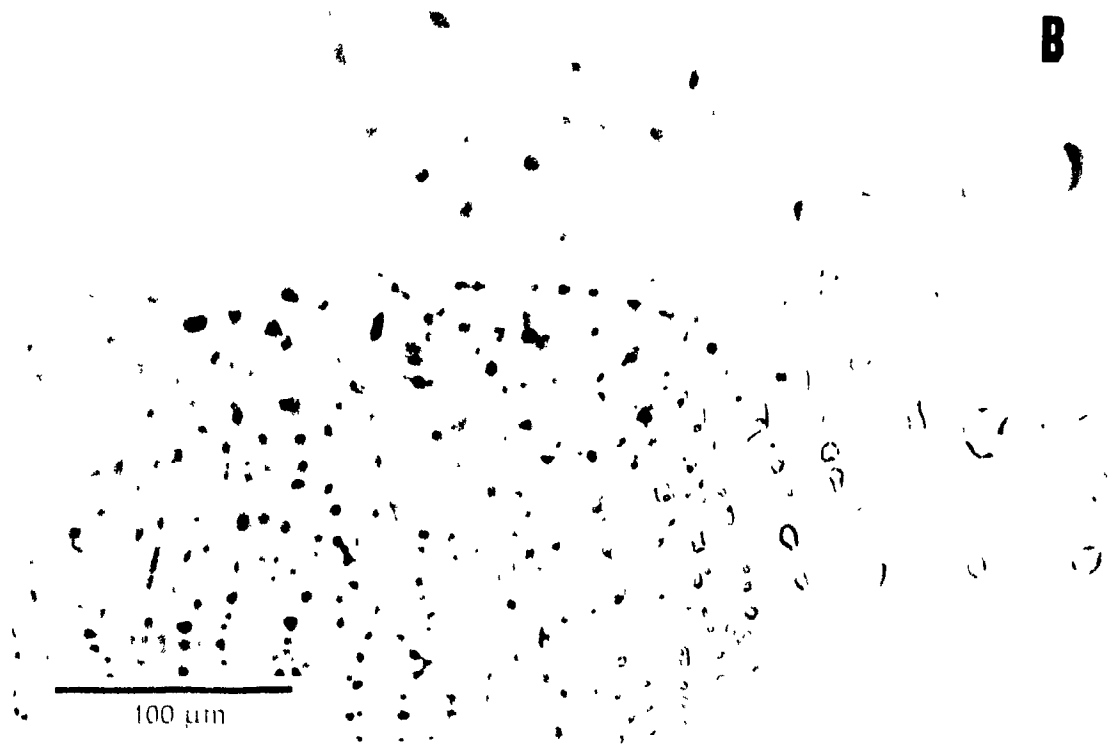
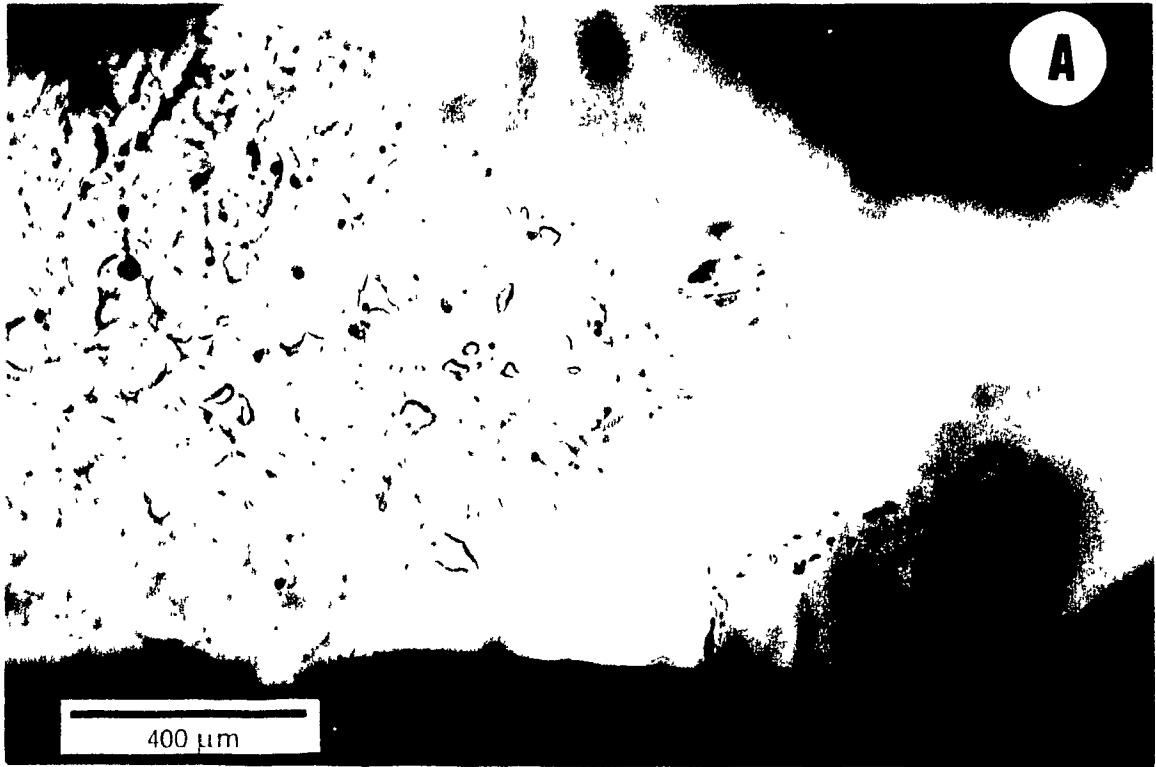
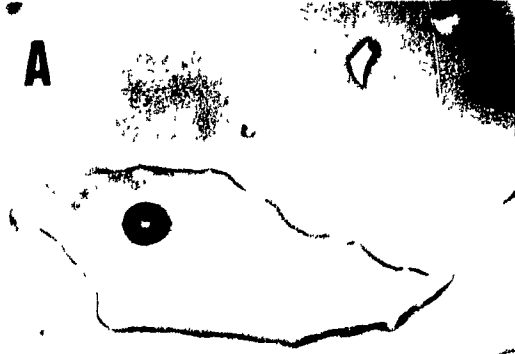


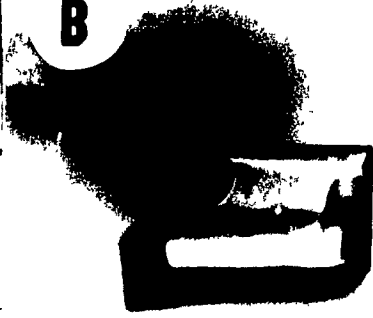
Figure 3.16 A) A large, primary liquid-vapor fluid inclusion in fluorite; B) A primary, liquid-vapor fluid inclusion in fluorite displaying a negative-crystal habit C) A primary liquid-vapor fluid inclusion in quartz; D) A liquid-only fluid inclusion in quartz; E) Coexisting liquid-only and vapor-rich fluid inclusions in quartz.

A



100 μ m

B



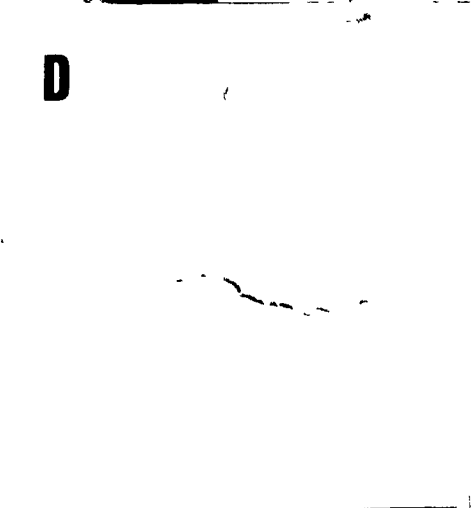
100 μ m

C



40 μ m

D



100 μ m

E



40 μ m

which comprise over 90% of all inclusions; and liquid-only inclusions. In liquid-vapor inclusions, the vapor bubble generally occupies no more than 10% of the volume of the inclusion. Liquid-vapor ratios in primary inclusions are consistent throughout the deposit. Liquid-only inclusions occur together in random, three-dimensional clusters and do not result from necking-down. Many of these inclusions fit the criteria proposed for primary inclusions by Roedder (1984). Secondary inclusions have a similar distribution of liquid-vapor and liquid-only types.

Inclusions in Quartz

Fluid inclusions are present in quartz from barren veins and associated silicification as well as quartz lining walls of fluorite bodies, but are considerably less abundant than in fluorite. Inclusions were considered primary on the basis of isolation from other inclusions or the random orientation of inclusions in three dimensional arrays.

Fluid inclusions in barren quartz veins are generally irregular in shape, and typically measure from a few microns to approximately 50 microns in diameter. Quartz associated with fluorite mineralization contains only small numbers of recognizable inclusions due to the fine-grained nature of the host mineral. These inclusions are small, round and less than 5 microns in diameter.

Inclusions in quartz are of three types: liquid-vapor (Fig. 3.16C), liquid-only (Fig. 3.16D) and vapor-rich (Fig. 3.16E). The liquid-only inclusions are by far the most common, comprising over 95% of inclusions in both barren vein quartz and quartz coating the walls of fluorite bodies. Liquid-vapor inclusions in quartz veins typically have liquid-vapor ratios of greater than 10:1, while in quartz associated with fluorite these ratios are greater than 20:1 and the vapor bubble

shows high degrees of pseudo-Brownian motion. Upon cooling and reheating of the samples, approximately 10% of liquid-only inclusions nucleate a vapor bubble. Very rarely, vapor rich inclusions were identified in quartz from barren veins. These fluid inclusions were small (<10 microns in diameter), and were not easily studied.

Secondary inclusions were easily identified by their occurrence along planar structures, interpreted to be healed fractures due to the decrease in the size of the inclusions towards the end of a plane. They are similar in size, shape and type to the primary inclusions.

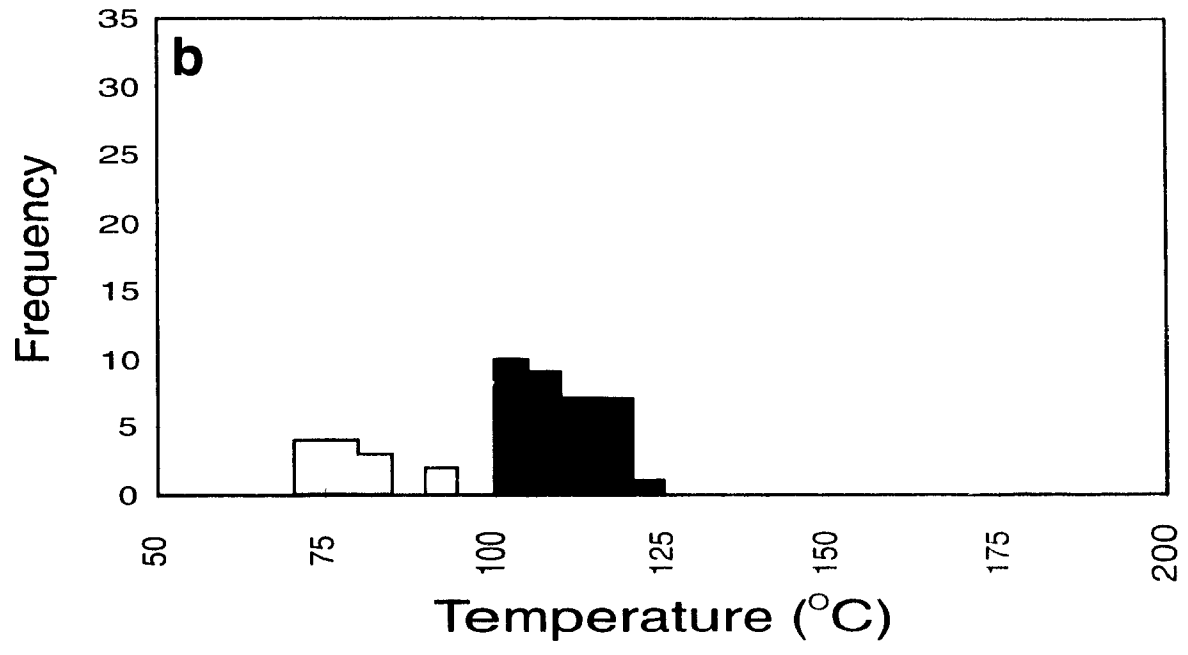
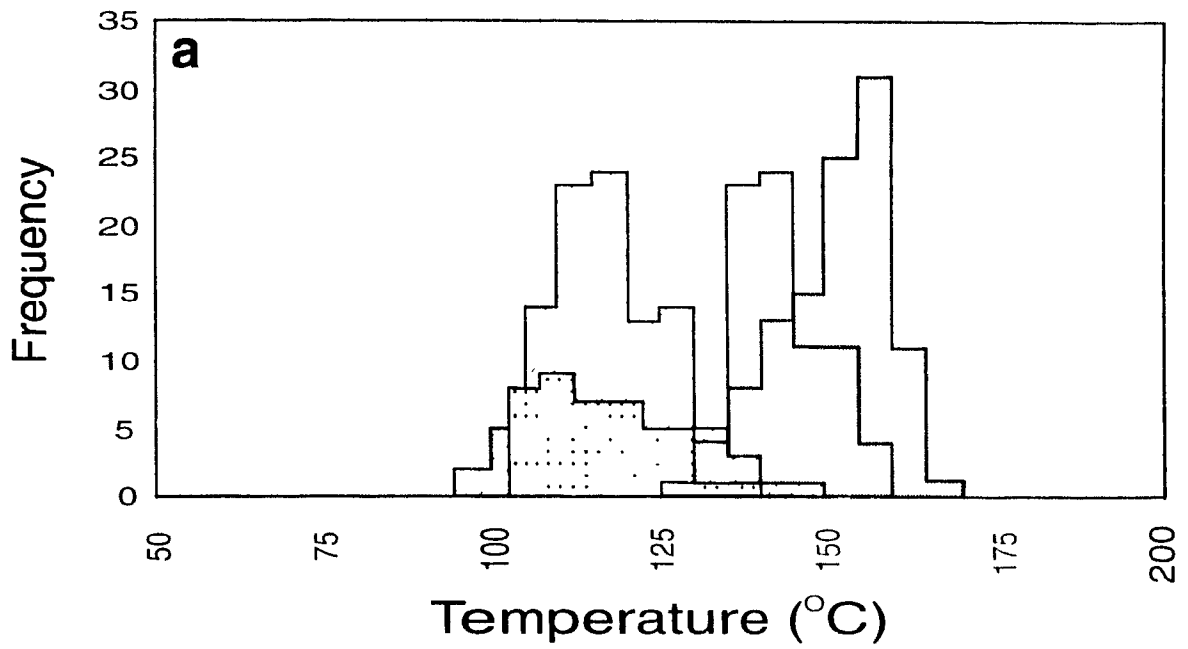
Microthermometry

Microthermometric studies were undertaken on primary fluid inclusions in fluorite from all parts of the deposit, and elsewhere in the complex, quartz from quartz veins associated with silicification, and quartz associated with fluorite mineralization. Analyses were performed on a Fluid Inc. modified U. S. G. S. gas flow heating/freezing system (Reynolds, 1992). Calibration was accomplished using synthetic CO₂ and H₂O inclusions. With this method of calibration, accuracies of +/- 0.2°C for subzero temperatures and +/- 1.0°C for higher temperatures were achieved.

Homogenization data for inclusions in fluorite and quartz are presented in Figures 3.17a and 3.17b, respectively. All inclusions homogenized to liquid.

Fluid inclusions in fluorite show an overall range of homogenization temperatures from 95.5 to 167.8°C, indicating a low temperature of formation. However, the early and late fluorite hosted inclusions yield significantly different distributions of homogenization temperatures. Inclusions in blue fluorite have the

Figure 3.17 Histograms of homogenization temperatures for liquid-vapor fluid inclusions in a) fluorite; b) and quartz.



FLUORITE

BLUE

PURPLE

YELLOW

COLORLESS

QUARTZ

BARREN VEINS

QUARTZ WITH FLUORITE

highest temperatures of homogenization, ranging from 134.2 to 167.8°C with a mean value of 152.1°C and the bulk of the temperatures falling between 150 and 160°C. Inclusions in purple fluorite have the next highest homogenization temperatures, ranging between 127.4 and 159.8°C, with a mean of 143.6°C and most temperatures falling between 135 and 145°C. The ranges for inclusions in yellow and colorless fluorite show considerable overlap from 95.5 to 145.4°C and 100.1 to 136.0°C, respectively. The mean homogenization temperatures for the two varieties are essentially the same, 117.9°C and 117.1°C, respectively. However, the bulk of the temperatures for yellow fluorite fall between 110 and 120°C, while those of the colorless variety fall between 100 and 110°C.

Fluid inclusions in quartz from barren veins and quartz lining the walls of fluorite bodies show an overall range in homogenization temperatures of 71.3°C to 120.7°C. Inclusions in barren quartz have the highest homogenization temperatures, ranging from 100.9 to 120.7°C, with a mean of 109.5°C, and most temperatures between 100 and 110°C. Inclusions in quartz associated with fluorite show much lower homogenization temperatures, ranging between 71.3°C and 93.7°C. The mean homogenization temperature for these inclusions is 79.4°C and the temperatures generally group between 70 and 80°C. Only one vapor-rich inclusion was found in which phase changes could be observed to any degree. The fluid inclusion appeared to homogenize, to vapor, in the same temperature range as the liquid-vapor inclusions. A more accurate estimate of temperature of homogenization could not be made due to the inherent difficulties in observing phase changes in these types of inclusions (Roedder, 1984).

Cryogenic experiments were conducted on inclusions in samples representing each of the varieties of fluorite and quartz from both associations in order to determine the salinities of the aqueous fluid. Samples were initially cooled to the temperature of liquid nitrogen (-196°C) in order that no low

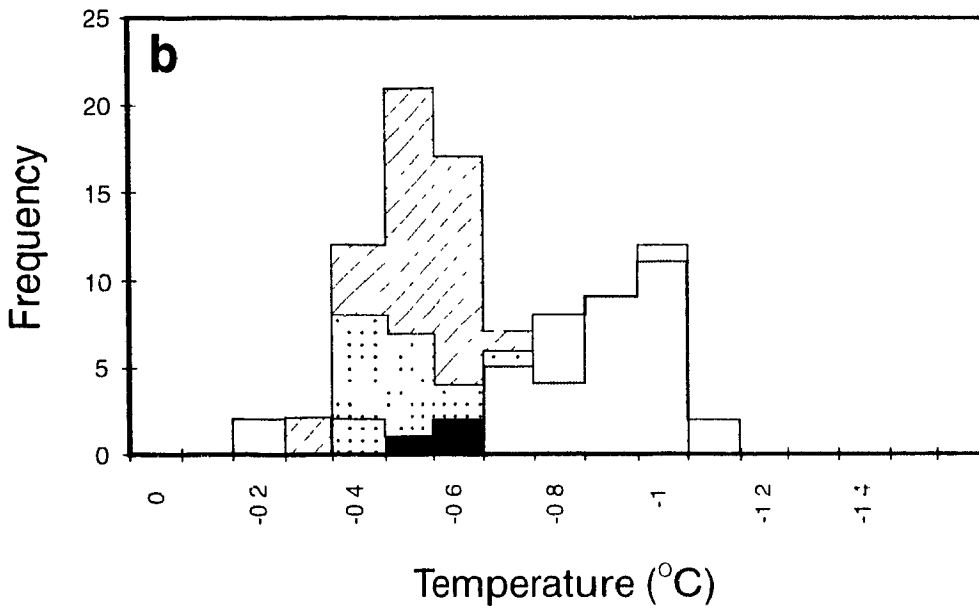
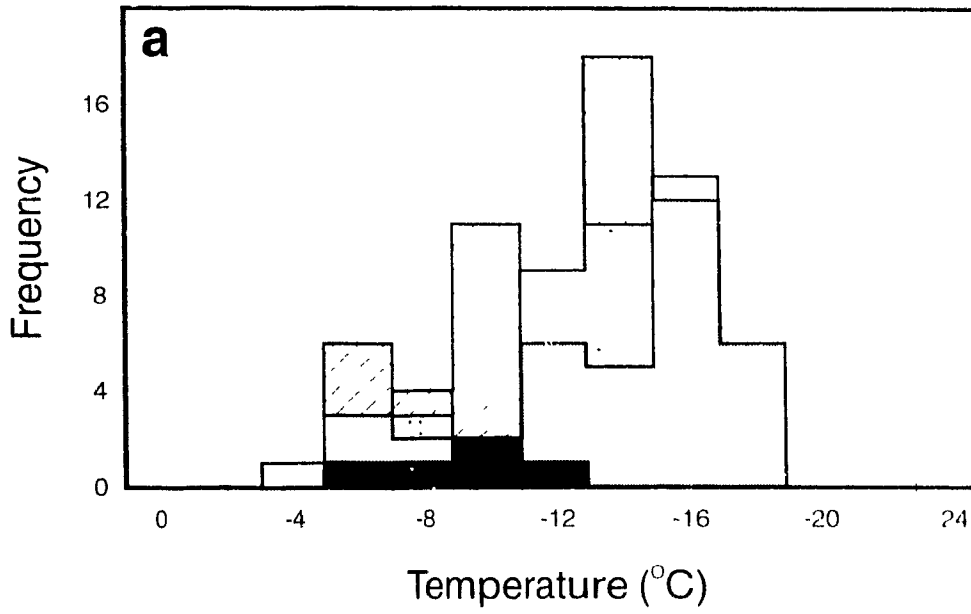
temperature phase changes would be missed. In over 80% of all liquid-vapor inclusions in blue and purple fluorite, and in quartz, and 50% of inclusions in yellow and colorless fluorite, the vapor bubble shrank or disappeared when the ice formed or when the latter was near its final melting temperature. This behavior indicates a low vapor pressure in the inclusions.

Figures 3.18a and 3.18b present initial ice melting ($T_{i,}$) and final ice melting ($T_{m(ice)}$) data, respectively, for liquid-vapor inclusions in fluorite and quartz in barren quartz veins. Owing to the low vapor pressure of the liquid-vapor inclusions, only a small number had a coexisting vapor phase in the presence of ice, and gave reliable cryogenic data. Inclusions in quartz crystals lining fluorite vein/vug walls were too small for phase changes to be observed. In all inclusions which displayed coherent melting phenomena (i.e. coexistence of liquid and vapor), the initial ice melting temperatures were significantly above -23°C (the eutectic temperature of the system $\text{NaCl-H}_2\text{O}$), ranging between -18°C and -14°C , with peaks in the distribution at -16°C , 14°C and -10°C , for the blue and purple fluorite, the yellow and colorless fluorite and for quartz, respectively.

As with homogenization temperatures, final ice melting temperatures of inclusions in fluorite distinguish the early blue and purple varieties from the late yellow and colorless fluorite. Liquid-vapor inclusions in blue fluorite had the lowest final ice-melting temperatures with a range between -1.1 and -0.4°C , and a mode of -0.9°C . Final ice-melting temperatures for inclusions in purple fluorite were similar, ranging between -1.0 and -0.5°C , with a mode of -1.0°C . Inclusions in yellow and colorless fluorite have similar ranges of final ice-melting temperature with values for yellow fluorite between -0.7 and -0.3°C and for colorless fluorite between -0.7 and -0.2°C . The modes for the two populations are the same, -0.5°C .

Owing to the limited number of usable inclusions in quartz from barren

Figure 3.18 a) Histogram of initial ice melting temperatures for liquid-vapor fluid inclusions in fluorite and quartz; b) Histogram showing the final ice melting temperatures for fluid inclusions in fluorite and quartz.



FLUORITE

QUARTZ

□ BLUE

▨ YELLOW

■ BARREN VEINS

□ PURPLE

▤ COLORLESS

quartz veins, only a small number of temperatures of final ice melting could be measured. These temperatures, representing fluid inclusions taken from two separate samples, show a narrow range of between -0.6 and -0.5°C .

Limited work on secondary inclusions in early and late fluorite, and quartz from barren systems showed that these inclusions have very similar homogenization and final ice melting temperatures to primary inclusions.

Crushing Experiments

Owing to the possibility that fluorite from the Amba Dongar deposit may be genetically linked to the host carbonatite, crushing tests were performed in order to establish if incondensable gases, specifically CO_2 , are present in the inclusions. Samples of fluorite from each of the color groups were decrepitated on a crushing stage using the method of Roedder (1934).

Upon crushing, the vapor bubble in fluid inclusions in all samples of fluorite, and quartz, from barren vein systems, expanded to completely fill the volume of the inclusion. This expansion of the vapor bubble indicates the presence of a significant concentration of incondensable gas(es) which, given the environment, is almost certainly CO_2 . The content of CO_2 was estimated by iterating Barton and Chou's (1993) equations A2 and A4, which yielded values of 2.1 atm for P_{CO_2} and $0.0764m$ for m_{CO_2} . A total pressure of approximately 12 bars was graphically estimated from Barton and Chou (1993, Fig 4), for the inclusions in blue and purple, and yellow and colorless fluorite, for temperatures of 150 and 125°C , respectively.

Estimates of Salinity Based on CO₂ Concentration

The cumulative measurement of CO₂ concentration is also useful for correcting salinity estimates based on measurements of the depression of the temperature of ice melting. Hedenquist and Henley, (1985) pointed out that the presence of dissolved CO₂ can significantly affect microthermometric estimates of the salinity of fluid inclusions. The equation of Hedenquist and Henley (1985) determine the "true" concentration of NaCl in the fluids:

$$T_{m-c} = -\{K_j \sum m_j + K_k \sum m_k\} \quad (2)$$

where T_{m-c} is the corrected final melting temperature of ice, $K_j \sum m_j$ is the sum of the molalities of electrolytes in solution multiplied by the molal freezing point depression constant, 1.72 for water (Potter *et al.*, 1978), and $K_k \sum m_k$ is the sum of the molalities of non-electrolytes multiplied by the molal freezing point depression constant, 1.86 for CO₂ (Hedenquist and Henley, 1985). Ratios of Ca/Na and K/Na and SO₄/Na were determined from leachate/decrepitate analyses and the molality of CO₂ was calculated from Barton and Chou (1993). The results of these calculations show that the salinity (equivalent wt % NaCl), calculated using the equations of Oakes *et al.* (1990), is considerably lower than that calculated using the measured T_m (Table 3.4), ignoring CO₂. The corrected average salinity for fluids from blue fluorite is 0.62 wt % NaCl, for inclusions in purple fluorite, 0.50 wt.% NaCl, for inclusions in yellow and colorless fluorite, 0.36 wt.% and the average salinity for fluids which deposited quartz in barren quartz veins is 0.58 wt.% NaCl. There is a clear trend of decreasing salinity

Table 3.4 Wt % NaCl and molal concentrations for fluid inclusions in fluorite and quartz, determined from calculated (Tm-cc) and measured (Tm) final ice melting temperatures

Sample	Color	Uncorrected			Corrected*		
		Tm (deg C)	wt % NaCl*	molality	Tm-cc (deg C)	wt % NaCl**	molality
AD026Q	quartz	-0.54	0.94	0.16	-0.54	0.60	0.11
AD053Q	quartz	-0.50	0.87	0.15	-0.50	0.55	0.10
AD066X	blue	-0.84	1.46	0.26	-0.84	0.63	0.11
AD066Z	blue	-0.80	1.39	0.24	-0.80	0.60	0.10
AD066Z	blue	-0.84	1.46	0.26	-0.84	0.63	0.11
AD066W	purple	-0.86	1.49	0.26	-0.86	0.50	0.09
AD050Y	yellow	-0.50	0.87	0.15	-0.50	0.32	0.06
AD008F	yellow	-0.55	0.96	0.17	-0.55	0.37	0.06
AD066XY	yellow	-0.59	1.03	0.18	-0.59	0.40	0.07
AD050C	colorless	-0.53	0.93	0.16	-0.53	0.35	0.06

*Corrected salinities using the equations of Hedenquist and Henley (1985) and fluid inclusion leachate data.

**Calculated using equations from Oakes et al (1990).

from the early blue and purple fluorite to the late yellow and colorless varieties
Fluid inclusions in quartz have salinities similar to those in the early fluorite

Leachates

Analyses of leachates, prepared by crushing fluid inclusion-bearing samples in the presence of water, were performed in order to gain further information about the composition of the fluid(s) responsible for fluorite deposition and wall rock silicification. Eight samples of fluorite were analyzed, three each of blue and yellow fluorite, and one each of purple and colorless fluorite. Two samples of quartz from barren quartz veins were also analyzed. The samples were considered representative of their respective paragenetic sequences.

Samples were prepared and the fluids extracted using the methods of Roedder (1958) and Poty *et al.* (1974). However, because of the high solubility of fluorite in acid solutions, samples were cleaned using nanopure water rather than dilute HCl and HNO₃ as recommended by these authors. Recently, Bottrell *et al.* (1988) have drawn attention to the problem of adsorption of doubly charged cations on the host mineral. They have therefore recommended the use of a 0.13M HNO₃ + 200 ppm LaNO₃ leachate solution to minimize those problems. Because of the solubility of fluorite in this solution, it was, however, necessary to use nanopure water.

Samples consisted of 4g aliquots of sieved and hand-separated quartz or fluorite. They were cleaned, crushed and leached with 10 ml of nanopure water. Blanks were prepared by running 10 ml of nanopure water over the clean, uncrushed sample. Analyses for Na, K, Ca, Mg and Fe were carried out by

flame atomic absorption spectrophotometry, Al by graphite furnace atomic absorption spectrophotometry and Cl, F, SO₄, P₂O₅ and Br by ion chromatography. Detection limits, calculated from analyses of calibration standards, were 0.01, 0.01, 0.04, 0.07, 0.004 ppm and <0.001 ppm for the cations, and 0.04, 0.08, 0.01, 0.05 and 0.006 ppm, for the anions, respectively.

Results

The results of analyses for eight samples of fluorite, two samples of quartz and four blanks are shown in Table 3.5 and 3.6. Calcium and fluorine are the dominant cation and anion in the solutions, suggesting that fluorite dissolution may have contaminated the leachate with these elements. In order to correct for this, the stoichiometric proportions of Ca and F in fluorite were subtracted from the analyses, on the assumption that all F was due to fluorite dissolution. Even after this correction the concentration of Ca in the fluid was an order of magnitude greater than those of the other cations. The next most important cations are Na and Al, followed by K and Mg. Iron concentration was below the limit of detection of the apparatus. Chlorine is the most abundant anion, which was analyzed for, and SO₄ is only significant in the purple fluorite sample (AD 066w) and the two quartz samples. Bromine was below detection in all samples and P₂O₅ was not detected in fluorite samples, but was detected in both quartz leachates. The sum of the charge-normalized atomic proportions of cations in all samples is significantly greater than that for the anions, suggesting the presence of other anions in solution. Given the geological setting (i.e. carbonatite, calcareous sandstone and limestone), the most likely candidate would be dissolved CO₂, (H₂CO₃, HCO₃⁻ or CO₃²⁻). An interesting observation is that the proportion of Na and K is similar to that of Cl, suggesting that Ca was introduced

Table 3.5 Fluid inclusion leachate compositions from fluonite and quartz

Sample	Color	Concentration (ppm)										
		Ca	Al	Na	K	Mg	P ₂ O ₅	Fe	I	Cl	%Cl	Br
AD026Q	quartz	0.22	0.15	0.06	0.07	0.01	0.03	0.07	0.17	0.12	0.15	0.006
AD053Q	quartz	0.08	0.17	0.11	0.09	0.02	0.16	0.07	0.08	0.19	0.16	0.006
AD066X	blue	11.8	0.16	0.19	0.06	0.02	0.05	0.07	0.25	0.1	0.07	0.006
AD066Z	blue	16.9	0.2	0.15	0.18	0.02	0.05	0.07	0.95	0.15	0.01	0.006
AD066Z	blue	11.4	0.15	0.09	0.02	0.02	0.05	0.07	0.8	0.19	0.01	0.006
AD066W	purple	13.3	0.17	0.19	0.05	0.02	0.05	0.07	0.19	0.20	0.01	0.006
AD050Y	yellow	9.1	0.14	0.07	0.02	0.02	0.05	0.07	0.78	0.1	0.01	0.006
AD008F	yellow	7.8	0.2	0.1	0.02	0.02	0.05	0.07	0.94	0.16	0.01	0.006
AD066XY	yellow	10.9	0.17	0.07	0.02	0.02	0.05	0.07	0.99	0.09	0.01	0.006
AD050C	colorless	8.7	0.15	0.07	0.02	0.02	0.05	0.07	0.97	0.11	0.01	0.006

Table 3.6 Calculated compositions of bulk fluids for fluonite and quartz

Sample	Color	Salinity		molality							Atomic ratios		
		wt%NaCl	Ca*	Al	Na	K	Mg	P ₂ O ₅	Cl	%Cl	Na/K	Ca/K	Al/K
AD026Q	quartz	0.60	0.000	0.170	0.081	0.056	0.013	0.026	0.105	0.048	1.46	0.00	0.77
AD053Q	quartz	0.55	0.018	0.110	0.085	0.041	0.015	0.030	0.095	0.030	2.08	0.11	0.89
AD066X	blue	0.63	0.271	0.08	0.107	0.020	0.011	0.007	0.110	0.003	5.39	1.57	0.90
AD066Z	blue	0.60	0.404	0.180	0.160	0.113	0.020	0.013	0.104	0.003	1.42	3.57	1.51
AD066Z	blue	0.63	0.202	0.110	0.080	0.010	0.017	0.011	0.110	0.002	7.65	19.29	0.73
AD066W	purple	0.50	0.229	0.070	0.091	0.014	0.009	0.006	0.087	0.096	6.46	16.29	1.05
AD050Y	yellow	0.32	0.152	0.100	0.060	0.010	0.016	0.010	0.056	0.096	5.95	15.00	1.08
AD008F	yellow	0.37	0.155	0.110	0.062	0.007	0.012	0.007	0.064	0.001	8.50	21.43	0.96
AD066XY	yellow	0.40	0.212	0.170	0.084	0.014	0.023	0.015	0.070	0.003	5.95	15.00	1.20
AD050C	colorless	0.35	0.151	0.090	0.060	0.010	0.016	0.010	0.061	0.002	5.95	15.00	0.98

*Ca values corrected using Ca = 4.39*Na obtained from decrepitate results

with another anion(s)

Within the various color groups of fluorite, and between fluorite and quartz, a number of differences occur. Generally, the Na concentration in leachates decreases from the blue and purple fluorite to the yellow and colorless varieties. Concentrations of Na in leachates from quartz are similar to those obtained from the yellow fluorite samples. Chlorine shows a strong dependence on Na, decreasing in concentration from blue to yellow fluorite samples. Potassium also follows a similar trend, decreasing along with Na and Cl. Quartz-derived leachates gave the only significant amounts of P_2O_5 . These trends are consistent with microthermometric estimates of salinity and the lower abundance of fluid inclusions in yellow/colorless fluorite.

Atomic ratio of Na/K for the fluorite samples ranges between 5.39 and 8.5, except for the anomalously low value for one sample of blue fluorite (AD066z) of 1.42, but does not correlate with fluorite color. The corresponding ratios for quartz samples are lower, 1.42 and 2.08. The atomic ratio of Ca/K for fluorite samples is also higher than that for quartz, and ranges from 13.57 to 21.43, except for that of sample AD066z which is again anomalously low (3.57). The Ca/K ratio for fluid leached from the quartz samples is 0.0 and 0.43. Comparison of the ratios within the various fluorite color groups reveals no distinguishing trends.

Decrepitate Residues

Semi-quantitative analyses of precipitates from opened fluid inclusions in blue, purple and yellow fluorite, and quartz were performed using a JSM-840A scanning electron microscope with a Tracor Northern energy dispersive x-ray

spectrometer. The system was equipped with an extra thin Al window thereby allowing the detection of elements as light as C (A=6). The analyses were accomplished using the technique of Haynes *et al* (1988). Doubly polished thin sections were cleaned and heated until the fluid inclusions decrepitated. They were then coated with carbon and analyzed immediately. Analyses were conducted using a rastering method, in order that a large area of the decrepitate residue would be analyzed. Owing to the inherent errors of analyzing for Ca on a Ca-bearing substrate, such as fluorite, a number of chips were decrepitated onto silica plates. The polished sample was placed on a silica-glass plate and heated. Fluids from decrepitated inclusions leaked onto the plate and precipitated solids (Fig. 3 19A). These solids were then coated with carbon and analyzed in the same manner as those precipitated on the fluorite and quartz chips. Six solution standards, three containing known amounts of Na, K, Ca, Cl and P and three containing known amounts of K, Na, Cl and S were used to prepare residues by evaporating drops of solutions on silica plates heated to approximately 60°C. These residues were analyzed as described above and the results used to construct calibration curves for these elements (Appendix 1).

Results

The results of the decrepitate analyses for samples AD066x (blue fluorite), AD066w (purple fluorite), AD066xy (yellow fluorite) and AD026 (quartz, barren vein) are presented in Table 3 7. Concentrations of Ca are corrected values using data for residues precipitated onto quartz plates. The Ca/Na ratios of the residues analyzed on these plates were remarkably consistent, and, when regressed linearly, yielded the relationship: wt % Ca = 4.93 wt % Na which was used to correct the other analyses.

Figure 3.19 A) An SEM photomicrograph of a fluid inclusion decrepitate residue on a silica plate; B) Energy dispersive scan from a typical Ca-, Na-, K-, Mg-, Fe-, C-, S- and Cl-bearing residue.

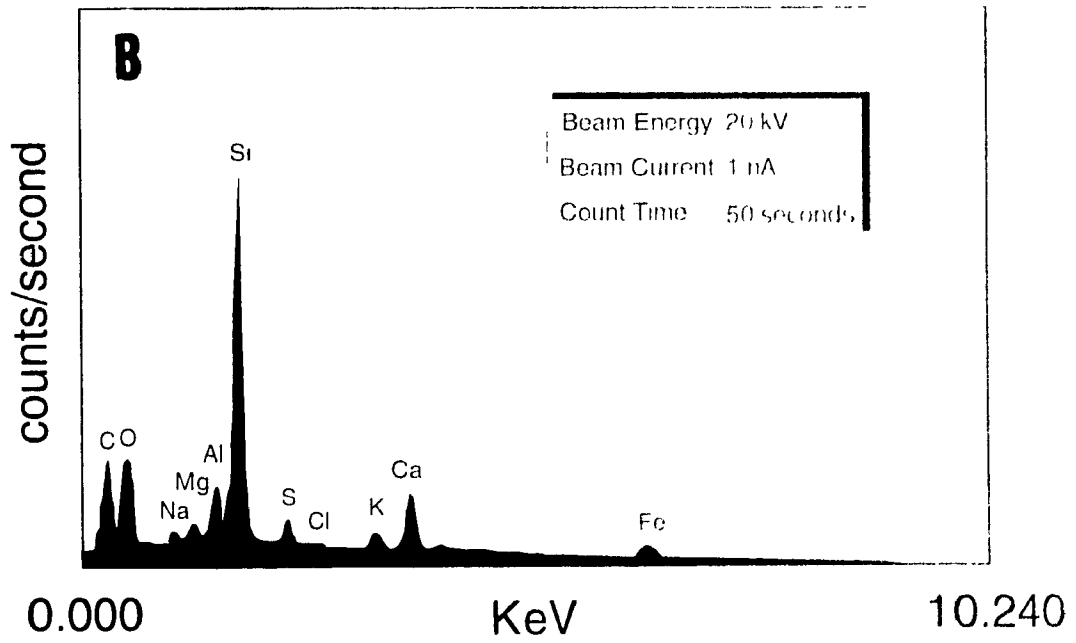
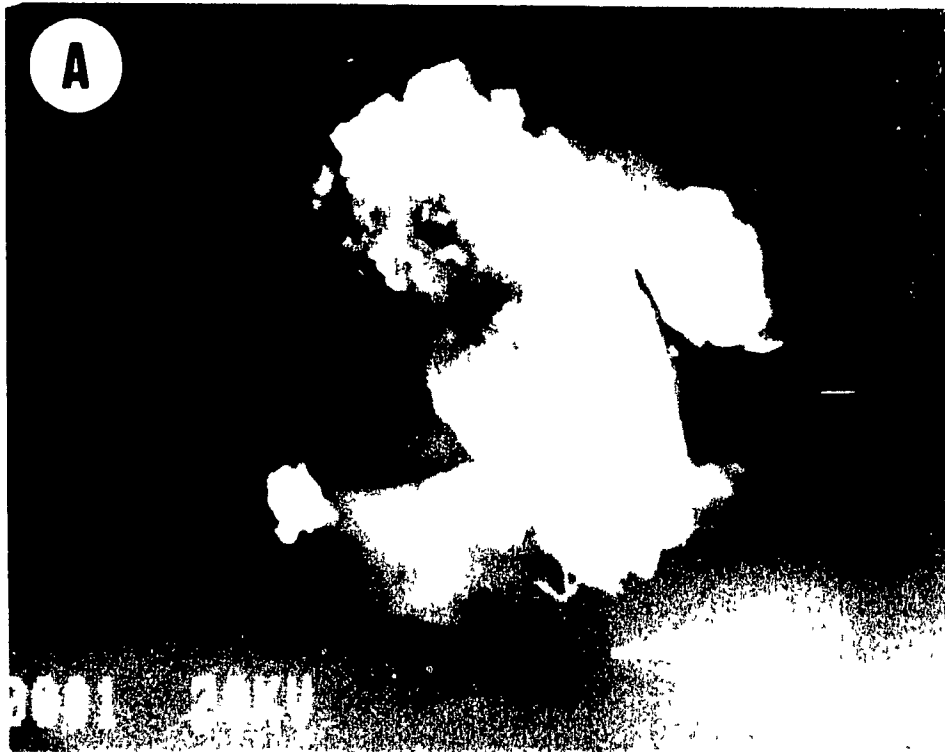


Table 3.7 Chemical analyses of decrepitate residues from fluid inclusions in fluorite and quartz, calculated as molality equivalent to salinity, measured from fluid inclusions, and corresponding atomic ratios

Sample	Salinity		molality								Atomic Ratios		
	wt% NaCl	Si	Al	Ca**	Na*	K*	Mg	P*	Cl*	S*	Na/K	Ca/K	Na/Cl
AD026Q quartz	0.60	3.57	0.39	3.79	0.04	0.00	0.17	0.16	0.10	0.33	N/A	N/A	0.41
		1.79	0.15	2.77	0.07	0.03	0.09	0.02	0.10	0.31	2.08	81.65	0.74
		1.22	0.23	0.34	0.08	0.08	0.08	0.09	0.10	0.06	0.99	4.18	0.83
AD066X blue	0.63	0.04	0.04	0.25	0.10	0.01	0.04	0.00	0.11	0.06	6.83	17.20	0.91
		0.42	0.11	0.28	0.11	0.04	0.05	0.00	0.11	0.08	3.06	7.71	1.02
		0.12	0.12	0.29	0.12	0.05	0.05	0.01	0.11	0.04	2.45	6.19	1.05
		0.05	0.04	0.26	0.10	0.04	0.03	5E-03	0.11	0.04	2.40	6.04	0.93
AD066X+ blue	0.63	N/A	N/A	N/A	N/A	N/A	N/A	N/A	0.00	N/A	3.20	7.82	N/A
		N/A	N/A	N/A	N/A	N/A	N/A	N/A	0.00	N/A	N/A	N/A	N/A
		13.87	1.92	3.27	1.13	0.92	0.88	0.22	0.11	1.25	1.22	3.55	10.23
		3.92	2.89	3.35	1.29	0.53	0.62	0.00	0.11	0.46	2.44	6.31	11.75
AD066W purple	0.50	0.28	0.29	0.85	0.34	0.02	0.19	0.02	0.09	0.27	15.04	37.89	3.88
		0.31	0.20	0.76	0.30	0.02	0.26	0.03	0.09	0.24	12.93	32.57	3.47
		0.23	0.14	0.48	0.19	0.02	0.18	0.00	0.09	0.23	10.02	25.24	2.17
		0.33	0.17	0.57	0.22	0.03	0.15	0.02	0.09	0.04	8.59	21.64	2.58
		0.31	0.14	0.50	0.20	0.04	0.12	0.04	0.09	0.04	5.48	13.80	2.27
AD066XY yellow	0.40	0.31	0.11	0.29	0.11	0.03	0.09	0.00	0.06	0.08	4.01	10.11	1.79
		0.30	0.28	0.94	0.37	0.05	0.16	0.00	0.06	1.75	7.80	19.66	5.80

*Calibrated values using standards

**Ca concentrations corrected using the equation $Ca = 4.39 * Na$, derived from sample AD 066x* (corrections exclude sample AD 066x*)

+Decrepitate analyses of samples prepared on silica plates

N/A-Not Available

Data unavailable for sample AD066X due to the absence of Cl, in the analyses, which is used to calculate molality at average salinity

The corrected results show that Si, Al, Ca, Na, K and Mg are the dominant cations in the residues. Cl and S were the only anions detected. The average values for the atomic ratios Na/K (1.56, 3.68, 10.41 and 5.91 for quartz and blue, purple and yellow fluorite, respectively) and Ca/K (9.28, 26.23 and 14.88 for blue, purple and yellow fluorite, respectively) are similar to those obtained from leachate results, except for the Ca/K ratio for quartz which is anomalously high (42.92). However, there is a significant difference in the average Na/Cl ratios from the those obtained from leachate data. The main reason for these departures from the leachate results lies in the semi-quantitative nature of the residue analyses, and the low concentrations of the elements in the precipitates. The latter can cause large errors when concentrations are close to background values.

In addition to the above elements, a significant peak was obtained for carbon (Fig. 3.19B). This would further support the presence of dissolved CO₂, and provide another possible anion (i.e. H₂CO₃, HCO₃⁻ or CO₃²⁻) to compensate for the charge imbalance in the leachate data.

Oxygen and Hydrogen Isotopes

Analyses of oxygen, hydrogen and carbon isotopes of fluids from opened fluid inclusions were obtained in order to gain insight into the source of the mineralizing fluids. One sample each of blue and yellow fluorite were analyzed by the Isotope Laboratory at the University of Saskatchewan. Oxygen and hydrogen compositions were determined using the CO₂-H₂O equilibration (Kishima and Sakai, 1980) and uranium reduction techniques (Bigeleisen *et al.*, 1952). Data uncertainties in micro-equilibration analyses are $\pm 5\%$ for δD_{H_2O} , \pm

2‰ for $\delta^{18}\text{O}_{\text{H}_2\text{O}}$ and $\pm 0.2\text{‰}$ for both $\delta^{13}\text{C}_{\text{CO}_2}$ and $\delta^{18}\text{O}_{\text{CO}_2}$. Results are reported in δ notation relative to Standard Mean Ocean Water (SMOW) for oxygen and hydrogen and to the Chicago PDB standard, and are presented in Table 3.8a.

The values of δD are similar for fluids released from inclusions in blue and yellow fluorite, -46‰ and -50‰ , respectively. Oxygen isotopes show a decrease from blue to yellow (-5.4 to -6.4‰). Carbon isotopes from CO_2 released from fluid inclusions, upon decrepitation, yield values of -2.0‰ and $+8.8\text{‰}$, for blue and yellow fluorite, respectively. The $\delta^{18}\text{O}_{\text{CO}_2}$ values for blue and yellow fluorite are 29.4‰ and 51.1‰ , respectively.

Discussion

Pressure and Temperature

On the basis of published measurements of stratigraphic thicknesses (Wadia, 1957), we estimate that approximately 250 to 500m of Bagh sediments and Deccan volcanics have been eroded from the Amba Dongar area since the emplacement of the carbonatite. This corresponds to a lithostatic pressure of 75 to 150 bars or a hydrostatic pressure of 25 to 50 bars. A minimum estimate of the fluid pressure associated with fluorite deposition and silicification is provided by data collected for aqueous, liquid-vapor inclusions in fluorite. As discussed above, these inclusions are estimated to contain approximately 0.1 m NaCl eq. and 0.08 m CO_2 and homogenized at an average temperature of 150°C . At this temperature, the corresponding vapor pressure is 12 bars (Barton and Chou, 1993). Thus in summary, it would appear that the fluid pressure was <150 bars, and given the open-space nature of the fluorite mineralization, was probably

Table 3.8a Oxygen, hydrogen and carbon isotopic data for fluids extracted from fluid inclusions in fluorite

Sample	Color	H ₂ O			CO ₂		
		umol	dD (SMOW)	d18O (SMOW)	umol	d13C (PDB)	dO (SMOW)
AD066Z	Blue	93.95	-46	-5.4	18.38	-2.0	29.4
AD066XY	Yellow	171.19	-50	-6.4	32.02	8.8	51.1

Uncertainties are +/- 2 and +/- 5 o/oo, for oxygen and hydrogen, respectively, for H₂O and +/- 0.2 o/oo for both oxygen and carbon in CO₂
 All data reported in delta notation, units are per mil (o/oo)

Table 3.8b Oxygen and carbon isotopic data for carbonatite samples.

Sample	d18O* (SMOW)	d13C* (PDB)
Calcitite	9.4	-4.28
	9.6	-5.11
Ankeritic Carbonatite	12	-4.15

*Data taken from Gwalani et al. (1993)

All data reported in delta notation, units are per mil (o/oo)

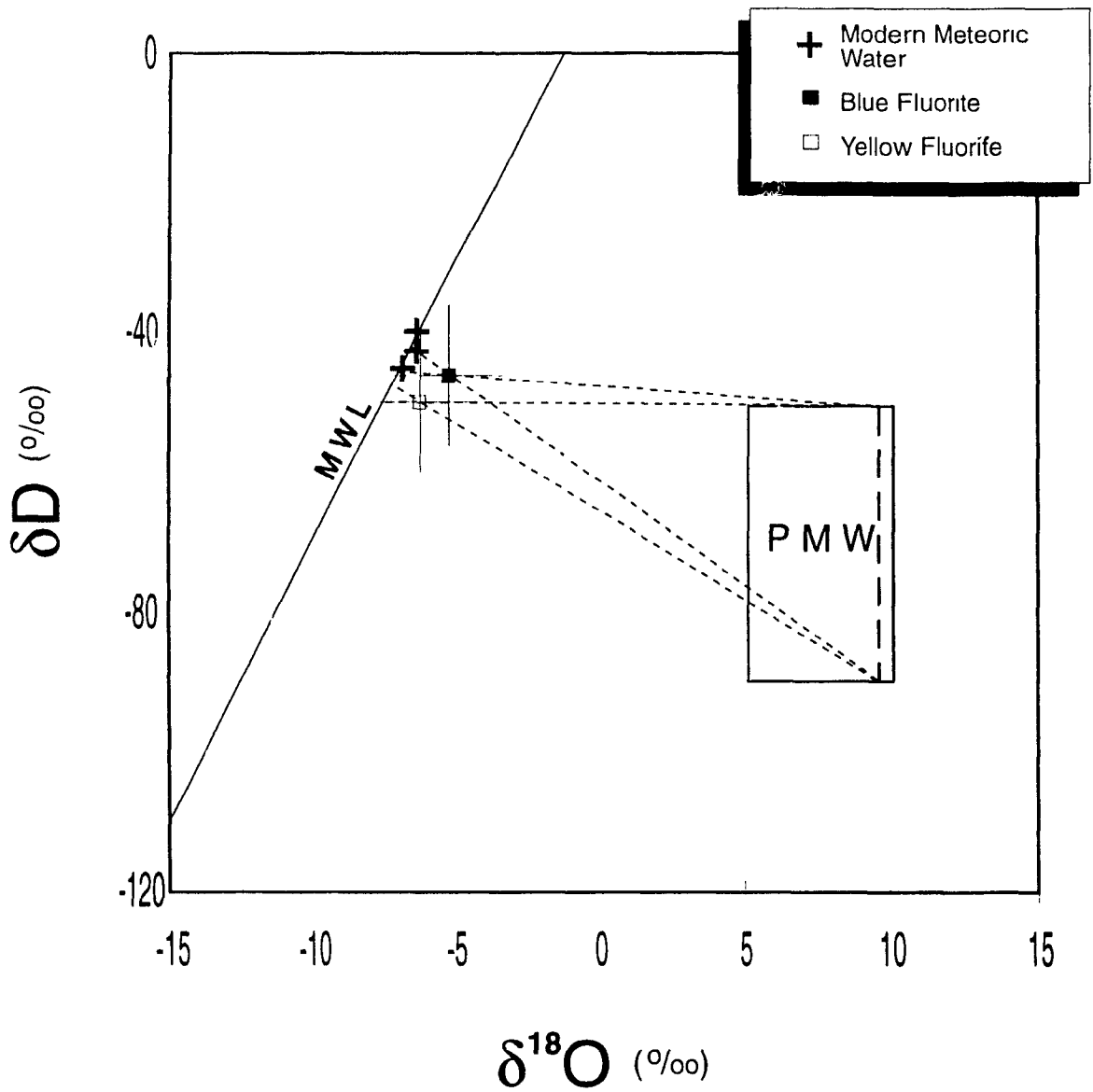
between 12 and 50 bars. At such low pressures, fluid inclusion homogenization temperatures can be used to estimate formation temperature without correction for pressure (The latter is $<5^{\circ}\text{C}$). We accordingly conclude that during deposition of the blue and purple fluorite, the temperature of the fluid was approximately 150°C , and decreased to approximately 115°C during deposition of the yellow and colorless varieties. By contrast, quartz associated with fluorite, but deposited before it, appears to have formed at a temperature of only 80°C . Quartz in barren quartz veins was precipitated at a temperature of approximately 110°C .

Fluid Origin

Although most studies of carbonatite-hosted fluorite deposits have concluded, from the geological setting, that the ore fluids were orthomagmatic, Deans and Powell (1968), Lahiry (1976) and Simonetti and Bell (1993) have proposed, on the basis of strontium isotope data, that the fluid at Amba Dongar had a large meteoric component. Oxygen and hydrogen isotopic compositions of aqueous fluids extracted from blue and yellow fluorite, during the course of the present study, appear to support the latter conclusion.

As can be seen from the plot of δD versus $\delta^{18}\text{O}$ shown in Figure 3.20, the compositions of the fluids from these samples plot near the meteoric water line, and close to the composition of present day meteoric water from the same area of India (Krishnamurthy and Bhattacharya, 1991). Furthermore, the latter is probably similar to the composition of meteoric water present during the emplacement of the carbonatite, as there has been little change in the latitude of Amba Dongar since the Late Eocene (Dietz and Holland, 1970;

Figure 3.20 Oxygen and hydrogen isotopic data for Eocene and later, fluorite-hosted inclusion fluids and modern meteoric water. The meteoric water line (MWL) and primary magmatic water box (PMW) are shown in relation to the samples. The heavy dashed line in the field of PMW represents the typical $\delta^{18}\text{O}$ value for Amba Dongar carbonatites (Gwalani *et al.*, 1993). The lighter dashed lines between the meteoric water line and primary magmatic waters represent mixing lines for the Amba Dongar ore fluid.



Johnson *et al.*, 1976).

The carbon and oxygen isotopic compositions of CO₂ released from fluid inclusions in blue fluorite are also consistent with a meteoric origin for the fluid. As reported earlier, the $\delta^{13}\text{C}$ and $\delta^{18}\text{O}$ values of CO₂ from this fluorite are -2 and -29.4‰, respectively. Calcite in equilibrium with such CO₂ at 150° C would have $\delta^{13}\text{C}$ and $\delta^{18}\text{O}$ values of -0.6 and 18.5‰, respectively (Bottinga, 1968), i.e. very similar to that of limestone (Ohmoto and Rye, 1979, Taylor, 1979). By contrast calcite in the Amba Dongar carbonatite typically has $\delta^{13}\text{C}$ and $\delta^{18}\text{O}$ values of -5 and +10‰, respectively (Table 3.8b). We therefore conclude that the CO₂ composition reflects equilibration of meteoric fluids with Bagh limestone or carbonate cement in Bagh sandstone. The CO₂ from yellow fluorite, however, yielded $\delta^{13}\text{C}$ and $\delta^{18}\text{O}$ values which are far too high to represent original compositions. A possible explanation for the higher values in yellow fluorite could be that small amounts of CO₂ effervesced from the ore fluid, removing isotopically light C, thereby enriching the fluid in the heavier ¹³C (Richet *et al.*, 1977).

On the basis of the data discussed above, we conclude that the principal fluid was meteoric and that this fluid entered the carbonatite after circulating extensively in the Bagh sediments. However, the small positive departure of its $\delta^{18}\text{O}$ and δD compositions from the meteoric water line suggests, either that it evolved as a result of water-rock interaction or mixed with an isotopically heavier, e.g. orthomagmatic, fluid.

Support for a fluid mixture is provided by the chemical composition of the inclusion fluid as deduced from bulk analyses of leachates and the analyses of residues of decrepitated inclusions. These data, particularly the high contents of sulfur and aluminum, point to an orthomagmatic fluid source. Sulfur and aluminum are typically in low concentrations in most common hydrothermal fluids

but have been shown to be at elevated levels in orthomagmatic fluids exsolved from carbonatites (Samson *et al.*, in press) and associated phonolitic magmas (Vard and Williams-Jones, 1993). A feature of the leachate data which is consistent with two sources of fluid is that, although there is abundant Ca, the concentration of Na is almost perfectly balanced by that of Cl, suggesting that Na and Cl were introduced separately from Ca, the fluids in equilibrium with carbonatite and phonolite melts, referred to above, are essentially Ca-free. Two sources of fluid are also suggested by the Sr isotope data (Deans and Powell, 1968, Simonetti and Bell, 1993) which show that the composition of fluorite (0.7082-0.71729) is intermediate between that of calcitite (0.70549-0.70628) and Bagh sandstone (0.7164-0.78274). It would thus appear that although the fluid was largely meteoric, it did include a small proportion of orthomagmatic fluid exsolved from the carbonatite.

In view of the above evidence for an ore fluid consisting of a mixture of meteoric and orthomagmatic fluids, we have tried to estimate the relative contributions of these two components. Application of the Lever Rule to mixing lines between meteoric water and magmatic water for Amba Dongar fluorite, on a plot of δD versus $\delta^{18}O$ (Fig. 3 20), shows that the fluid which deposited blue fluorite consisted of approximately 89-92% meteoric and 8-11% orthomagmatic water. The corresponding proportions of these fluids which deposited yellow fluorite are interpreted to have composed approximately 92-95% and 5-8%, respectively. The composition of the mixture can also be estimated by comparing the salinity of the fluid in this deposit with that of a pure orthomagmatic fluid. Samson *et al.* (in press) have determined that fluids exsolved from the carbonatite magma which formed the Oka complex contained approximately 15 wt.% NaCl eq. A similar composition was estimated by Vard and Williams-Jones for fluids exsolved from phonolite magma in the Francon

Quarry, Montreal. By contrast, the salinity of the fluids which deposited blue and yellow fluorite at Amba Dongar were 0.6 and 0.35 wt % NaCl eq., respectively. These data are consistent with a mixture comprising 92 and 95% salt-free meteoric water and 8 and 5% orthomagmatic water, respectively.

Log f_{O_2} -pH Conditions

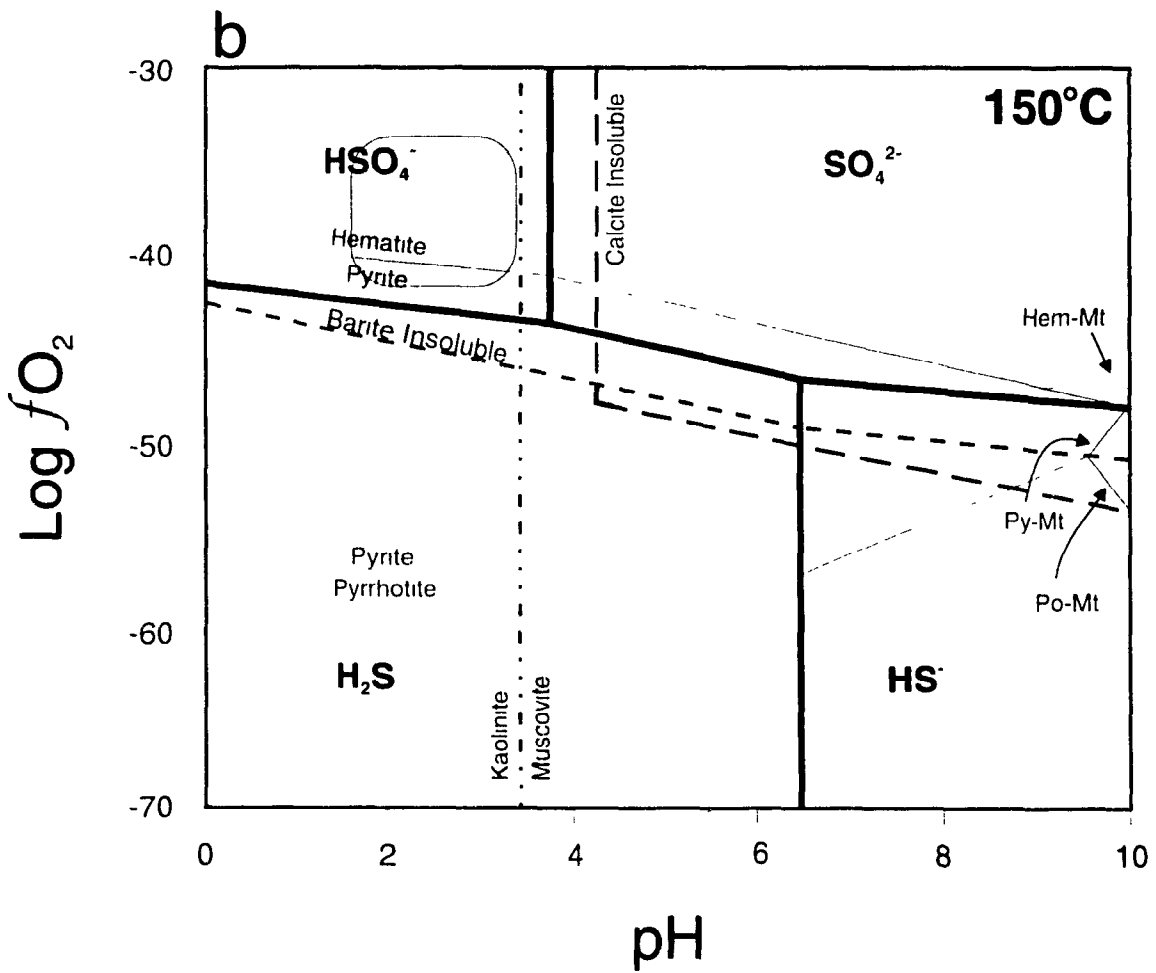
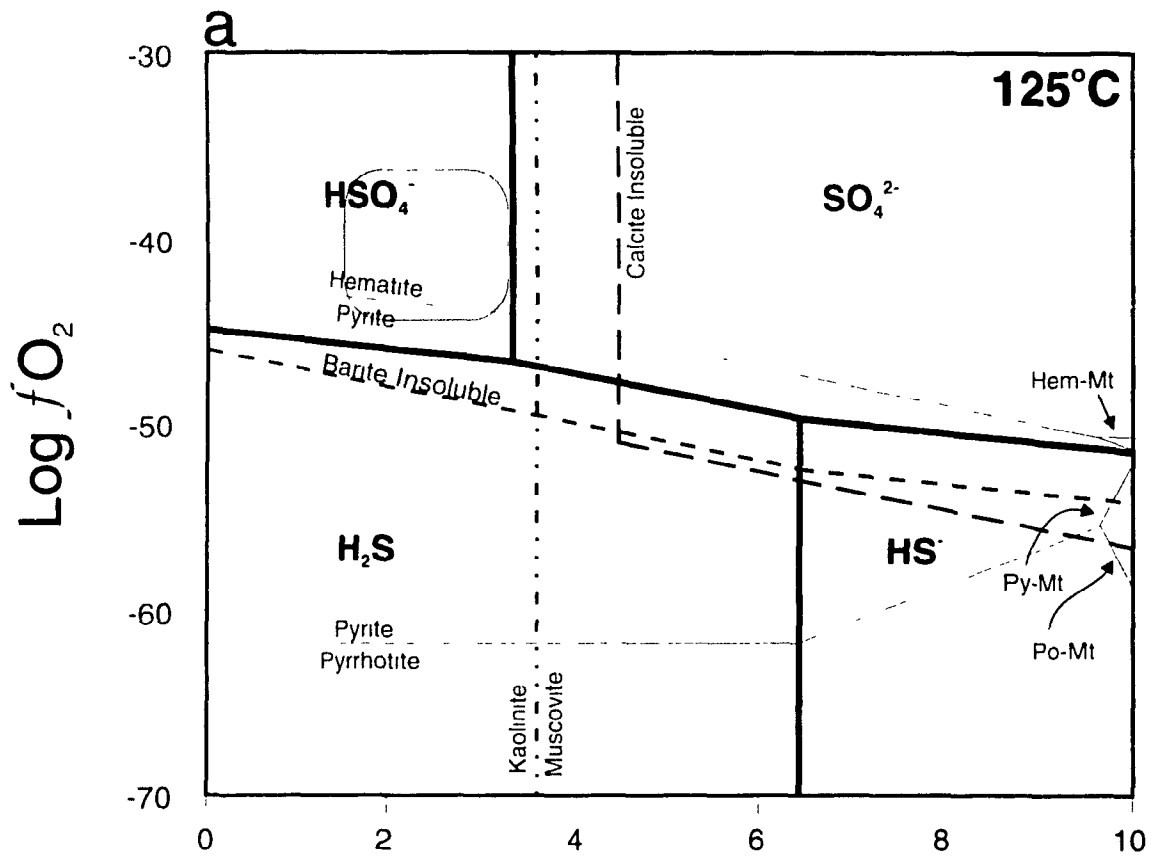
Log f_{O_2} -pH conditions during fluorite deposition have been estimated from the solubility and stability of several key minerals found in the deposit. The common occurrence of barite, in the early stage fluorite, requires that the fluid was saturated in this mineral. By contrast, calcite was removed in large quantities from the host rock meaning that the fluid was undersaturated with respect to this phase. The dominant Fe-bearing mineral, in all cases, is hematite, although rare pyrite and chalcopyrite has been observed in fluorite, which constrains log f_{O_2} -pH conditions to have been in the field of hematite stability, but close to the hematite-pyrite equilibrium boundary. Finally, the occurrence of a kaolinite group mineral as the only Al-bearing phase, in fluorite and quartz, implies that the pH conditions were below the kaolinite-muscovite boundary.

Log f_{O_2} -pH diagrams were constructed for temperatures of 125 and 150°C using log K values for the relevant mineral dissolution reactions, mineral stability equilibria and reactions amongst the aqueous sulfur species, calculated using the Supcrt92 software package and its thermodynamic database (Johnson *et al.*, 1991). The concentrations of Ca^{2+} , K^+ , S and Al were estimated from a combination of leachate, decrepitate and microthermometric data, to be 0.25, 0.01, 0.01 and 0.1 *m*, respectively, for blue fluorite (150°C) and 0.15, 0.01, 0.01

and 0.1 *m*, respectively, for yellow and colorless fluorite and quartz (125°C). The composition of the fluid which precipitated purple fluorite (150°C) is similar to that for blue fluorite, with the exception of S, which has a concentration of 0.1 *m*. The molality of dissolved carbon was estimated from the expansion of the vapor bubble on crushing of fluid inclusions and the equations in Barton and Chou (1993) to be 0.076 *m*, for both fluorite and quartz. The concentration of Ba²⁺ was arbitrarily assumed to be the same as that of ΣS.

Figures 3.21a and b show the probable log *f*O₂-pH conditions which existed at the time of fluorite deposition. Based on evidence of calcite dissolution and the presence of barite, hematite and a kaolinite group mineral, the conditions of fluorite deposition are constrained to a region of low pH and high *f*O₂ (pH <3.5, log *f*O₂ >-39 and -42, for blue and yellow fluorite, respectively). The high *f*O₂ is predictable given the shallow nature of the system, and is consistent with the lack of a negative Eu anomaly in fluorite. Owing to its large size, Eu²⁺ may be partitioned into early formed phases leaving the later stage fluids Eu-depleted, which gives REE profiles a negative Eu anomaly (Ekambaram *et al.*, 1986). However, under oxidizing conditions Eu²⁺ will convert to Eu³⁺ and can substitute for Ca, leaving a profile with either no anomaly or a positive anomaly, depending on the relative amounts of Eu²⁺ and Eu³⁺ (Whittaker and Muntus, 1970; Moller and Morteani, 1983; Constantopoulos, 1988). The low pH is also not unexpected given the low temperature, high *f*O₂ and high content of S of the fluid. Indeed, it is precisely these conditions that produce the very low pH fluids which are responsible for the formation of acid-sulfate epithermal Au deposits (Stoffregen, 1987). It is also worth noting that fluorite solubility is greatest at low pH (Richardson and Holland, 1979a) and that Al, which is relatively abundant in the fluid, is only mobile at either low or high

Figure 3.21 The fO_2 -pH stability fields of Fe-S-O minerals, calcite, barite, kaolinite, muscovite and the aqueous sulfur species at a) 125°C (yellow and colorless fluorite) and b) 150°C (blue and purple fluorite). Activities of ΣS , ΣC , Ba^{2+} , K^+ and Ca^{2+} in the ore fluid were determined to be 10^{-2} , 10^{-11} , 10^{-2} , 10^{-2} and $10^{-0.8}$, respectively, for yellow and colorless fluorite (125°C), and 10^{-1} , 10^{-11} , 10^{-1} , 10^{-1} and $10^{-0.6}$, respectively, for blue and purple fluorite (150°C). The shaded area in each of the diagrams represents the probable log fO_2 and pH conditions of the ore fluid at the time of fluorite deposition.

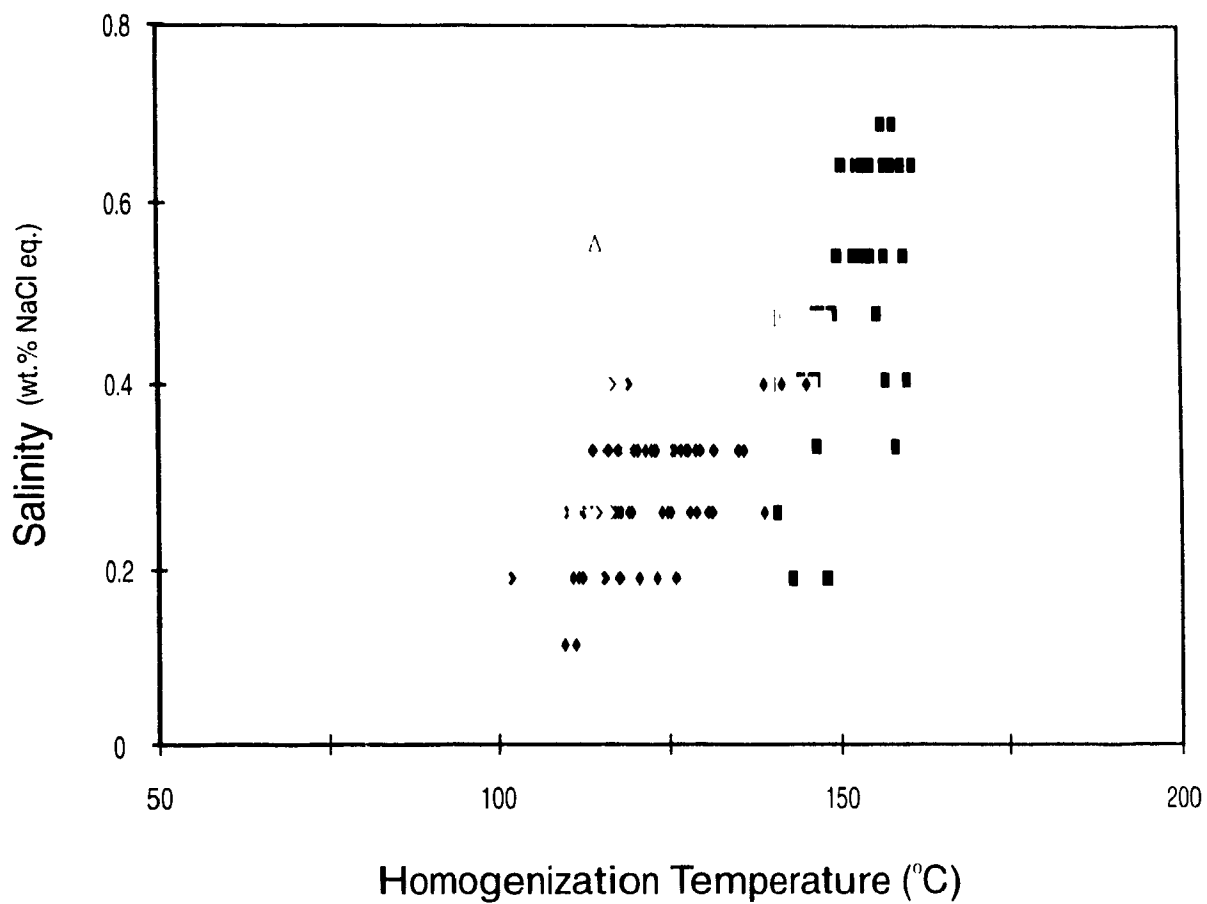


pH (Castet, 1991).

Fluid Evolution

The color zonation of fluorite (i.e. blue/purple \Rightarrow white \rightarrow yellow/colorless) suggests that fluids which deposited fluorite evolved during the mineralizing episode. This is confirmed by the microthermometric data obtained from fluid inclusions in the various varieties of fluorite. In a plot of salinity (wt.‰ NaCl eq.) versus temperature of homogenization for fluid inclusions from fluorite and quartz (Fig. 3.22), it is evident that salinity and temperature decreased from blue fluorite to colorless fluorite deposition. Fluid inclusions in quartz (from barren silicification) plot to the left of, and near the high salinity end of, the trend in Figure 3.22, i.e. they have a salinity similar to the fluid which deposited blue fluorite but were trapped at lower temperature. The trend of fluid evolution during fluorite deposition is a direct consequence of the fluid mixing model discussed above. In the context of this model the trend implies that the proportion of orthomagmatic fluid (high temperature, high salinity) was higher initially, and decreased during the later stages of fluorite deposition as the hydrothermal system became progressively more dominated by meteoric fluid. In keeping with the place of quartz in the paragenesis, the salinity of the quartz-hosted inclusions is similar to that of inclusions in blue fluorite. However, the temperature is unexpectedly low. We believe that the reason for this lies in the fact that this fluid was cooled by reacting with the cold calcite, whereas the slightly later fluid which deposited blue fluorite was not cooled. This is supported by the presence of vapor-rich, CO_2 inclusions in quartz (CO_2 released during the reaction of the acid ore fluid with the calcite), and the absence of these

Figure 3.22 A plot of salinity (wt.% NaCl eq.) versus homogenization temperature for fluid inclusions in fluorite and quartz.



FLUORITE

QUARTZ

■ BLUE

◆ YELLOW

BARREN VEINS

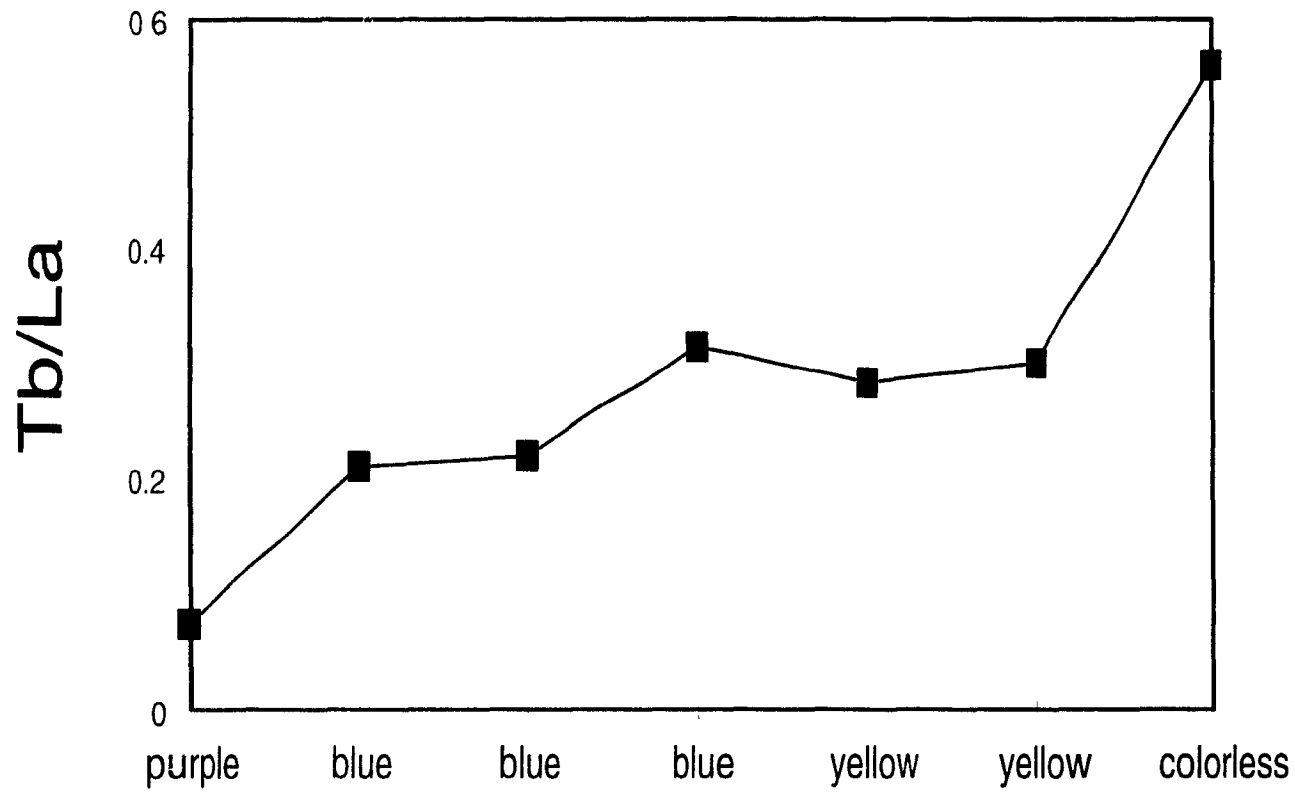
■ PURPLE

◆ COLORLESS

inclusions in fluorite, which grew in an open space environment. Although these data are based on barren-vein quartz, it is reasonable to assume that the quartz associated with fluorite and quartz from barren vein systems are one and the same, based on the evidence of fluorite replacement of silicification in the fluorite alteration zone.

The changing composition of the REE in fluorite can also be used to follow the evolutionary path of the fluid which precipitated fluorite. Although all varieties of the fluorite show strong HREE enrichment (Fig. 3.10), it is clear from the plot of Tb/La (Fig. 3.23) that this enrichment increases progressively from early blue and purple to late yellow and colorless fluorite (Tb is preferred to Lu as an indicator in fluorite because the coordination of Ca in fluorite restricts substitution of the very heaviest REE in the structure (Moller and Morteani, 1983)). Similar behavior has been reported by Collins and Strong (1992) for the St. Lawrence fluor spar district, Newfoundland. The higher proportion of La in the early blue and purple fluorite is readily explained by the relative stability of REE complexes. Wood (1990) has shown that REE form their strongest complexes with F, and that the stability of these complexes increases steadily from La to Lu. It is thus reasonable to conclude that the La-complex, being the weakest, would be the first to destabilize and thus cause substitution of La for Ca in the early blue and purple fluorite. With increasing dilution of the fluid and continued precipitation of fluorite, F⁻ activity would have decreased, thereby destabilizing progressively higher REE complexes. Therefore, based on REE composition, the chronological order of fluorite deposition is interpreted to be purple, blue, yellow and colorless, which is consistent with the zoning observed in the deposit.

Figure 3.23 A plot of Tb/La versus fluorite color showing the chemical evolution from early purple and blue fluorite to the later yellow and colorless varieties.



Transport and Deposition

The evidence presented earlier indicates that the fluorite at Amba Dongar was deposited from a fluid composed of a mixture of meteoric and orthomagmatic fluids from the surrounding sediments and the carbonatite, respectively. Moreover, the evidence also suggests that the orthomagmatic component supplied Na, Al, Fe, Ba, F, Cl and S, whereas the meteoric water was probably only responsible for providing calcium, strontium and CO₂, which it leached from calcite in the surrounding sandstones and limestones

A number of factors, i.e. [Ca²⁺] and [F⁻], temperature, salinity, pH, have been shown to influence fluorite solubility (Booth and Bidwell, 1950, MacDonald and North, 1974; Richardson and Holland, 1979a; Holland and Malinin, 1979) Fluorite solubility, in dilute NaCl solutions (<0.5 M NaCl), is at its highest in the temperature range 100 to 150°C. Lowering salinity and/or acidity has the effect of decreasing fluorite solubility.

As mentioned above, the fluid responsible for depositing fluorite at Amba Dongar was a low temperature (100-150°C), low salinity (<0.65 m), low pH (<3.6) mixture of two fluids, one carrying Ca and the other transporting F. Although temperature has a great effect on fluorite solubility, the temperatures of fluorite formation at Amba Dongar would preclude this as a limiting factor in fluorite deposition as this occurred at the temperature maximum of fluorite solubility. By contrast, mixing of the orthomagmatic, F-bearing fluid with large volumes of Ca-enriched meteoric fluids at the site of deposition could be a very effective method for depositing fluorite. Not only would the increase in calcium activity promote fluorite deposition but the dilution would decrease pH and salinity, further enhancing fluorite insolubility.

Depositional Model

A model is proposed in which a carbonatite magma was emplaced at shallow crustal levels (<500 m), based on thickness measurements of cover rocks and fluid inclusion data) into Deccan volcanics and Bagh sediments. Intrusion was accomplished as a series of ring dykes, formed as a result of an initial fluidization event which deposited the carbonatite breccia. Following this a number of distinct pulses of magma were injected, resulting in the formation of a calcite ring and numerous ankeritic carbonatite plugs. Emplacement of the carbonatite was accompanied by separation of volatiles from the melt which resulted in the development of large zones of potassic and sodic fenitization in the sandstone surrounding the carbonatite. The intrusion of the magma and the release of fluids produced numerous faults in the surrounding country rocks and the solidified sections of the carbonatite, typically at an angle perpendicular to the ring. The early orthomagmatic fluid, based on observations of fenite mineralogy and studies of other complexes, was composed predominantly of Na, K, Al, Cl and S. With the collapse of this system, a meteoric water-dominated system in the surrounding sediments became the principal hydrothermal unit, forming large convection cells, due to the heat from the intrusion. A silica-calcium bearing fluid was introduced into the carbonatite, along the previously formed fractures, where it mixed with, and oxidized, the small quantities of orthomagmatic brines which were still exsolving from the carbonatite magma. This produced a highly acidic fluid which dissolved carbonatite, replacing it with silica and small quantities of fluorite to produce zones of intense silicification. Water/rock ratios at this stage were low, and the interaction of this fluid with the cold carbonatite caused cooling, which helped promote silica deposition. In

some places the silica sealed the conduits, thereby terminating hydrothermal activity at these localities. Elsewhere, particularly along the outer margins of the carbonatite, the conduits remained open and further mixing of orthomagmatic and meteoric fluids caused open space deposition of fluorite at high water/rock ratios. Partly in response to the higher water/rock ratio and partly because of the insulating effects of the silicified wallrocks, temperature increased thereby largely terminating precipitation of quartz. With time, the fluid depositing fluorite became progressively more meteoric-dominated and temperature and salinity both decreased. The concentration of the elements, originating from the ore fluid, also decreased as a result of this dilution. The earliest fluorite to precipitate was the purple variety, followed closely by blue fluorite, this recorded the peak temperature and salinity, i.e. the height of late orthomagmatic inundation. The white fluorite, which was temporally next, marked the time when temperature decreased and pH increased to a level where the fluid became saturated with a kaolinite group mineral. The late yellow and colorless fluorite were deposited during the waning stages of orthomagmatic activity, when proportions of meteoric water were higher and temperatures and salinities were therefore lower. Fluorite deposition was finally halted as the orthomagmatic component was diminished to the point that the system was solely meteoric in composition. At this time, the fluid locally deposited small amounts of quartz on the surface of fluorite.

Comparison To Other Deposits

A small number of carbonatite hosted fluorite deposits are known throughout the world. The Okorusu deposit, Namibia is similar to Amba Dongar,

both in geological setting and size. Fluid Inclusion studies performed on inclusions in fluorite from this deposit indicate that the fluid which precipitated fluorite was of low temperature (<160°C), moderate salinity (≈ 5 wt % NaCl eq., based on freezing point depression) and low CO₂ content (<0.2 m) (Roedder, 1973). The Mato Preto deposit, Brazil is of lower tonnage but significantly higher grade (Table 3.1) Fluid Inclusion studies of fluorite from this deposit reveal that the ore fluid was of low temperature (<120°C, although fluid inclusions in "remobilized ore" gave much higher temperatures, ranging between 220 and 260°C) and low to moderate salinity (0-15 wt.% NaCl eq.) (Santos, 1988). Fluorite deposits hosted by carbonatites in Tuva and Eastern Sayan are similar to Amba Dongar in geological setting, but show vastly different fluid properties. Fluid inclusion studies of fluorite from these deposits indicate that the ore fluid was of high temperature (200-500°C) and high salinity (20-50 wt.% NaCl eq.), i.e. dominantly orthomagmatic in origin.

From these few studies it would appear that carbonatite-hosted fluorite deposits show a wide range in the composition of the fluids responsible for their formation. However it can be observed that the lower temperature deposits have consistently lower salinities. In view of this, and the fact that the deposits all have similar geological setting, it is probable that they differ from one another only in the proportions of orthomagmatic fluids that were involved in deposition. It would thus seem that the model developed for the formation of Amba Dongar is applicable to carbonatite-hosted fluorite deposits in general.

Conclusions

The Amba Dongar fluorite deposit consists of 11.6 mt of 30% CaF₂ as

veins and vug fillings, and is hosted by a carbonatite ring dyke which was intruded, at shallow levels, into Late Cretaceous Bagh sandstones and Late to Early Eocene Deccan basalts. From the results of geochemical, fluid inclusion and stable isotopic studies it can be concluded that the ore fluid consisted of a mixture of meteoric and orthomagmatic fluids and was of low temperature (<160°C) and low salinity (<0.65 wt % NaCl). The meteoric fluid, which dominated the system, was responsible for providing Ca, while orthomagmatic fluids provided F. The mixing of a S-bearing, orthomagmatic fluid with an oxidizing meteoric water produced very acidic conditions under which silicification of the calcitite took place, this was followed by deposition of fluorite at the site of mixing, near the contact between the sandstone and the carbonatite.

CHAPTER IV: CONCLUSIONS

General Conclusions

The Amba Dongar deposit belongs to a poorly understood class of carbonatite-hosted fluorite deposits. The principal conclusions of this study are:

- 1) The Amba Dongar complex consists of a ring structure intrusion of carbonatite breccia, calcitite and ankeritic carbonatite, and a number of randomly dispersed syenitic plugs. These were intruded into Late Cretaceous Bagh sandstones and Late to Early Eocene Deccan volcanics, at shallow crustal levels (<500 m).
- 2) An initial stage of hydrothermal activity resulted in extensive potassic and sodic fenitization of the surrounding sandstones by orthomagmatic fluids exsolved from the carbonatitic magma during emplacement.
- 3) A later hydrothermal system resulted in extensive silicification of the host calcitite and deposition of vast amounts of fluorite, as veins and vug fillings, in the calcitite, near its contact with sandstone. During fluorite deposition, early quartz in the wallrock was partially replaced by fluorite. The fluorite occurs in purple, blue, white, yellow and colorless varieties, which were deposited in that order.
- 4) Fluorite deposition was localized along faults and fractures in the calcitite, formed during emplacement of the carbonatite and by overpressure

caused by the earlier fenitizing fluid.

- 5) Silicification and fluorite deposition were caused by a low temperature (<160°C), low salinity (<0.65 wt % NaCl eq) fluid. Log f_{O_2} and pH conditions of the ore fluid, at the time of deposition, were greater than -4.2 and less than 3.5, respectively
- 6) Oxygen, hydrogen and carbon isotopic data for fluids from fluid inclusions in fluorite indicate that the ore fluid was dominantly meteoric, and that it had equilibrated with sedimentary limestones
- 7) Chemical analyses of fluid inclusion leachates and decrepitate residues from fluorite and quartz show significant concentrations of Ca, Al and S, in addition to Na and Cl, in the ore fluid
- 8) The small positive departure of the fluorite hosted fluid from the meteoric water line, and the significant amounts of Al, S, Na and Cl in solution, suggest a small contribution of orthomagmatic fluids to the ore-forming fluid.
- 9) The initial mixing of the orthomagmatic fluid with an oxidizing meteoric water produced a fluid with high acidity, causing intense silicification of the host calcite. The interaction of this fluid with the cold carbonatite, at low water/rock ratios, resulted in cooling. Silicification provided an insulating layer for later fluids, allowing for higher temperatures
- 10) Fluorite deposition resulted from the interaction of a Ca-bearing meteoric

fluid with a F-bearing orthomagmatic fluid, at high water/rock ratios, at the site of mixing. The increase in pH as a result of this dilution enhanced fluorite deposition.

Contributions to Knowledge

- 1) This study provides the first comprehensive investigation of: 1) of the fluids involved in the formation of a carbonatite-hosted fluorite deposit; and 2) the physico-chemical controls of fluorite deposition in this environment.
- 2) An interesting conclusion of this study is that the Ca in the fluorite was derived from an external source and not, as might be expected, from the carbonatite. The orthomagmatic fluids, as implied by this study and shown by other recent studies of carbonatites and associated silicate magmas, are NaCl brines with elevated concentrations of Al and S.
- 3) The very low solubility of fluorite requires that Ca and F be transported separately. It therefore follows that formation of economic carbonatite-hosted fluorite deposits is favored by settings in which the exsolved orthomagmatic fluids have access to external Ca-bearing fluids.
- 4) Carbonatite-hosted fluorite deposits, other than those interpreted to be primary magmatic in origin, appear to differ only in the proportions of meteoric and orthomagmatic fluids in the ore forming fluid. Therefore, the results of this study can be applied to other deposits of the same affinity.

REFERENCES

- Andersen, T., 1986, Magmatic fluids in the Fen carbonatite complex, S.E. Norway: *Contrib. Mineral. Petrol.*, v. 93, p. 491-503.
- Andersen, T. and Austrheim, H., 1991, Temperature-HF fugacity trends during crystallization of calcite carbonatite magma in the Fen complex, Norway: *Mineralogical Magazine*, v. 55, p. 81-94.
- Barbieri, M., Tolomeo, L., and Voltaggio, M., 1983, Yttrium, lanthanum, and manganese geochemistry in fluorite deposits from Sardinia (Italy): *Chem. Geol.*, v. 40, p. 43-50.
- Barton, P.B., and Chou, I.M., 1993, Refinement of the evaluation of the role of CO₂ in modifying estimates of the pressure of epithermal mineralization: *Economic Geology*, v. 88, p. 873-884.
- Bigeleisen, J., Perlman, M.L., and Prosser, H.C., 1952, Conversion of hydrogenic materials to hydrogen for isotopic analysis: *Analytical Chemistry*, v. 24, p. 1356.
- Booth, H.S. and Bidwell, R.M., 1950, Solubilities of salts in water at high temperatures: *J. Am. Chem. Soc.*, v. 72, p. 2567-2575.
- Bose, P.K. and Das, N.G., 1986, A transgressive storm- and fair-weather wave dominated shelf sequence: Cretaceous Nimar Formation, Chakrud, Madhya Pradesh, India: *Sedimentary Geology*, V. 46, p. 147-167.
- Bottinga, Y., 1968, Calculation of fractionation factors for carbon and oxygen isotopic exchange in the system calcite-carbon dioxide-water: *The Journal of Physical Chemistry*, v. 72, (3), p. 800-807.
- Bottrell, S.H., Yardley, B., and Buckley F., 1988, A modified crush-leach method for the analysis of fluid inclusion electrolytes: *Bull. Mineral.*, v. 111, p. 279-290.
- Boynnton, W.V., 1983, Cosmochemistry of the rare earth elements: meteorite studies: in P. Henderson (ed.), *Rare Earth Element Geochemistry, Developments in Geochemistry*, 2nd ed., Elsevier Science Publishers, Amsterdam, p. 63-114.

- Bredikhina, S.A., and Bobrov, V.A., 1993, REE in fluorites from carbonatite deposits, *in* P. Fenoo Hach-Ali, J. Torres-Ruiz and F Gervilla (eds), Current Research in Geology Applied to Ore Deposits (Supplementary Abstracts): Proceedings of the second biannual S.G.A. Meeting, Granada, p.S1-S4
- Castet, S., 1991, Solubilité de la boehmite et spéciation de l'aluminium dissous dans les solution aqueuses à haute température (90-350C) détermination expérimentale et modélisation: unpublished Ph.D. Thesis, Paul Sabatier University, Toulouse, France, 116p.
- Chatterjee, S.C., 1964, An alkaline-olivine basalt sub-province in the Deccan Traps: In: Proceedings of the 22nd International Geological Congress, New Delhi, Pt. 7, p. 35-41.
- Chiplonkar, G.W., Ghare, M.A. and Badve, R.M., 1977, Bagh Beds - their fauna, age and affinities: A retrospect and prospect. *Biovigyanam*, v. 3, p. 33-60
- Collins, C.J., and Strong, D.F., 1992, The distribution of REE in hydrothermal vein fluorite and calcitite from the St. Lawrence fluorspar district, Newfoundland GAC-MAC Abstracts, v. 17, p.A19-A20.
- Constantopoulos, J., 1988, Fluid inclusions and rare earth element geochemistry of fluorite from South-Central Idaho: *Economic Geology*, v. 83, p. 626-636.
- Courtillot, V.F., Maluski, H., Vandamme, D., Moreau, M.G. and Besse, J., 1988, Deccan flood basalts and the Cretaceous-Tertiary boundary. *Nature*, v. 333, p. 843-846
- Currie, K.L. and Ferguson, J., 1971, A study of fenitization around the alkaline complex at Callender Bay, Ontario, Canada: *Canadian Journal of Earth Sciences*, v. 8, p. 498-517.
- Dawson, J.B., 1989, Sodium carbonatite extrusions from Oldoinyo Lengau, Tanzania. implications for carbonatite complex genesis: *in* K. Bell (ed.), *Carbonatites: genesis and evolution*: London, Unwin Hyman, p 255-276.
- Deans, T., and Powell, J.L., 1968, Trace elements and strontium isotopes in carbonatites, fluorites and limestones from India and Pakistan: *Nature*, v. 218, p. 750-752.
- Deans, T., Sukheswala, R.N., Sethna, S.F. and Viladkar, S.G., 1972, Metasomatic feldspar rocks (potash fenites) associated with the fluorite deposits and carbonatites of Amba Dongar, Gujarat, India: *Trans. Inst. Min. Metall. (sect. B. earth sci.)*, v. 81, p. B1-B9.

- Deans, T., Sukheswala, R.N., Sethna, S.F. and Viladkar, S.G., 1973, Metasomatic feldspar rocks (potash fenites) associated with the fluorite deposits and carbonatites of Amba Dongar, Gujarat, India: Discussion and contributions: Trans. Inst. Min. Metall. (sect B: earth sci), v 82, p. B33-B40.
- Dietz, R.S. and Holden, J.C., 1970, Reconstruction of Pangaea: breakup and dispersion of continents, Permian to Present: J. Geophys. Res., v. 75 (26), p. 4939-4956.
- Eggler, D.H., 1989, Carbonatites, primary melts, and mantle dynamics: in Bell, K., ed., Carbonatites: genesis and evolution: London, Unwin Hyman, p.149-176.
- Ekambaram, V, Brookins, D.G, Rosenberg, P.E., and Emanuel, K.M., 1986, Chemical Geology, v. 54, p. 319-331.
- Flegg, A.M., Clarke, M.C.G., Sutherland, D.S. and Le Bas, M.J., 1977, Homa Mountain II: The main carbonatite center: in M.J. Le Bas (ed.), Carbonatite-Nephelinite Volcanism: An African case history: Wiley-Interscience, Toronto, p. 222-232.
- Ganzeyev, A. A, and Sotskov, Y. P., 1976, Rare earth elements in fluorites of different origin: Geokhimiya, No. 3, p. 390-395.
- Gittins, J., 1989, The origin and evolution of carbonatite magmas: in Bell, K., (ed.), Carbonatites: genesis and evolution: London, Unwin Hyman, p.149-176.
- Gittins, J., Beckett, M F., and Jago, 1990, Composition of the fluid accompanying carbonatite magma: A critical examination, American Mineralogist, v. 75, p. 1106-1109.
- Grant, J.A., 1986, The isocon diagram-a simple solution to Gresens' equation for metasomatic alteration: Economic Geology, v. 81, p. 1976-1982.
- Gresens, R.L., 1967, Composition-volume relationships of metasomatism: Chem. Geol. v 2, p. 47-65
- Gupta, M.L. and Gaur, V.K., 1984, Surface heat flow and probable evolution of Deccan volcanism. Tectonophysics, v. 105, p. 309-318.
- Gwalani, M.L., 1981, Petrology of Deccan Traps and Bagh beds of Dugdha-Naswadi, Gujarat: Somaiya Publications, Bombay, 107p..
- Gwalani, L.G., Rock, N.M.S., Chang, W.J., and Fernandez, S., 1993, Alkaline rocks and carbonatites of Amba Dongar and adjacent areas, Deccan Igneous Province, Gujarat, India: 1. Geology, Petrography and Petrochemistry: Mineralogy and Petrology, v. 47, p. 219-253.

- Hall, W.E. and Friedman, I., 1963, Composition of fluid inclusions, Cave-in Rock fluorite district, Illinois and Upper Mississippi Valley zinc-lead district: *Economic Geology*, v. 58, p. 886-911.
- Hamilton, D.L., Bedson, P., and Esson, J., 1989, The behavior of trace elements in the evolution of carbonatites: in K. Bell (ed), *Carbonatites: genesis and evolution*: Unwin Hyman, London, p.405-427.
- Haynes, F.M., Sterner, S.M., and Bodnar, R.J., 1988, Synthetic fluid inclusions in natural quartz.IV. Chemical analyses of fluid inclusions by SEM/EDA: Evaluation of method: *Geochim. et Cosmochim. Acta*, v. 52, p. 969-977.
- Hedenquist, J.W. and Henley, R.W., 1985, The importance of CO₂ on freezing point measurements: Evidence from active geothermal systems and implications for epithermal ore deposition: *Economic Geology*, V. 80, p. 1379-1406.
- Hein, U. F., Möller, P., and Schneider, H.-J., 1984, Rare earth element fractionation in fluorite as a geochemical indicator of ore deposition in Triassic carbonate rocks of the Eastern and Southern Alps: *N. Jb. Miner. Mh* , p 305-316.
- Heinrich, E.Wm., 1966, *The Geology of Carbonatites*. Rand McNally & Company, Chicago, 553p.
- Hogarth, D.D., 1989, Pyrochlore, apatite and amphibole. distinctive minerals in carbonatite: in K. Bell (ed), *Carbonatites: genesis and evolution*. Unwin Hyman, London, p.105-148.
- Holland, H.D., and Malinin, S.D., 1979, The solubility and occurrence of non-ore minerals: in H.L. Barnes (ed.), *Geochemistry of hydrothermal ore deposits*, Wiley-Interscience, Toronto, p. 461-508.
- Jago, B.C. and Gittins, J., 1991, The role of fluorine in carbonatite magma evolution, *Nature*, v. 349, p. 56-58.
- Johnson, B.D., Powell, C.McA., and Veevers, J.J., 1976, Spreading history of the eastern Indian Ocean and Greater India's northward flight from Antarctica and Australia: *Geol. Soc. Am. Bull.*, v. 87, p. 1560-1566.
- Johnson, J.W., Oelkers, E.H., and Helgeson, H.C., 1991, Supcrt92: a software package for calculating the standard molal thermodynamic properties of minerals, gases, aqueous species, and reactions from 1 to 5000 bars and 0° to 1000°C: developed at the Earth Sciences Department, Lawrence Livermore National Laboratory and Department of Geology and Geophysics, University of California, Berkeley.

- Jones, A.P. and Wyllie, P.J., 1983, Low-temperature glass quenched from a synthetic, rare earth element carbonatite: implications for the origin of the Mountain Pass Deposit, California. *Economic Geology*, v. 78, p. 1721-1723.
- Karkare, S.G. and Srivastava, R.K., 1990, Regional dyke swarms related to the Deccan Trap Alkaline province, India: *in* A.J. Parker, P.C. Rickwood and D.H. Tucker (eds.), *Mafic Dykes and Emplacement Mechanisms, Proceedings of the Second International Dyke Conference, Adelaide, South Australia, September, 1990*, p. 335-347.
- Kaul, K., Rao, C.N., Sanyal, T., and Akhtar, S.H., 1988, Fluorite crystallization temperatures: evidence from thermoluminescence characteristics and fluid inclusion studies; *Indian Journal of Geology*, v. 60, (4), p. 258-265.
- Kessen, K.M., Woodruff, M. S., and Grant, N. K., 1981, Gangue mineral $^{87}\text{Sr}/^{86}\text{Sr}$ ratios and the origin of Mississippi Valley-type mineralization: *Econ. Geol.*, v. 76, p. 913-920.
- Kishima, N , and Sakai, H., 1980, Oxygen-18 and deuterium determination on a single water sample of a few milligrams: *Analytical Chemistry*, v. 52, p. 356-358.
- Krishnamurthy, R.V., and Bhattacharya, S.K., 1991, Stable Oxygen and Hydrogen isotope ratios in shallow ground waters from India and a study of the evapotranspiration in the Indian monsoon: *in* H.P. Taylor, J.R. O'Neil, and I.R. Kaplan (eds.), *Stable isotope Geochemistry: A tribute to Samuel Epstein: The Geochemical Society, San Antonio*, p. 187-194.
- Krishnan, M.S., 1982, *Geology of India and Burma: CBS Publishers and Distributors*, 536p.
- Kuellermer, F.J., Visocky, A.P. and Tuttle, O.F., 1966, Preliminary survey of the system barite-calcite-fluorite at 500 bars: *in* O.F. Tuttle and J. Gittins (eds.), *Carbonatites: Wiley-Interscience, New York*, p. 353-364.
- Lahiry, A., 1976, Observations on fluorspar mineralization at Amba Dongar, Gujarat based on fluid inclusion data: *Indian Journal of Earth Sciences*, v. 3, (1), p. 37-43.
- Le Bas, M.J., 1989, Diversification of Carbonatites: *in* K. Bell (ed.), *Carbonatites: genesis and evolution: Unwin Hyman, Boston*, p. 428-447.
- Le Bas, M.J. and Rubie, D.C., 1977. Kisingiri I: An ijolite-carbonatite-nephelinite volcanic complex in western Kenya: *in* M.J. Le Bas (ed.), *Carbonatite-nephelinite volcanism: John Wiley and Sons, Toronto*, p. 39-46.
- MacDonald, R.W. and North, N.A., 1974, The effect of pressure on the solubility of CaCO_3 , CaF_2 , and SrSO_4 in water: *Can. J. Chem.*, v. 52, p. 3181-3186.

- MacLean, W.H. and Kranidiotis, P., 1987, Immobile elements as monitors of mass transfers in hydrothermal alterations: Phelps Dodge massive sulfide deposit, Matagami, Quebec: *Economic Geology*, v. 82, p. 951-962
- Mariano, A.N., 1989, Nature of economic mineralization in carbonatites and related rocks: in K. Bell (ed.), *Carbonatites: genesis and evolution*: Unwin Hyman, London, p.149-176.
- Möller, P., and Morteani, G., 1983, On the geochemical fractionation of rare earth elements during the formation of Ca-minerals and its application to problems of the genesis of ore deposits: in Augustithis, S. S., ed., *The significance of trace elements in solving petrogenetic problems*, Athens, Theophrastus, p. 747-791.
- Oakes, C.S., Bodnar, R.J., and Simonson, J.M., 1990, The system NaCl-CaCl₂-H₂O; I. The ice liquidus at 1 atm. total pressure: *Geochim. Cosmochim. Acta*, v. 54, p. 603-610.
- Ohmoto, H., and Rye., R.O., 1979, Isotopes of sulfur and carbon: in H.L. Barnes (ed.), *Geochemistry of hydrothermal ore deposits*, Wiley-Interscience, Toronto, p. 509-567.
- Potter, R.W., II, Clyne, M.A., and Brown, D.L., 1978, Freezing point depression of aqueous sodium chloride solutions: *Economic Geology*, V. 73, p 284-285.
- Poty, B.P., Stalder, H.A., and Weisbrod, A.M., 1974, Fluid inclusion studies in quartz from fissures of Western and Central Alps: *Schweiz. Mineral. Petrogr. Mitt.*, v 54, p. 717-752.
- Puzanov, L.S., 1975, Genesis of fluorite-barite-iron ore mineralization in Tuva: *Doklady Akademii Nauk SSSR*, v. 225, (3), p. 669-672.
- Puzanov, L.S., 1977, Origin of fluorite mineralization in carbonatite of the Bol'shaya Tagna pluton, Eastern Sayan: *Doklady Akademii Nauk SSSR*, v. 233, (3), p. 463-466.
- Reynolds, T.J., 1992, Fluid Inc. adapted U.S.G.S. gas-flow heating/freezing system, Instruction manual.
- Richardson, C. and Holland, D., 1979a, The solubility of fluorite in hydrothermal solutions, an experimental study: *Geochimica et Cosmochimica Acta*, v. 43, p. 1313-1325.
- Richardson, C. and Holland, H.D., 1979b, Fluorite deposition in hydrothermal systems: *Geochimica et Cosmochimica Acta*, v. 43, p. 1327-1335.

- Richet, P., Bottinga, Y., and Jovy, M., 1977, A review of hydrogen carbon, nitrogen, oxygen, sulphur and chlorine stable isotope fractionation among gases molecules: *Ann. Rev. Earth Planet. Sci.*, v. 5, p. 65-110.
- Roedder, E., 1958, Technique for the extraction and partial chemical analysis of fluid-filled inclusions from minerals: *Economic Geology*, v. 53, (3), p. 235-266.
- Roedder, E., 1973, Fluid inclusions from the fluorite deposits associated with carbonatite at Amba Dongar, India, and Okorusu, South West Africa: Metasomatic feldspar rocks (potash fenites) associated with the fluorite deposits and carbonatites of Amba Dongar, Gujarat, India: Discussion and contributions: *Trans. Inst. Min. Metall. (sect. B: earth sci)*, v. 82, p. B35-B39.
- Roedder, E., 1984, Fluid Inclusions: Reviews in Mineralogy Vol. 12, P.H. Ribbe (ed.), Mineral. Soc. Am., 644p.
- Roedder, E., Heyl, A V and Creel, J.P., 1968, Environment of ore deposition at the Mex-Tex deposits, Hansonbourg district, New Mexico, from studies of fluid inclusions: *Economic Geology*, v. 63, p. 336-348.
- Ronchi, L. H., Touray, J.-C., Michard, A., and Dardenne, M. A., 1993, The Ribeira fluorite district, southern Brazil: *Mineral. Deposita.*, v. 28, p. 240-252.
- Ruiz, J., Kesler, S. E., Jones, L. M., and Sutter, J. F., 1980, Geology and geochemistry of the Las Cuevas fluorite deposit, San Luis Potosi, Mexico: *Econ. Geol.*, v. 75, p. 1200-1209.
- Samson, I.M., Weining, L., and Williams-Jones, A.E., The nature of orthomagmatic hydrothermal fluids in the Oka carbonatite, Quebec: evidence from fluid inclusions: *Geochim. Cosmochim. Acta*, (in press).
- Santos, R.V., 1988, Geologia e geoquímica do depósito de fluorita do complexo alcalina carbonatítico de Mato Preto-Parana: M.Sc. Thesis no.47, Brasilia University.
- Simonetti, A., and Bell, K., 1993, Nd, Pb and Sr isotopic data from the fluorite mineralization at Amba Dongar, Gujarat, India: EUG VII, Terra Nova Abstract Supplement 2, p. 48.
- Srivastava, R.K., 1989, Evolution of alkaline carbonatitic complex of Ambadungar, District Baroda, Gujarat: *Indian Journal of Geochemistry*, v. 4, (1), p. 1-38.
- Srivastava, R.K., and Karkare, S.G., 1989, Sulphide mineralization around Ambadungar, Baroda District, Gujarat: *Current Science*, v. 59, (17), p. 962-964.

- Srivastava, R.K., and Karkare, S.G., 1991, Economic potential of the alkaline carbonatitic complex of Ambadungar, District Baroda, Gujarat.: The Mining, Geological and Metallurgical Institute of India, v. 88, (2), p. 94-112.
- Stoffregen, R., 1987, Genesis of acid-sulfate alteration and Au-Cu-Ag Mineralization at Summitville, Colorado: *Economic Geology*, v. 82, p.1575-1591.
- Strong, D. F., Fryer, B. J., and Kerrich, R., 1984, Genesis of the St. Lawrence Fluorspar deposits as indicated by fluid inclusion, rare earth element, and isotopic data: *Econ. Geol.*, v. 79, p. 1142-1158.
- Sukheswala, R.N. and Udas, G.R., 1963, Note on the carbonatite of Amba Dongar (Gujarat State) and its economic potentialities: *Science and Culture*, v. 29, p. 563-568.
- Sukheswala, R.N., Sirivastava, A.N., Mahambre, S.J. and Gwalani, L.G., 1976, Geology of Bakhatgarh-Phulmahal and Dugdha-Naswadi sectors in the Malwa region of the lower Narmada valley: In: Report on the geology of the Deccan Trap in southern part of Malwa Region, University Grants Commission, India, 19p..
- Taylor, H.P. Jr., 1979, Oxygen and hydrogen Isotope relationships in hydrothermal mineral deposits: *in* H.L. Barnes (ed.), *Geochemistry of hydrothermal ore deposits*, Wiley-Interscience, Toronto, p. 236-277
- Taylor, R.G. and Pollard, P.J., 1985, Pervasive hydrothermal alteration in tin-bearing granites and implications for the evolution of ore-bearing magmatic fluids *in* R.P. Taylor and D.F. Strong (eds.), *Recent advances in the geology of granite-related mineral deposits: Special volume 39, Canadian Inst. of Min. and Metall.*, p. 86-95.
- Treiman, A.H. and Essene, E.J., 1984, A periclase-dolomite-calcite carbonatite from the Oka complex, Quebec, and its calculated volatile composition: *Contrib. Mineral. Petrol.*, v. 85, p. 149-157.
- Vard, E., and Williams-Jones, A., 1993, A fluid inclusion study of vug in dawsonite-altered phonolite sills, Montreal, Quebec: implications for HFSE mobility: *Contrib. Mineral. Petrol.*, v. 113, p. 410-423.
- Viladkar, S.G., 1981, The carbonatites of Amba Dongar, Gujarat, India: *Bulletin of the Geological Society of Finland*, v. 53, p. 17-28.
- Viladkar, S.G., 1984, Alkaline rocks associated with the carbonatites of Amba Dongar, Chhota Udaipur, Gujarat, India: *The Indian Mineralogist*, p. 130-135.

- Viladkar, S.G., 1986, Fenitization at the Amba Dongar Carbonatite alkalic complex, India: *in* M. Gabriel (ed), Symposium New Mineral Raw Materials: Proceedings, p. 170-189.
- Viladkar, S G and Wimmenauer, W., 1992, Geochemical and Petrological Studies on the Amba Dongar Carbonatites (Gujarat, India): *Chem Erde*, v. 52, p. 277-291.
- Wadia, D.N., 1957, *Geology of India (3rd Ed.)*: MacMillan, London.
- Wellman, P. and McElhinny, M.W., 1970, K-Ar age of the Deccan Trap, India: *Nature*, v. 227, p. 595-596.
- Whittaker, E.J W., and Muntus, R., 1970, Ionic radii for use in geochemistry, *Geochim. Cosmochim. Acta*, v. 34, p. 945-956.
- Wood, S.A , 1990, The aqueous geochemistry of the rare-earth elements and yttrium: 1. Review of available low-temperature data for inorganic complexes and the inorganic REE speciation of natural waters: *Chemical Geology*, v. 82, p. 159-186.
- Woolley, A.R., 1989, The spatial and temporal distribution of carbonatites. *in* K. Bell (ed.), *Carbonatites: genesis and evolution*: London, Unwin Hyman, p. 15-37.
- Woolley, A.R. and Kempe, D.R.C., 1989, Carbonatites: nomenclature, average chemical compositions, and element distribution: *in* K. Bell (ed.), *Carbonatites: genesis and evolution*: London, Unwin Hyman, p.1-37.
- Wyllie, P.J., 1989, Origin of carbonatites: evidence from phase equilibrium studies: *in* K. Bell (ed.), *Carbonatites: genesis and evolution*: London, Unwin Hyman, p.149-176.
- Wyllie, P J. and Tuttle, O.F., 1960, The system CaO-CO₂-H₂O and the origin of carbonatites. *Journal of Petrology*, v. 1, p. 1-46.
- Zhou, Z., Li Gongyuan, Sung Tongyun and Liu Yuguan, 1980, On the geological characteristics and the genesis of the dolomitic carbonatites at Bayan, Obo, Inner Mongolia: *Geological Review*, v. 26, (1), p. 35-42.

APPENDIX

Analytical Equipment and Methodology

Fluid Inclusion Microthermometry

Microthermometric studies were undertaken on primary fluid inclusions in fluorite from all parts of the deposit, and elsewhere in the complex, quartz from quartz veins associated with silicification, and quartz associated with fluorite mineralization. Analyses were performed on a Fluid Inc. modified U S G S. gas flow heating/freezing system (Reynolds, 1992). Calibration was accomplished using synthetic CO₂ and H₂O inclusions. With this method of calibration, accuracies of +/- 0.2°C for subzero temperatures and +/- 1.0°C for higher temperatures were achieved.

Owing to the soft nature of fluorite, heating experiments were performed first to minimize stretching of the inclusions, which occurs as a result of ice expansion during cooling.

Leachate Analyses

Samples were prepared and the fluids extracted using the methods of Roedder (1958) and Poty *et al.* (1974). However, because of the high solubility of fluorite in acid solutions, samples were cleaned using nanopure water rather

than dilute HCl and HNO₃ as recommended by these authors. Recently, Bottrell *et al.* (1988) have drawn attention to the problem of adsorption of doubly charged cations on the host mineral. They have therefore recommended the use of a 0.13M HNO₃ + 200 ppm LaNO₃ leachate solution to minimize these problems. Because of the solubility of fluorite in this solution, it was, however, necessary to use nanopure water.

Samples consisted of 4g aliquots of sieved and hand-separated quartz or fluorite. They were cleaned, over a period of 14 days, in nanopure water which was changed every two days. Prior to crushing, samples were placed in an ultrasonic bath. In this step the nanopure water was replaced every ten minutes. Samples were then heated to 80°C, in order to drive off all traces of the cleaning solution. Crushing was then performed in an agate mortar and pestle with the sample submerged in 10 ml of nanopure water, which acted as the leachate medium. Blanks were prepared by running 10 ml of nanopure water over the clean, uncrushed sample. Analyses for Na, K, Ca, Mg and Fe were carried out by flame atomic absorption spectrophotometry, Al by graphite furnace atomic absorption spectrophotometry and Cl, F, SO₄, P₂O₅ and Br by ion chromatography.

Decrepitate Analyses

Semi-quantitative analyses of precipitates from opened fluid inclusions in blue, purple and yellow fluorite, and quartz were performed using a JSM-840A scanning electron microscope with a Tracor Northern energy dispersive x-ray spectrometer. The system was equipped with an extra thin Al window thereby allowing the detection of elements as light as C (A=6). The analyses were accomplished using the technique of Haynes *et al.* (1988). Doubly polished thin

sections were cleaned and heated until the fluid inclusions decrepitated. They were then coated with carbon and analyzed immediately. Analyses were conducted using a rastering method, in order that a large area of the decrepitate residue would be analyzed. Owing to the inherent errors of analyzing for Ca on a Ca-bearing substrate, such as fluorite, a number of chips were decrepitated onto silica plates. The polished sample was placed on a silica-glass plate and heated. Fluids from decrepitated inclusions leaked onto the plate and precipitated solids (Fig. 3.19A). These solids were then coated with carbon and analyzed in the same manner as those precipitated on the fluorite and quartz chips.

Six solution standards, three containing known amounts of Na, K, Ca, Cl and P and three containing known amounts of K, Na, Cl and S were used to prepare residues by evaporating drops of solutions on silica plates heated to approximately 60°C. These residues were analyzed as described above and the results used to construct calibration curves for these elements (Fig. 1.00).

Measured Concentration

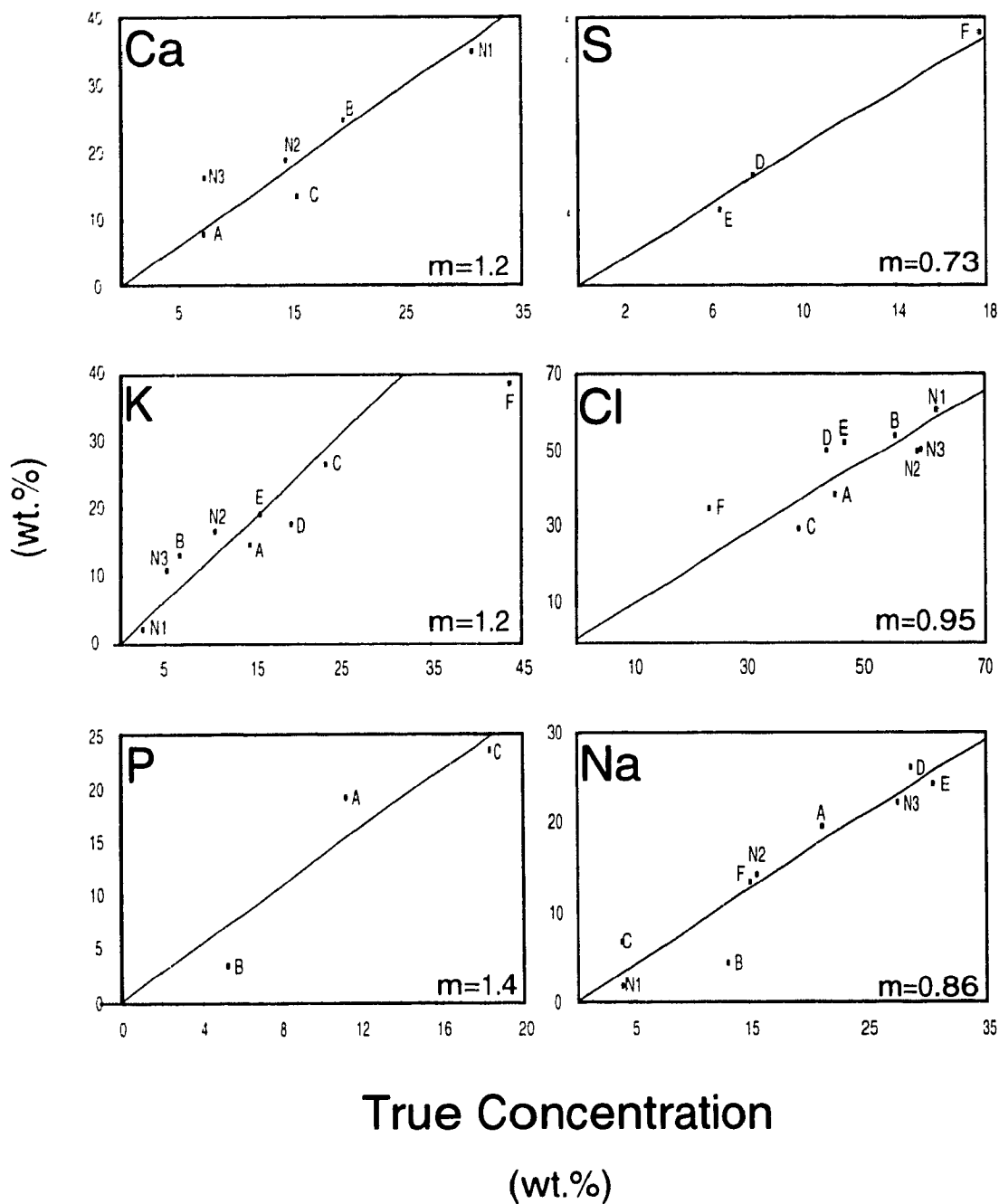


Figure 1.00 Calibration curves for decrepitate analyses based on true and measured concentrations. Analyses A to F are from this study. Data for N1 to N3 taken from Guillemette (1991).